A BIO AND SYNTHETIC POLYMER BASED NERVE GUIDE TESTED UNDER
IN VITRO AND IN VIVO CONDITIONS

A THESIS SUBMITTED TO
THE GRADUATE SCHOOL OF NATURAL AND APPLIED SCIENCES
OF
MIDDLE EAST TECHNICAL UNIVERSITY

BY

TUĞBA DURSUN USAL

IN PARTIAL FULFILLMENT OF THE REQUIREMENTS
FOR
THE DEGREE OF DOCTOR OF PHILOSOPHY
IN
BIOTECHNOLOGY

SEPTEMBER 2019

Approval of the thesis:

A BIO AND SYNTHETIC POLYMER BASED NERVE GUIDE TESTED UNDER IN VITRO AND IN VIVO CONDITIONS

submitted by **TUĞBA DURSUN USAL** in partial fulfillment of the requirements for the degree of **Doctor of Philosophy in Biotechnology Department, Middle East Technical University** by,

Prof. Dr. Halil Kalıpçılar
Dean, Graduate School of **Natural and Applied Sciences**   _____

Assoc. Prof. Dr. Can Özen
Head of Department, **Biotechnology**   _____

Prof. Dr. Vasıf Hasırcı
Supervisor, **Biotechnology, METU**   _____

Assist. Prof. Dr. Deniz Yücel
Co-Supervisor, **Histology Embryology Dept., Acıbadem Uni.**   _____

Examining Committee Members:

Prof. Dr. Tülin Güray
Biological Sciences Dept., METU   _____

Prof. Dr. Vasıf Hasırcı
Biotechnology, METU   _____

Prof. Dr. Mehmet Yıldırım Sara
Medical Pharmacology Dept., Hacettepe University   _____

Assoc. Prof. Dr. Halime Kenar
Arslanbey Vocational School, Kocaeli University   _____

Assist. Prof. Dr. Erkan Kiriş
Biological Sciences Dept., METU   _____

Date: 06.09.2019

I hereby declare that all information in this document has been obtained and presented in accordance with academic rules and ethical conduct. I also declare that, as required by these rules and conduct, I have fully cited and referenced all material and results that are not original to this work.

Name, Surname: Tuğba Dursun Usal

Signature:

ABSTRACT

A BIO AND SYNTHETIC POLYMER BASED NERVE GUIDE TESTED UNDER IN VITRO AND IN VIVO CONDITIONS

Dursun Usal, Tuğba
Doctor of Philosophy, Biotechnology
Supervisor: Prof. Dr. Vasıf Hasırcı
Co-Supervisor: Assist. Prof. Dr. Deniz Yücel

September 2019, 143 pages

Damages to the peripheral nervous system due to age, diseases or trauma may lead to gap formation in nervous tissue and inhibit signal transfer. Nerve guides are used to bridge the neural gaps created as a result of these events. This study describes the design, construction, and testing of a nerve guide which carries inner guidance elements to provide an appropriate microenvironment for peripheral nerve regeneration. A methacrylated gelatin-poly(2-hydroxyethyl methacrylate) (GelMA-pHEMA) hydrogel and 3D printed polycaprolactone (PCL) tube were produced as the exterior part of the nerve guide. Inner guidance elements, gelatin-poly(3-hydroxybutyrate-co-3-hydroxyvalerate) (PHBV) aligned fibers, were produced to provide PC12 cell alignment. Both GelMA-pHEMA hydrogels and PCL tube were suitable for Schwann cell (SC) attachment and proliferation. PC12 cells, seeded on gelatin-PHBV aligned fibrous mats, were aligned along the fiber axis and showed neurite outgrowth. Gelatin-PHBV fibrous mats were rolled and implanted into the 3D printed PCL tube to obtain a whole nerve guide structure. Over three weeks, cell number increased significantly. SCs were attached to the PCL tube, connected to each other and showed myelination. PC12 cells were also attached, proliferated and migrated from proximal to distal part on the gelatin-PHBV aligned mats. The increase

in expression of neuronal markers such as beta-III tubulin and NeuN indicated the differentiation of PC12 cells into neurons. This composite nerve guide was tested under *in vivo* conditions. 10 mm sciatic nerve defect was created in rats and different types of nerve guides were implanted at the injury site. Both walking track analysis and electrophysiology studies showed that there is a functional recovery in the groups having PCL tube and PCL tube with gelatin-PHBV mat and SCs. These results show the potential of the developed nerve guide for the peripheral nerve regeneration under *in vitro* and *in vivo* conditions.

Keywords: Nerve Tissue Engineering, Nerve Guide, Peripheral Nerve Injury, 3D Printing, Electrospinning

ÖZ

BİYOLOJİK VE SENTETİK POLİMER TEMELLİ BİR SİNİR TÜPÜNÜN İN VİTRO VE İN VİVO KOŞULLARDA SINANMASI

Dursun Usal, Tuğba
Doktora, Biyoteknoloji
Tez Danışmanı: Prof. Dr. Vasıf Hasırcı
Ortak Tez Danışmanı: Dr. Öğr. Üyesi Deniz Yücel

Eylül 2019, 143 sayfa

Yaş, hastalık ya da travma gibi nedenlerle periferal sinir sistemine verilen hasarlar sinir dokusunda boşluk oluşumuna neden olabilir ve sinyal iletimini engelleyebilir. Sinir tüpleri bu olaylar sonucunda oluşan sinir kopukluklarını birleştirmekte kullanılmaktadır. Bu çalışma, periferik sinir yenilenmesi için uygun bir mikroortam sağlamak amacıyla iç kılavuz elemanları taşıyan bir sinir tüpünün tasarımını, üretimini ve test edilmesini açıklamaktadır. Sinir tüpünün dış kısmı olarak bir metakrilat jelatin-poli (2-hidroksietil metakrilat) (GelMA-pHEMA) hidrojel ve 3 boyutlu yazıcı tekniği ile polikaprolakton (PCL) tüp üretilmiştir. İç kılavuz elemanları, jelatin-poli (3-hidroksibutirat-ko-3-hidroksivalerat) (PHBV) yönlü lifler, PC12 hücre yönlenmesini sağlamak için üretilmiştir. Hem GelMA-pHEMA hidrojellerin hem de PCL tüpün Schwann hücresi (SC) yapışması ve çoğalması için uygun olduğu görülmüştür. Jelatin-PHBV yönlü fiberler üzerine ekilmiş PC12 hücreleri, fiberler boyunca yönlenmiş ve sinir hücresi uzantıları göstermiştir. Jelatin-PHBV fiberler bütün bir sinir kılavuzu yapısı elde etmek için rulo haline getirilip ve 3 boyutlu yazıcı tekniği ile üretilen PCL tüpün içine yerleştirilmiştir. Hücre sayısının üç hafta boyunca önemli ölçüde arttığı gözlenmiştir. Schwann hücreleri, PCL tüpe yapışmış, birbirlerine bağlanmış ve miyelinleşme göstermiştir. PC12 hücreleri de jelatin-PHBV yönlü

fiberler üzerine yapışmış, çoğaltılmış ve proksimal uçtan distal uca doğru göç etmişlerdir. Beta-III tubulin ve NeuN gibi nöronal markerların ekspresyonunun artması PC12 hücrelerinin nörona farklılaşmasını göstermiştir. Bu kompozit sinir tüpü *in vivo* koşullarda test edilmiştir. Sıçanlarda 10 mm siyatik sinir hasarı oluşturulmuş ve yaralanma bölgesine farklı tipte sinir tüpleri yerleştirilmiştir. Hem yürüyüş yolu analizi hem de elektrofizyoloji çalışmaları, PCL tüpü ve PCL tüpü, jelatin-PHBV mat ve Schwann hücrelerinin bulunduğu gruplarda fonksiyonel bir iyileşme olduğunu göstermiştir. Bu sonuçlar, *in vitro* ve *in vivo* koşullar altında periferik sinir yenilenmesi için geliştirilen sinir tüpünün potansiyelini göstermektedir.

Anahtar Kelimeler: Sinir Doku Mühendisliği, Sinir Tüpü, Periferal Sinir Yaralanması, 3 Boyutlu Basım, Elektroeğirme

Dedicated to my beloved family

ACKNOWLEDGEMENTS

TABLE OF CONTENTS

LIST OF TABLES

TABLES

LIST OF FIGURES

FIGURES

LIST OF ABBREVIATIONS

ABBREVIATIONS

μCT	Microcomputed tomography
μm	micrometer
2D	Two Dimensional
3D	Three Dimensional
ANAs	Acellular Nerve Allografts
APS	Ammonium Persulfate
ATDSCs	Amniotic Tissue-derived Stem Cells
ATR	Attenuated Total Reflection
BDNF	Brain-derived Neurotrophic Factor
b-FGF	Basic Fibroblast Growth Factor
BMSC	Bone Marrow Stem Cell
BSA	Bovine Serum Albumin
Ca	Calcium
CAD	Computer-aided Design
cAMP	Cyclic Adenosine Monophosphate
CLSM	Confocal Laser Scanning Microscopy
cm	Centimeter
CNS	Central Nervous System
CNTF	Ciliary Neurotrophic Factor
CO	Cut-off
CO_2	Carbon Dioxide
CSF	Cerebrospinal fluid
D_2O	Deuterium oxide
Da	Dalton
DAPI	4', 6-Diamidino-2-Phenylindole
DHT	Dehydrothermal
DM	Degree of Methacrylation
DMEM	Dulbecco's Modified Eagle Medium
DMSO	Dimethyl Sulfoxide
DPSCs	Dental Pulp Stem Cells
ECM	Extracellular Matrix
EGDMA	Ethylene Glycol Dimethacrylate
ESC	Embryonic Stem Cell
FADH	Flavin Adenine Dinucleotide
FBS	Fetal Bovine Serum

FDM	Fused Deposition Modelling
FITC	Fluorescein Isothiocyanate
FTIR	Fourier-transform Infrared Spectroscopy
g	Gram
GABA	Gamma-aminobutyric Acid
G-CSF	Granulocyte Colony-stimulating Factor
GDNF	Glial Cell Line-derived Neurotrophic Factor
GelMA	Methacrylated Gelatin
GFAP	Glial Fibrillary Acidic Protein
h	Hour
HA	Hyaluronic Acid
HAc	Acetic Acid
HE	Hematoxylin and Eosin
HFIP	1,1,1,3,3,3-hexafluoroisopropanol
HFSCs	Hair Follicle Stem Cells
HLF	Human Ligament Fibroblast
IGF1	Insulin-like Growth Factor 1
iPSCs	induced Pluripotential Stem Cells
kDa	Kilo Dalton
L	Liter
M	Molarity
mA	milliampere
MA	Methacrylic Acid
MBP	Myelin Basic Protein
MDSPCs	Muscle-derived Stem/Progenitor Cells
mg	Milligram
MHz	Megahertz
min	Minute
mL	Milliliter
mm	Millimeter
mM	Millimolar
MSC	Mesenchymal Stem Cell
MTC	Masson's Trichrome
MW	Molecular Weight
Na	Sodium
Na_2HPO_4	Disodium Hydrogen Phosphate
NaCl	Sodium Chloride
NADH	Nicotinamide Adenine Dinucleotide
NADPH	Nicotinamide Adenine Dinucleotide Phosphate
NaH_2PO_4	Sodium Dihydrogen Phosphate
ng	Nanogram
NG	Nerve Guide

NGC	Nerve Guide Channel
NGF	Nerve Growth Factor
nm	Nanometer
NMR	Nuclear Magnetic Resonance
NSC	Neural Stem Cell
NT	Neurotrophin
NT-3	Neurothrophin-3
OCT	Optimal Cutting Temperature
OEC	Olfactory Ensheathing Cells
PANI	Polyaniline
PBS	Phosphate Buffer Saline
PCL	Poly(ε-caprolactone)
PDMS	Poly(dimethylsiloxane)
PE	Polyethylene
PEG	Polyethylene Glycol
Pen/Strep	Penicillin/Streptomycin
PGA	Poly(glycolic acid)
PHB	Poly(3-hydroxybutyrate)
PHBV	Poly(3-hydroxybutyrate-co-3-hydroxyvalerate)
PHEMA	Poly(2-hydroxyethyl methacrylate)
PLA	Poly(lactic acid)
PLGA	Poly(Lactic Acid-co-Glycolic Acid)
PLLA	Poly(L-Lactic Acid)
PMMA	Poly(methyl methacrylate)
PNI	Peripheral Nerve Injury
PNS	Peripheral Nervous System
PPy	Polypyrrole
PU	Polyurethane
PVA	Polyvinyl Alcohol
RP	Rapid Prototyping
rpm	Rotation per minute
RT	Room Temperature
s.d.m	Standard Deviation of the Mean
SC	Schwann cell
SEF	Solvent-based Extrusion Freeforming
SEM	Scanning Electron Microscopy
SF	Silk Fibroin
SKP-SCs	Skin-derived Precursor Stem Cells
SLA	Stereolithography
SLS	Selective Laser Sintering
SSI	Static Sciatic Index
T_c	Critical Temperature

TEMED	N,N,N′,N′-Tetramethylethane-1,2-Diamine
T_g	Glass Transition Temperature
T_m	Melting Temperature
UC-MSCs	Umbilical Cord-derived MSCs
UV	Ultraviolet
UV-Vis	UV-Visible
v/v	Volume/Volume
w/v	Weight/Volume
WC	Water Content
WJMSCs	Wharton's Jelly MSC

CHAPTER 1

INTRODUCTION

1.1. Nervous System

The nervous system is divided into central nervous system (CNS) and peripheral nervous system (PNS) (Figure 1.1). The CNS consists of the brain and the spinal cord. The PNS consists of cranial nerves, sensory nerve bundles which arise from the brain, the spinal nerves originate from the spinal cord and ganglions. The PNS delivers sensory information to the CNS and carries motor commands from the CNS to peripheral tissues and systems (Hasirci and Hasirci, 2018).
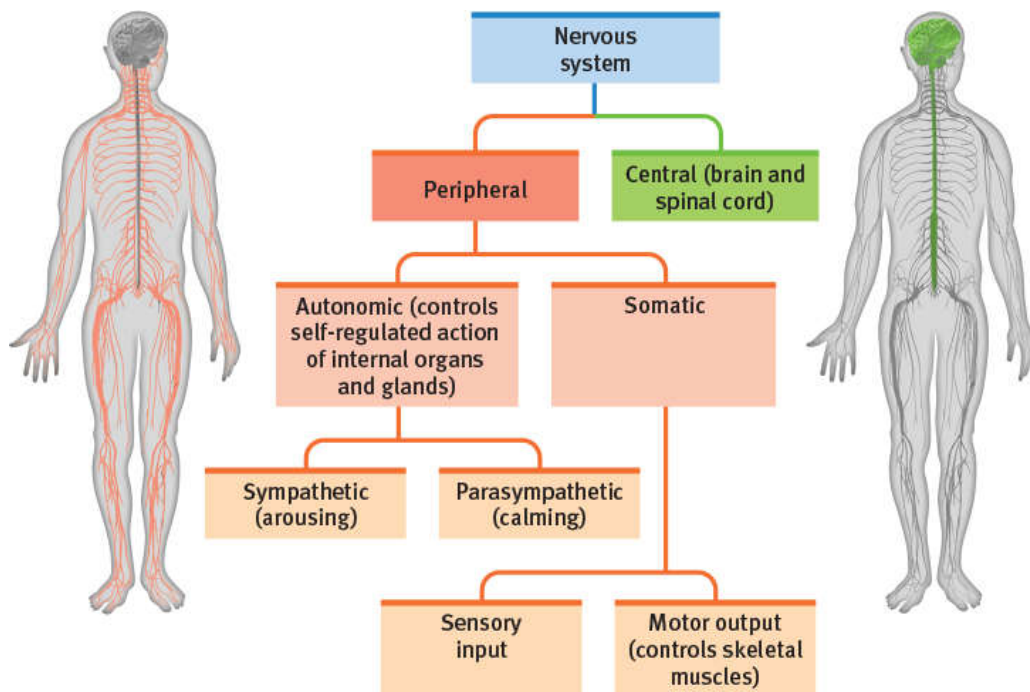
Figure 1.1. Classification of the nervous system (Myers and DeWall, 2017).

1.1.1. The Peripheral Nervous System

The peripheral nervous system (PNS) consists of two parts; somatic and autonomic. Somatic nervous system monitors sensory input and triggers motor output, controlling the skeletal muscles. Autonomic nervous system controls the glands and the muscles of the internal organs, including heart and digestive system. Autonomic nervous system is also divided into two parts named as sympathetic and parasympathetic nervous system. The dual functions of the autonomic nervous system are presented in Figure 1.2. The autonomic nervous system controls the more autonomous internal functions. Its sympathetic division arouses and expends energy. Its parasympathetic division calms and conserves energy, allowing routine maintenance activity. The sympathetic and parasympathetic divisions work together to steady the internal state of the body (Myers and DeWall, 2017).
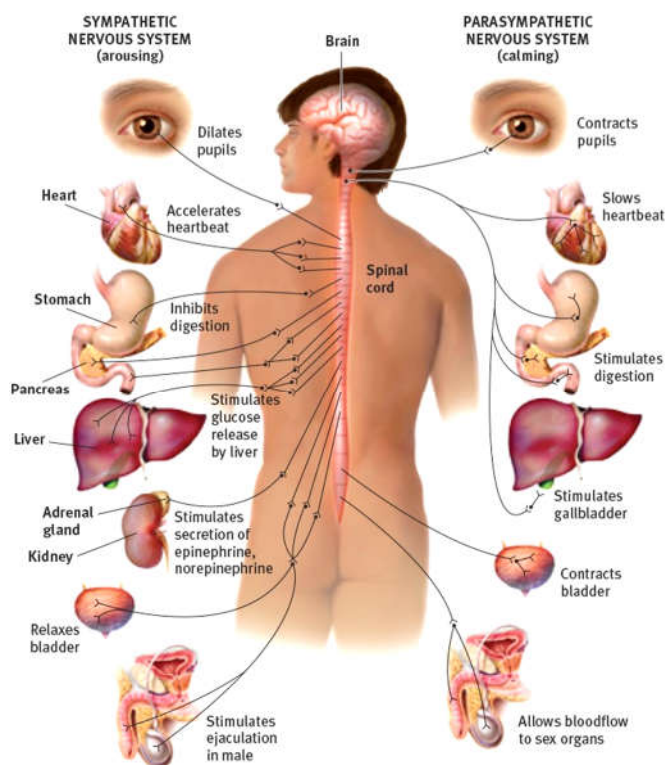
Figure 1.2. The dual functions of the autonomic nervous system (Myers and DeWall, 2017).

1.1.2. The Central Nervous System

The central nervous system (CNS) consists of the brain and the spinal cord. It has three layers of protective coverings called meninges which is derived from the Greek and means membranes (Molnar and Gair, 2015). Dura mater is the outermost layer and carries blood from the brain toward the heart. Arachnoid mater which has a web-like structure is the middle layer. Pia mater which directly contacts and covers the brain and spinal cord is the inner layer. The space between the arachnoid and pia maters is filled with cerebrospinal fluid (CSF). The brain floats in CSF, which acts as a cushion and shock absorber (Figure 1.3).
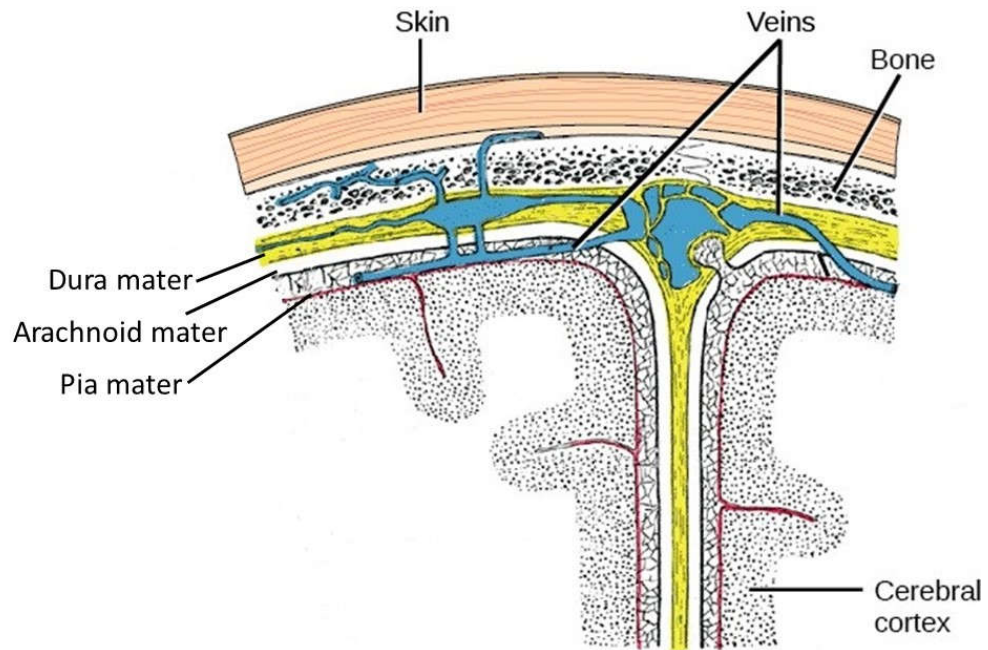
Figure 1.3. The cerebral cortex is covered by three layers of meninges: the dura, arachnoid, and pia maters (credit: modification of work by Gray's Anatomy) (Molnar and Gair, 2015).

1.1.3. Neurons and Glial Cells

Neurons and glial cells are the two main classes of cells of the nervous system. Neurons generate signals and transfer these signals between nerve cells. Glial cells

cover the axons and produce the growth factors such as nerve growth factor (NGF), brain-derived neurotrophic factor (BDNF) and the neurotransmitters such as acetylcholine, gamma-aminobutyric acid (GABA), and dopamine (Caon, 2018). Different types of neuroglia in the central and the peripheral nervous system are shown in Figure 1.4. Certain types of neuroglia called astrocytes signal neurons to form and maintain synapses.
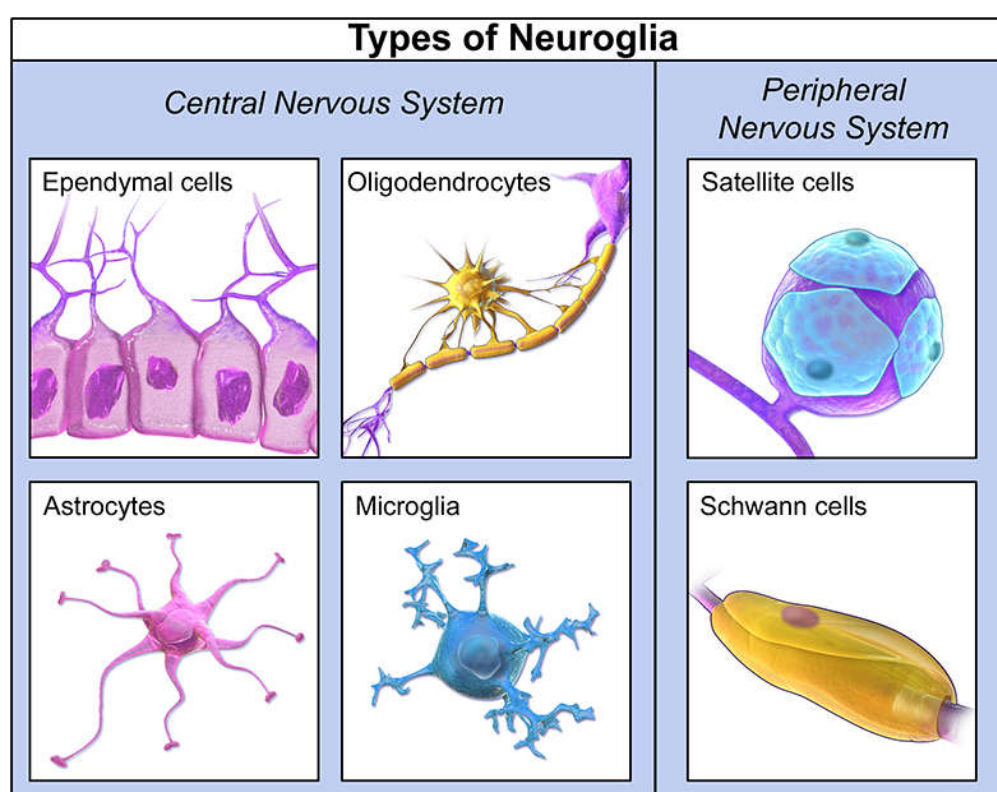
Figure 1.4. Major types of glial cells in the nervous system. Blausen.com staff (2014), CC by 3.0 via Commons.

Nerve cells are the main signaling units of the nervous system. A typical neuron has four morphologically defined regions: the cell body, dendrites, the axon, and presynaptic terminals (Figure 1.5A). The cell body, or soma, contains a large, round

4

nucleus. Dendrites, which extend from the cell body, are highly branched, and each has dendritic spines. An axon is a long cytoplasmic process capable of propagating an electrical impulse known as the action potential (Martini et al., 2018). All the behavioral functions of the brain are carried out by specific sets of interconnected neurons.

The junction between two cells is called a synapse. The gap between these two cells at a synapse is called a synaptic cleft. The impulse in the presynaptic neuron signals the postsynaptic cell during the synaptic transmission process (Guyton and Hall, 2006). Initially, a nerve impulse travels along the axon to a synapse. Then, neurotransmitters are secreted from axons into synaptic knobs at their distal ends. The neurotransmitter which diffuses across the synaptic cleft is released when a nerve impulse reaches the end of an axon (Figure 1.5B). Finally, the signal may be excitatory or inhibitory depending on the neurotransmitter reaching a postsynaptic neuron or another cell.
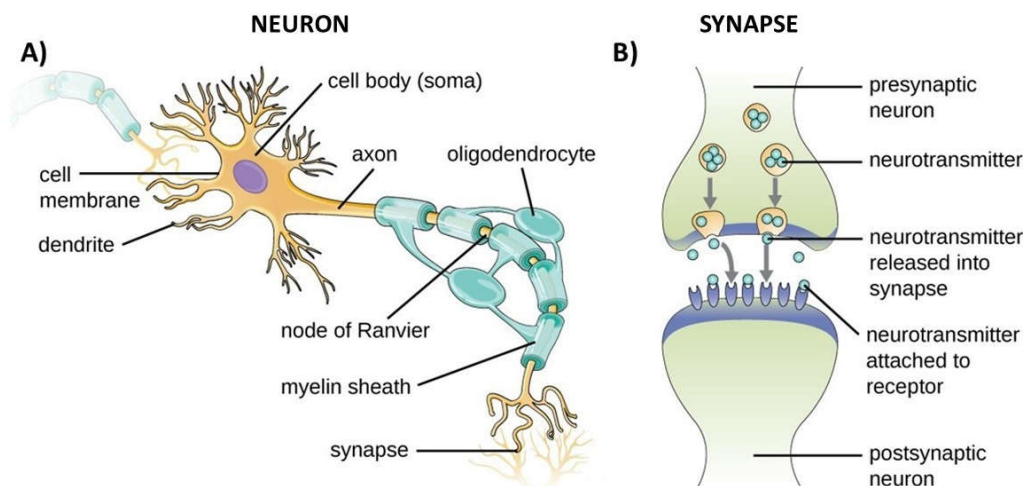
Figure 1.5. Structure of a nerve. (A) A myelinated neuron is associated with oligodendrocytes. Oligodendrocytes are a type of glial cell that forms the myelin sheath in the CNS that insulates the axon so that electrochemical nerve impulses are transferred more efficiently. (B) A synapse consists of the axonal end of the presynaptic neuron (top) that releases neurotransmitters that cross the synaptic space (or cleft) and bind to receptors on dendrites of the postsynaptic neuron (bottom). (https://courses.lumenlearning.com/microbiology/chapter/anatomy-of-the-nervous-system/)

1.1.4. Structure of a Peripheral Nerve Trunk

Peripheral nerves are composed of bundles of nerve fibers (Figure 1.6). A peripheral nerve trunk has three main parts (Arslantunali et al., 2014a). Endoneurium is the inner layer and composed of loose connective tissue. It surrounds each nerve fiber and the supporting Schwann cells. Perineurium is the middle layer and made of dense connective tissue. A bundle of nerve fibers is held together by collagen fibrils in the connective tissue and form fascicles surrounded by the perineurium. Epineurium is the outermost layer of connective tissue sheath. It covers entire nerve fascicles within a nerve trunk in a dense and irregular connective tissue. The thicknesses of nerve fascicle range from 1.3 to 100 μm (Kijeńska et al., 2014).
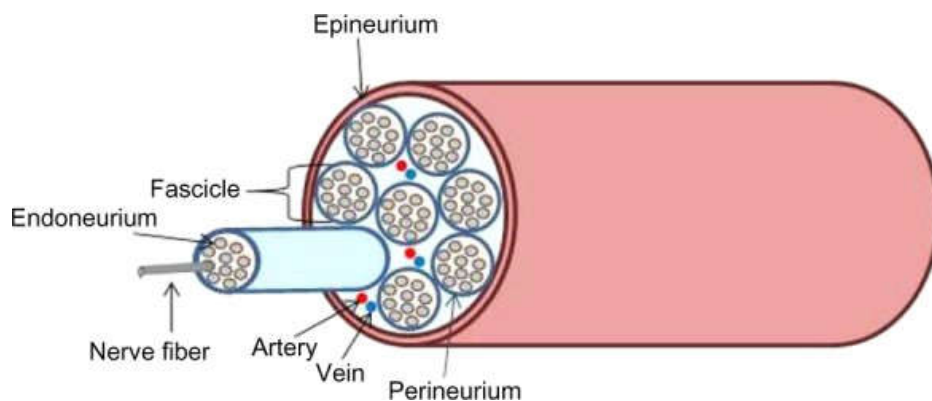
Figure 1.6. Structure of the peripheral nerve trunk. (Arslantunali et al., 2014a)

1.2. Peripheral Nerve Injury

The nervous system can be damaged by mechanical, thermal, chemical, or ischemic factors. This damage results in the interruption of communication between neurons and their targets. Therefore, various nervous system functions such as memory, cognition, language, and voluntary movement are impaired. The degree of the injury affects the functional outcome (Arslantunali et al., 2014a). Seddon's and Sunderland's classifications are used to assess the level of peripheral nerve injury (Seddon, 1943;

Sunderland, 1951). Seddon classified the peripheral nerve injuries as neurapraxia, axonotmesis, and neurotmesis. In neurapraxia, axons are not disrupted, however, there is a partial demyelination and impulses cannot be transmitted. These injuries recover with treatment within a few months. In axonotmesis, the endoneurium, the perineurium, the epineurium, and Schwann cells are intact but axon loss is observed. These injuries are regenerated slowly by the help of intact endoneurium (2-3 cm per month). In neurotmesis, the nerve trunk is transected completely and there is a scar formation. Therefore, neuroma and Wallerian degeneration are formed at the proximal and distal ends, respectively. In such severe injuries, surgical repair is required to connect the proximal and the distal ends of a nerve. Sunderland categorized the peripheral nerve injury as 1-5 degree injuries. Sunderland's first and second degree injury corresponds to neurapraxia and axonotmesis respectively in the Seddon classification. In the third degree injury, the perineurium and the epineurium are intact, but the endoneurium is disrupted. Recovery of motor and sensory function can be significantly delayed, and surgery is needed only if no recovery occurs in 2-3 months. In fourth degree injury, axons, endoneurium, and perineurium are disrupted, but the epineurium is intact. Removal of scar tissue and surgical repair of the nerve is needed in order to achieve regeneration because there is a higher degree of degeneration when compared with lower degree injuries. Sunderland's fifth degree injuries corresponds to neurotmesis. Classification of peripheral nerve injury is summarized in Figure 1.7.
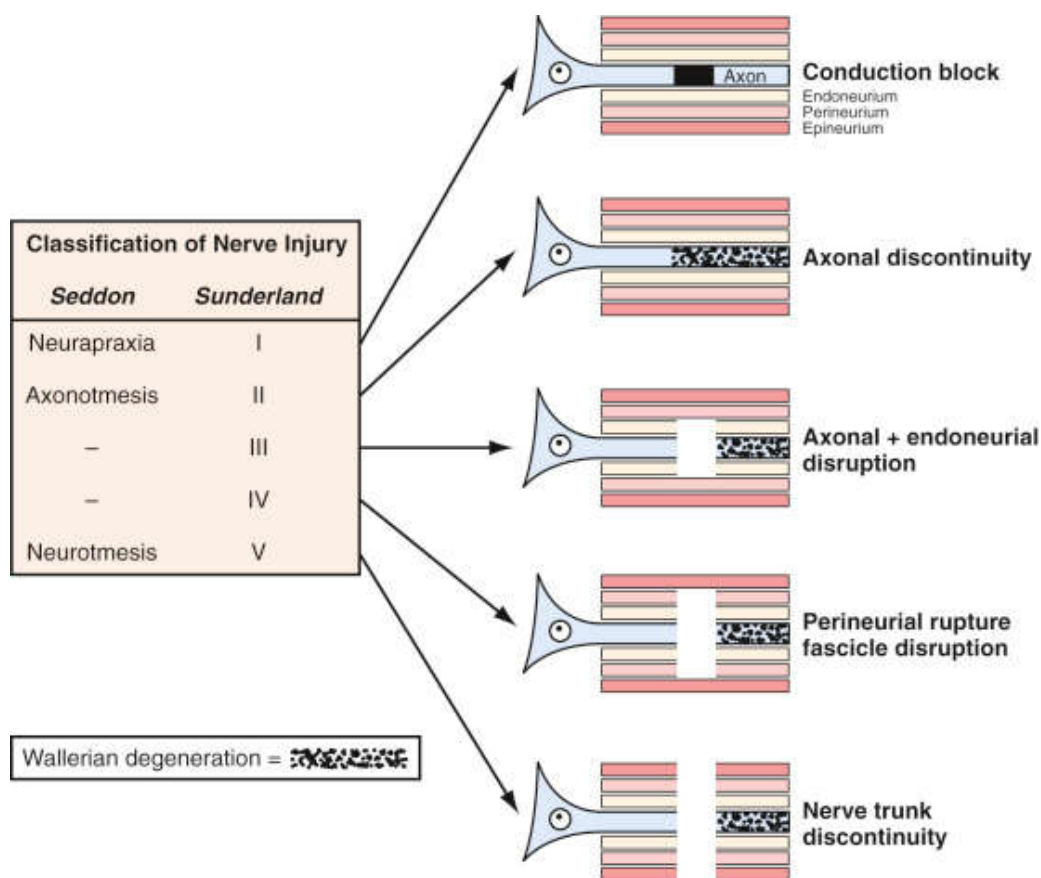
Figure 1.7. Seddon and Sunderland classification of nerve injuries. (Nadi and Midha, 2018)
Copyright © 2018 Elsevier Inc.

When the peripheral nerve injury occurs, the proximal end, the portion still connected to the cell body, may survive, but the distal end, the portion of the axon disconnected from the cell body, does not. The distal end is disconnected from the neural body undergoes Wallerian (anterograde) degeneration (Carroll and Worley, 2017). The ideal rate of axonal regrowth from the proximal end is 1 mm/day (Arslantunali et al., 2014a). However, if these axonal sprouts fail to cross the injury site, this leads to the formation of a neuroma and the denervated muscle fiber becomes atrophic. Cellular response to a peripheral nerve injury is shown in Figure 1.8.
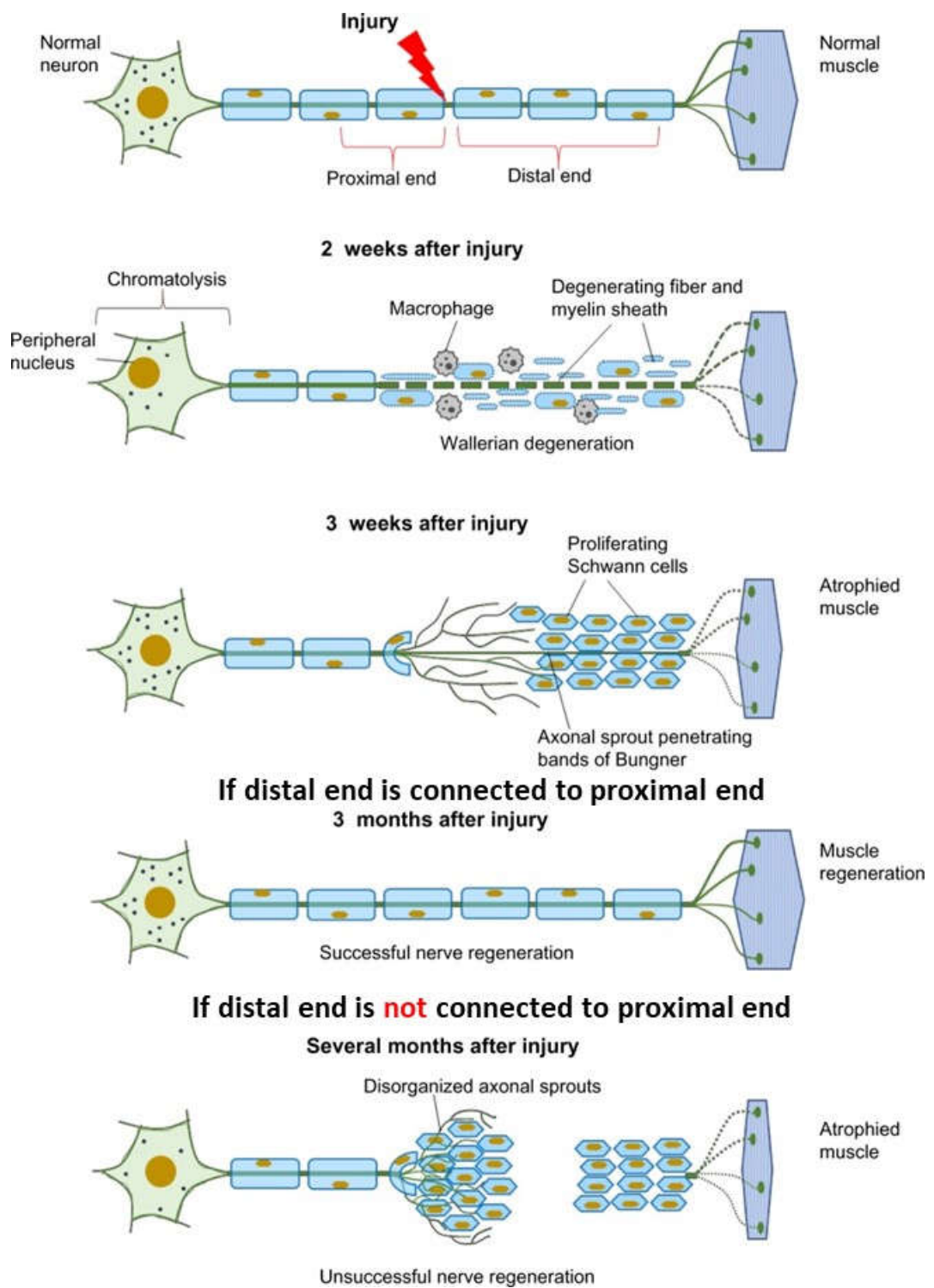
Figure 1.8. Cellular response to peripheral nerve injury. (Arslantunali et al., 2014a)

1.2.1. Treatment Strategies for Peripheral Nerve Injuries

Peripheral nerve injuries cause the motor and/or sensory loss which can affect the life of the patient (Bassilios Habre et al., 2018). The gold standard for the treatment of nerve section is end-to-end suturing of severed nerves (neurorrhaphy). However, in some cases, there is a segmental loss of the nerve trunk. End-to-end neurorrhaphy can be used if the gap is less than 1 cm. Autologous nerve grafting is the gold standard when the nerve gap exceeds 1 cm. Vascularized nerve grafts, cellular and acellular allografts, nerve conduits, and end-to-side neurorrhaphy are used as alternative treatments to overcome the limited availability and the donor site morbidity.

Poor nerve regeneration and incomplete functional recovery may occur after a peripheral nerve injury (Li et al., 2014). Spontaneous nerve regeneration may not be satisfactory to achieve proper functional recovery, especially in severe injuries. There are some current clinical approaches for the treatment of peripheral nerve injury; different treatment strategies are summarized in Figure 1.9.
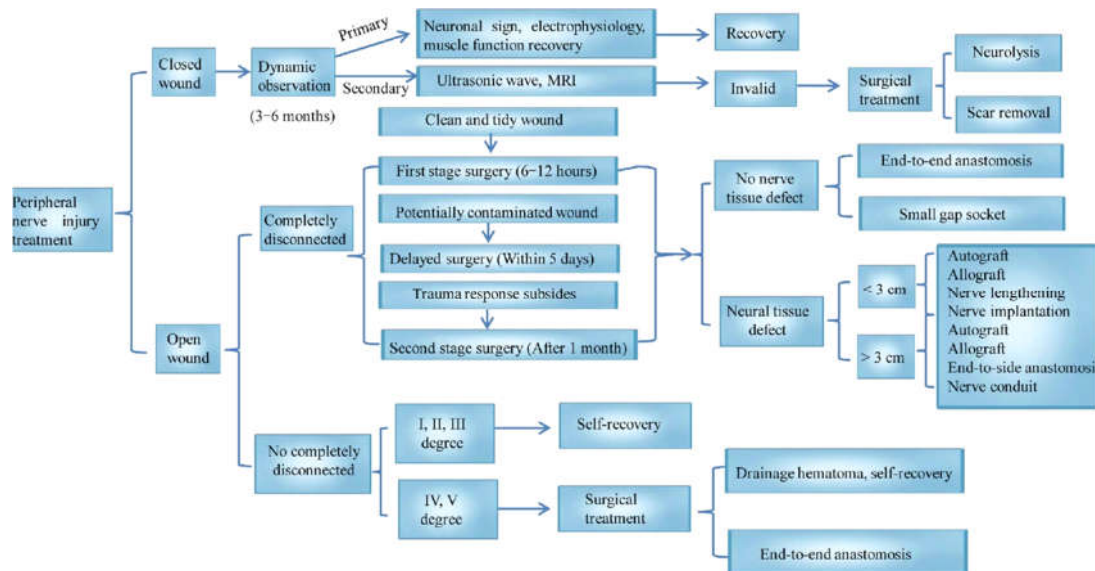
Figure 1.9. Main methods for the clinical treatment of different peripheral nerve injuries. Nerve implantation (the red color) indicates that it can be used whether the nerve defect is ≤ 3 cm or ≥ 3 cm. (Han et al., 2019).

1.2.1.1. Peripheral Nerve Grafts

1.2.1.1.1. Autografts

Autografts are the most widely used nerve repair materials and are considered as the gold standards in bridging nerve gaps. They provide structural connection for axonal progression from the proximal to the distal site. An autograft is commonly obtained from the sural nerve, medial antebrachial cutaneous nerve, or superficial radial nerve since these small-caliber grafts achieve better results (faster revascularization) than larger-caliber grafts (Nadi and Midha, 2018). However, there are significant limitations in the use of nerve autografts, such as the need for a second surgery site to harvest graft tissue from the donor site, which is associated with donor site morbidity and resultant loss of function. Autografts can be used for nerve gaps of up to 3-5 cm (Das and Srivastava, 2019).

1.2.1.1.2. Allografts

Nerve allograft is a technique used to bridge a peripheral nerve lesion with tissues derived from a different individual of the same species. However, the use of allografts has limitations such as immune rejection, secondary infection, risk of cross-contamination, and limited supply.

Cadaveric donor nerve grafts are used as allografts in the treatment of peripheral nerve injuries (Ramachandran and Midha, 2019). These grafts can supply viable Schwann cells for regenerating axons. Although nerve allografts are not as immunogenic as skin or muscle, the use of them almost always requires immunosuppressive therapies.

Acellular nerve allografts (ANAs) obtained from animals have been established as promising alternatives to autologous nerve grafts (Boriani et al., 2019). Noncellular-based stimulation of ANAs showed positive effects on nerve function recovery. However, neuroregenerative effect of autografts still appeared superior to acellular nerve allografts, even with noncellular enrichment of ANAs. On the other hand,

modified ANAs closely approached or even outperformed autografts in a few studies (Wang et al., 2017).

1.2.1.1.3. Xenografts

Xenografts are the graft materials taken from donors from another species than humans. Clinical surgery research has turned to nerve xenotransplantation, which offers a potentially unlimited source of donor nerves compared autografts and allografts (Deleyto and Lasso, 2017).

Acellular xenografts are obtained by chemically eliminating the cellular constituents which might cause immunogenic reactions. During this process, the native extracellular matrix that retains sufficient bioactivity to promote axonal regeneration should be preserved (Hudson et al., 2004). Acellular nerve xenografts, similarly to acellular nerve allografts, are found to be immunocompatible (Zhang et al., 2010). In this study, it was proposed that short defects can regenerate along acellular scaffolds but longer defects might require certain cellular stimuli which should be provided by added autologous stem cells. Functional rehabilitation efficacy of these acellular xenografts was proven comparable to autografting (Jia et al., 2012).

1.2.1.2. Nerve Conduits

Nerve conduits or nerve guides are artificial devices which bridge the proximal and the distal nerve ends in order to achieve nerve regeneration. Physical (internal guidance channels) and biochemical elements (growth factor release) can be incorporated into the nerve guide structure to improve its properties. Support cells, such as Schwann cells (SCs), can also be integrated into the nerve conduit to enhance the healing of the damaged tissue (Figure 1.10).
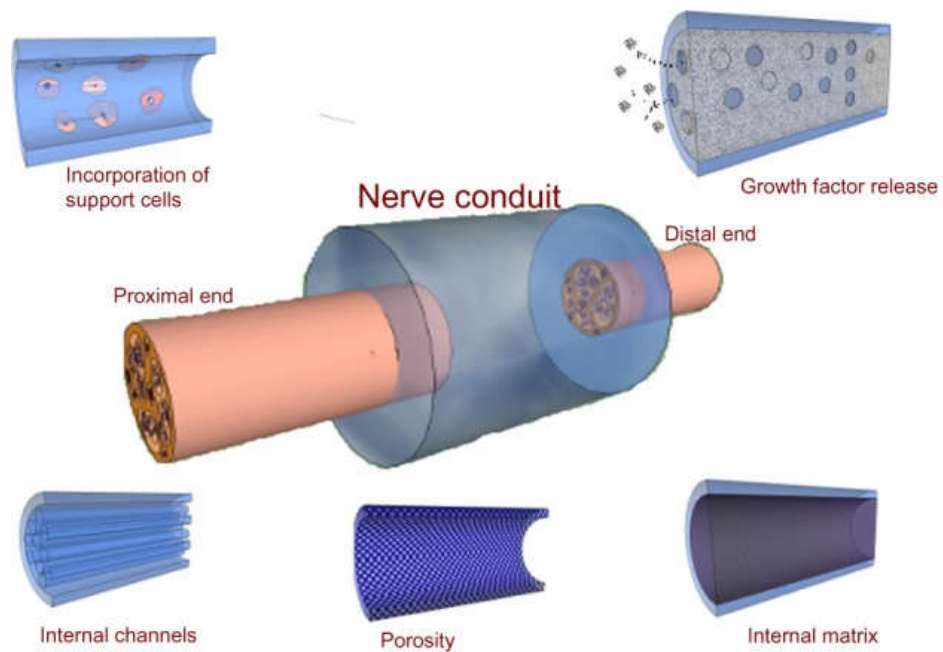
Figure 1.10. Examples for nerve conduit designs. (Arslantunali et al., 2014a)

An ideal scaffold requires should have a combination of optimal material, size, architecture, and surface properties to support peripheral nerve regeneration (Du et al., 2018). With the help of these features, a new extracellular matrix consisting of blood vessels, fibroblasts, and Schwann cells can be formed, creating a supportive environment for nerve regeneration. Various nerve conduits have been approved for clinical use are summarized in Table 1.1.

Table 1.1. *Commercially available FDA-approved nerve conduits. (Arslantunali et al., 2014a)*

Product Name	Material	Structure	Company
NeuraGen®	Collagen Type I	Semipermeable, fibrillar structure of the collagen	Integra LifeSciences Co, Plainsboro, NJ, USA
NeuroFlex™	Collagen Type I	Flexible, semipermeable tubular collagen matrix	Collagen Matrix, Inc., Franklin Lakes, NJ, USA
NeuroMatrix™	Collagen Type I	Semipermeable tubular collagen matrix	Collagen Matrix, Inc.
NeuraWrap™	Collagen Type I	Longitudinal slit in the tubular wall structure	Integra LifeSciences Co
NeuroMend™	Collagen Type I	Semipermeable collagen wrap designed to unroll and self-curl	Collagen Matrix, Inc.
Neurotube®	Polyglycolic acid	Absorbable woven PGA Mesh Tube	Synovis Micro Companies Alliance, Birmingham, USA
Neurolac™	Poly(D,L-lactide-co-ε-caprolactone)	Synthetic and transparent PLCL tubular structure	Polyganics BV, Groningen, Netherlands
Salutunnel™	Polyvinyl alcohol	Non-biodegradable PVA tubular structure	Salumedica LCC, Atlanta, GA, USA

1.2.1.2.1. Biological Nerve Conduits

Biopolymers as well as synthetic polymers are used for the fabrication of the nerve conduits. Bioactive properties of the bipolymers allow better interactions between the cells and the guides and enhance proliferation of the cells and regeneration of tissues (Arslantunali et al., 2014a). Even though biopolymers have high degrees of biocompatibility, they still show batch-to-batch variation (Schmidt and Leach, 2003). Bacterial polyesters (poly(3-hydroxybutyrate) (P3HB) and poly(3-hydroxybutyric acid-co-3-hydroxyvaleric acid) (PHBV), proteins (silk, collagen, gelatin, fibrinogen, elastin, keratin), and polysaccharides (hyaluronic acid, chitin, and alginate) are commonly used in the production of the biological nerve conduits.

14

1.2.1.2.2. Synthetic Nerve Conduits

Synthetic polymers are alternatives to the biopolymers and have some advantages over the biopolymers such as controllable mechanical properties and degradation rates, and functionalization with various groups that enhance tissue regeneration (Tian et al., 2012). In the recent years, the material preference has shifted towards synthetic polymers (Arslantunali et al., 2014a). Biodegradable polyesters, such as poly(lactic acid) (PLA), poly(glycolic acid) (PGA), poly(lactic acid-co-glycolic acid) (PLGA), poly(ε-caprolactone) (PCL), polyurethanes (PUs), trimethylene carbonate-co-ε-caprolactone, and poly(D,L-lactide-co-ε-caprolactone) are frequently used. Nonbiodegradable polymers such as methacrylate-based hydrogels, polystyrene, silicone, and poly(tetrafluoroethylene) are also used in nerve regeneration studies.

1.2.1.2.3. Hybrid Nerve Conduits

Both bio and synthetic polymers have their own advantages and disadvantages. Hybrid nerve conduits are produced to obtain superior properties. For example, most of the synthetic materials are hydrophobic and not suitable for cell adhesion and researchers started to treat the surfaces of the nerve conduits with ECM proteins or design hybrid nerve conduits with different compositions to overcome this problem (Lee et al., 2012). For example, polyesters (Yucel et al., 2010; Prabhakaran et al., 2013), polysaccharides (Entekhabi et al., 2016; Singh et al., 2019), and proteins (Dursun Usal et al., 2018; Yen et al., 2019) are combined with synthetic biomaterials for the fabrication of the hybrid nerve conduits.

1.3. Peripheral Nerve Tissue Engineering

Different types of strategies have been developed to produce an advanced peripheral nerve tissue engineering products. For example, cells are incorporated into the scaffolds to enhance axonal regeneration with neuroprotective therapies (Faroni et al., 2015). Advanced biomaterials such as collagen, laminin and fibrin hydrogels containing ECM proteins, are reported to be used in peripheral nerve repair due to their ability to support axonal outgrowth (Mobini et al., 2017). Different types of

scaffold production methods including electrospinning and 3D printing are used to fabricate highly aligned structures (Entekhabi and Nazarpak, 2018; Dursun Usal et al., 2019). Growth factors such as NGF and BDNF are also known to be incorporated in the nerve guide structure.

1.3.1. Cell Sources in Peripheral Nerve Tissue Engineering

Cells are the most essential part of a tissue engineering product. Schwann cells, neural stem cells, embryonic stem cells, and marrow stromal cells have been reported as the most studied support cells in the peripheral tissue engineering (Gu et al., 2011).

1.3.1.1. Stem Cells

Different types of stem cells; nerve, embryonic, adult, adipose-derived and bone marrow stem cells, are used in peripheral tissue engineering (Jiang et al., 2017). Different stem cell sources are presented in Figure 1.11.
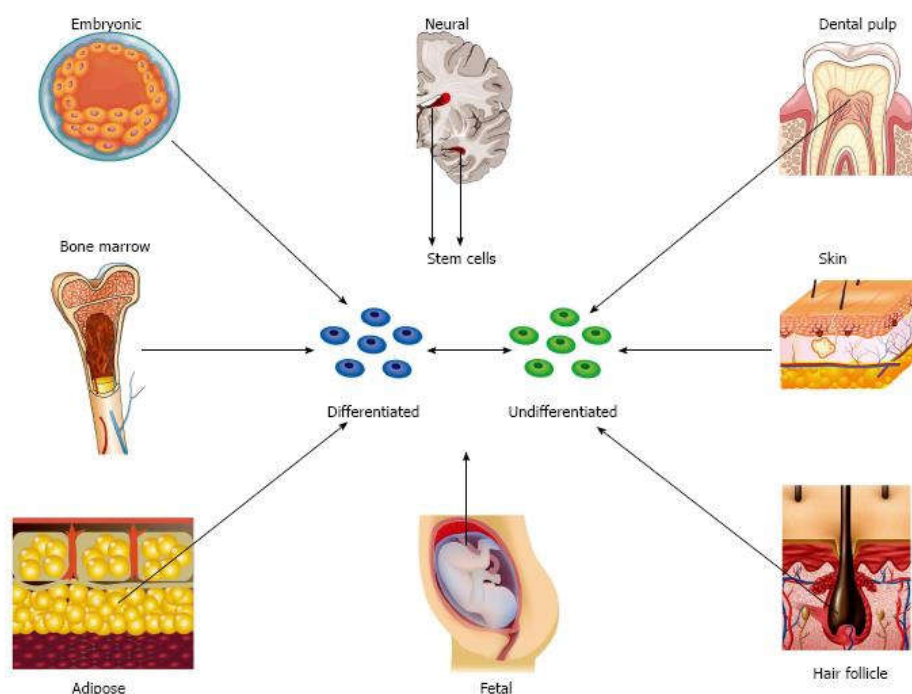
Figure 1.11. Different stem cell sources. (Fairbairn et al., 2015).

16

1.3.1.1.1. Nerve Stem Cells (NSCs)

Nerve stem cells (NSCs) can be derived from three different sources: 1) direct extraction from primary tissues, 2) differentiation from pluripotent stem cells and 3) transdifferentiation from somatic cells (Tang et al., 2017). NSCs can differentiate into neurons and glial cells (Fairbairn et al., 2015). Therefore, they have a unique role in neural regeneration. Nerve stem cell transplantation is very efficient for the treatment of nervous system diseases. Many studies reported positive effects of NSC implantation into peripheral nerve injury (Zhang et al., 2008; Guo and Dong, 2009; Fu et al., 2011; Liard et al., 2012; Lee et al., 2014). However, their use is limited due to the difficulties associated with the cell harvest.

1.3.1.1.2. Embryonic Stem Cells (ESCs)

Embryonic stem cells (ESCs) can be viewed as an immortal extension of short-lived pluripotent cells which exist in a preimplantation embryo (Klimanskaya, 2019). These pluripotent cells form all of the tissues of the body during embryo development. Embryonic stem cells are homogenous, are not susceptible to the detrimental impact of age and disease unlike adult stem cells (Rando, 2006). ESCs have been used in different studies for the peripheral nerve regeneration (Cui et al., 2008; Xie et al., 2009; Jones et al., 2018). However, differentiation into specialized neural cell lines is challenging and established protocols only exist for a limited number of lines (Zhang et al., 2008). Immunogenicity, tumorigenicity and potential ethical controversy are the common disadvantages associated with the usage of ESCs (Fairbairn et al., 2015).

1.3.1.1.3. Bone Marrow Mesenchymal Stem Cells (BMSCs)

Bone marrow mesenchymal stem cells or bone marrow stromal cells (BMSCs) are one of the most important stem cells in the field of neural tissue engineering. They localize in the stromal compartment of the bone marrow, support hematopoiesis, and differentiate into mesenchymal lineages (Klimczak and Kozlowska, 2016). BMSCs are used in various applications such as neural injury and disorders due to their easy

isolation through the aspiration of the bone marrow and expansion in a large scale by *in vitro* culture (Sun et al., 2015; Shirian et al., 2016; Chijimatsu et al., 2017; Jia et al., 2019). BMSCs have become an alternative to Schwann cells for use as support cells because autologous Schwann cells are difficult to obtain in large number, and allogeneic Schwann cells are involved in immunological rejections (Gu et al., 2014).

1.3.1.1.4. Adipose-Derived Stem Cells (ADSCs)

Adipose-derived stem cells (ADSCs) can be derived from adipose tissue obtained by liposuction (Jiang et al., 2017). When compared with BMSCs, ADSCs show higher proportion and superior proliferation and differentiation potential (Strem et al., 2005). ADSCs can be differentiated into a Schwann cell-like phenotype which shares morphological and functional properties with Schwann cells, thus representing a valid SC alternative (Kingham et al., 2007). Multiple *in vitro* studies have shown the differentiation of ADSCs into tissues similar to neural tissue under a range of stimuli (Zack-Williams et al., 2015). Therefore, some studies utilized nerve conduits combined with ADSCs to bridge the gap in the damaged peripheral nerves (Scholz et al., 2011; Kingham et al., 2014), while others used ADSC therapy with nerve allografts (Zhang et al., 2010; Marconi et al., 2012; Tajiri et al., 2014).

1.3.1.1.5. Other Stem Cells

Many types of other stem cells such as induced pluripotential stem cells (iPSCs) (Uemura et al., 2015; Srinivasan and Toh, 2019), skin-derived precursor stem cells (SKP-SCs) (Grimoldi et al., 2015; Zhu et al., 2018), hair follicle stem cells (HFSCs) (Amoh et al., 2012; Yamazaki et al., 2017), dental pulp stem cells (DPSCs) (Yamamoto et al., 2016; Carnevale et al., 2018), muscle-derived stem/progenitor cells (MDSPCs) (Guy et al., 2019; Lavasani et al., 2014; Vojnits et al., 2017), and fetal-derived stem cells including amniotic tissue-derived stem cells (ATDSCs) (Li et al., 2014; Su et al., 2018), umbilical cord-derived MSCs (UC-MSCs) (Zarbakhsh et al., 2016; Ma et al., 2019), Wharton's jelly MSCs (WJMSCs) (Peng et al., 2011; Millán-Rivero et al., 2018) are used for the peripheral nerve regeneration.

1.3.1.2. Schwann Cells (SCs)

Schwann cells (SCs) undergo a radical change and provide powerful support for regeneration after a peripheral nerve injury (Jessen and Mirsky, 2016). Schwann cell injury response to nerve injury is shown in Figure 1.12. The Schwann cell injury response has two components (Jessen and Arthur-Farraj, 2019). One is the reversal of myelin differentiation, and the other is the sequential activation of diverse features that support peripheral nerve repair.
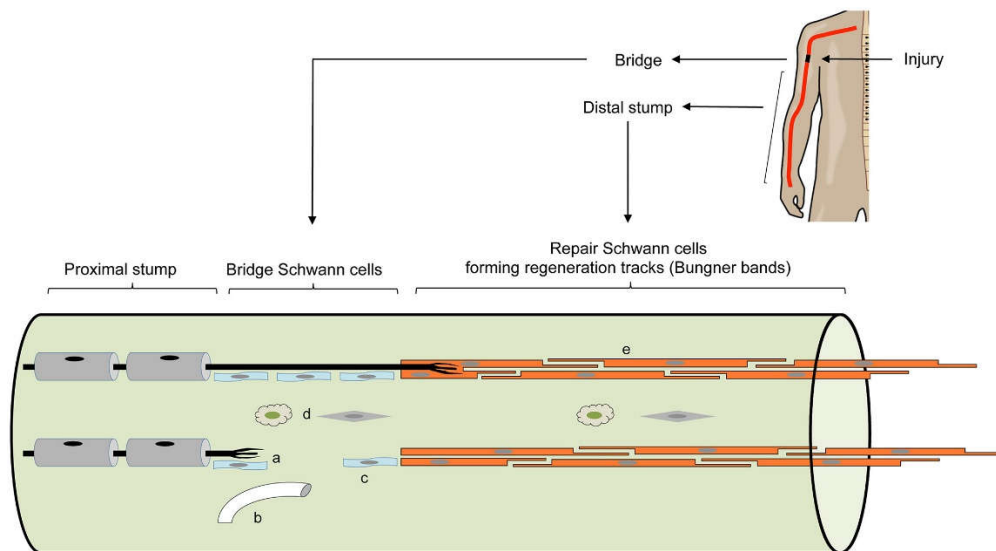
Figure 1.12. Major cell components of regenerating nerves. The diagram shows the proximal and distal ends and the guide that connects them. (a) Regeneration unit, (b) blood vessel, (c) Schwann cells migrating from the distal end, (d) macrophages and fibroblasts and (e) Bungner bands (Jessen and Arthur-Farraj, 2019) Copyright 2019 Wiley Periodicals, Inc.

Schwann cell transplantation has shown promise for peripheral nerve regeneration (Han et al., 2019). Schwann cells cultured *in vitro* formed normal myelin around the axons when implanted into rat sciatic nerve. Schwann cells are also used as the support cells in the nerve guide structure to provide enhanced peripheral nerve regeneration (Cattin et al., 2015; England et al., 2017; Gonzalez-Perez et al., 2018; Resch et al., 2018; Dursun Usal et al., 2019).

1.3.1.3. Olfactory Ensheathing Cells (OECs)

Olfactory ensheathing cells (OECs) are a type of macroglia found in the nervous system. Several studies revealed that transplantation of OECs enhances axonal regeneration and functional recovery following damage to the nervous system (Yang et al., 2015). Although they are usually used for the treatment of spinal cord injury, some of the studies have reported the positive effect of OECs for peripheral nerve regeneration (Kabiri et al., 2015; Goulart et al., 2016; Li et al., 2018; Zhang et al., 2019; Gu et al., 2019).

1.3.1.4. Neuronal Cell Lines

Neuronal cell lines are commonly used for *in vitro* neurobiology studies. They can be induced to differentiate into neuron-like cells which express neuronal markers and elaborate processes like axons and dendrites. The major advantages of cell lines are their indefinite growth, degree of reproducibility and simplicity (Barnes et al., 2001). The main disadvantage of these cell lines is their physiological differences from which they were derived. These cell lines are often induced to display a more neuronal phenotype by manipulations of the culture conditions such as the addition of specific growth factors (Gordon et al., 2013). SH-SY5Y (Arslantunali et al., 2014b; Yang et al., 2016; Qing et al., 2018; Nune et al., 2019), PC12 (Song et al., 2016; Oh et al., 2018; Wang et al., 2019), NT2 (Tegenge et al., 2011; Roloff et al., 2015), MN9D (Hei et al., 2016; Wei et al., 2019), and Cath.a (Haney et al., 2013; Wang et al., 2018) are the cell lines which are used in the peripheral nerve regeneration studies.

1.3.2. Scaffold Production Methods in Peripheral Nerve Tissue Engineering

Neural scaffolds can be fabricated by many different techniques, such as immersion precipitation particulate leaching, extrusion, injection molding, non-woven or woven mesh rolling, centrifugal casting, spinning mandrel technology, film casting plus rolling, and molding plus freeze-drying (Gu et al., 2014). Some advanced fabrication techniques have been used to manufacture more complex scaffolds, such as a

multichannel nerve guidance conduit (NGC), or a NGC containing longitudinally aligned fibers, microgrooves or hydrogels within their lumens. Different manufacturing methods, such as electrospinning, phase separation, self-assembly, and computer-aided design-based fabrication techniques, have been utilized for producing nanostructured scaffolds to enhance axonal regrowth.

1.3.2.1. Conventional Nerve Guide Fabrication Techniques

Conventional fabrication techniques include electrospinning, freeze drying, solvent casting and particle leaching, gas foaming, phase separation, and self-assembly.

1.3.2.1.1. Electrospinning

Electrospinning is an electrohydrodynamic process, during which a liquid droplet is electrified to form a jet, followed by stretching and elongation to generate fibers (Xue et al., 2019). A high-voltage power supply, a syringe pump, a spinneret, and a conductive collector are the main components of an electrospinning setup. The liquid is extruded from the spinneret to produce a droplet due to the surface tension. When an electrical field is applied, the electrostatic repulsion among the surface charges deforms the droplet into a Taylor cone, from which a charged jet is ejected. As the jet is stretched into finer diameters, it solidifies and leads to the deposition of solid fibers on the collector. All tissues and organs such as skin, collagen, dentin, cartilage, nerve, and bone have some resemblance to highly organized, hierarchical, nanosize fibrous structures (Haider et al., 2018). Therefore, electrospinning has been used in many studies to produce an aligned structure to provide cell elongation inside of the nerve guide (Yucel et al., 2010; Lee et al., 2017; Frost et al., 2018; Quan et al., 2019).

1.3.2.1.2. Freeze Drying

Freeze drying is a drying process for converting solutions into solids for distribution and storage for food science, pharmaceuticals, and enzyme stabilization applications (Lu et al., 2013). It has three major steps: 1) freezing of the solution at a low temperature (-80 °C); 2) putting of the the frozen sample in a chamber in which the

pressure is lowered through a partial vacuum, known as the primary drying process, in which the ice in the material is removed by direct sublimation; 3) removal of the unfrozen water in the material by desorption in a secondary drying process. Freeze drying method has been widely used for the fabrication of 3D porous scaffolds for nerve tissue engineering (Salvatore et al., 2014; Lin et al., 2017; Carvalho et al., 2018).

1.3.2.1.3. Solvent Casting and Particulate Leaching

Mineral and organic particles are dispersed in polymer solution in solvent casting and particulate leaching (Yadegari et al., 2017). Then, the solvent is evaporated by applying solvent casting techniques. Lastly, solid particles are leached out by selective dissolution to produce the polymeric matrix. Highly porous structures (more than 93%) and facile tailoring the crystallinity of matrix are the main advantages. This method is feasible to any polymer which is soluble in organic solvents. However, the removal of dissolved particles in polymer matrix restricts this technique only for producing thin membranes. This method have been utilized for the production of the nerve guides (Chung et al., 2011; Ho et al., 2019).

1.3.2.1.4. Gas Foaming

Gas foaming provides solvent-free formation of porous materials by the application of gas bubbles within a polymer (Hutmacher et al., 2014). Molded polymers can be pressurized with a gas, typically CO_2, until the polymer is saturated. The release of pressure results in nucleation and growth of the air bubbles up to 100 μm. The main disadvantage of this method is the limited interconnectivity, thus it is combined with particulate leaching. In some studies, gas foaming has been used to produce tissue engineering scaffolds (Kuang et al., 2017; Manavitehrani et al., 2019) and enhance peripheral nerve regeneration (Rao et al., 2019).

1.3.2.1.5. Phase Separation

A single-phase homogenous solution is critically quenched, causing separation into two phases; polymer-rich region and a solvent-rich region in the phase separation

process (Baghaban-Eslaminejad et al., 2017). It is a useful technique to fabricate nanofibrous scaffolds, which have interconnected porous structure for the biological applications. Porogens, such as sugar, salt, or paraffin are often added within a bulk material and then leached out following phase separation, leaving open pores, as well as nanofibers. This method has been used in different studies for the fabrication of the nerve guides (Kuo and Yeh, 2011; Zhang et al., 2013; Abzan et al., 2018).

1.3.2.1.6. Self-Assembly

The self-assembly process is an autonomous organization of components into patterns or structures without human intervention (Zhang et al., 2005). Self-assembly of biological molecules can be induced by noncovalent bonds or weak covalent interactions. Phospholipids are the typical example of molecular self-assembling into an ordered structure (Ma, 2008). Moreover, various nanoscale filaments of peptides can be assembled into nanofibers, which can mimic the physical microenvironment of cells *in vivo*. These nanofibers could wrap around cells covering long distances over their surfaces and act as cables that connect neighbor cells and mechanically support them by creating 3D networks in the body. Therefore, self-assembly has been used in peripheral nerve tissue engineering applications (Nune et al., 2016; Wu et al., 2017; Zhu et al., 2017; Lu et al., 2018; Li et al., 2019).

1.3.2.2. Rapid Prototyping (RP)

Rapid prototyping includes a group of techniques to fabricate highly precise scaffold structures directly from computer-aided design (CAD) data (Nguyen et al., 2015). RP is considered as a bottom-up approach because the resulting scaffold is constructed in a layer-by-layer manner. RP uses additive processes; its components are built up gradually in layers until the final geometry is obtained (Yeong et al., 2004).

Rapid prototyping technique can produce scaffolds for cell seeding and cell encapsulation and design 3D structures with predetermined micro and inner architecture (Billiet et al., 2014). An important property of RP is the ability to build

predefined macrostructures as well as microstructures which are not possible with the traditional fabrication methods. This property makes RP a potential technique for fabricating scaffolds with controlled structures and architectures for use in tissue engineering. Since the macroscopic shapes and form of the scaffolds determine the final appearance and the structure of tissue engineered product, RP can be used to reconstruct parts of the body. For example, an ear or a jaw can be constructed from the contours of the organ of the patient obtained directly from the patient by the magnetic resonance imaging (MRI), CT scans or other scanning methods (Ozbolat and Yu, 2013). Fused deposition modeling (FDM), stereolithography (SLA), selective laser sintering (SLS), solvent-based extrusion freeforming (SEF) and bioprinting are the different rapid prototyping techniques.

1.3.2.2.1. Fused Deposition Modeling (FDM)

A solid polymer is cast into a hot extrusion nozzle to be melted and extruded on the surface of a 3D object using a computer controlled extrusion and deposition processes in fused deposition modeling (Eltom et al., 2019). The scaffold is made layer-by-layer from adjacent microfilaments. The different components of FDM are shown in Figure 1.13A. Thermoplastic biopolymers such as polycaprolactone (PCL) are used in FDM technique. Fused deposition modeling has been used for the production of tissue engineering scaffolds (Hutmacher et al., 2001; Chin Ang et al., 2006; Rimington et al., 2017; Mohseni et al., 2018) and nerve guides (Hsieh et al., 2015).

1.3.2.2.2. Selective laser sintering (SLS)

Selective laser sintering (SLS) method uses a CO_2 or Nd:YAG laser beam for scanning successive layers of powdered materials to create a 3D object (Shirazi et al., 2015). The scanning patterns of each layer are automatically computed based on the slicing of the digital design. SLS technique includes two main steps: 1) CAD design of the structure, and 2) transfer of the CAD data to the SLS machine fabricate 3D structure with the desired powders (Figure 1.13B). SLS is a fast and economical process (Mazzoli, 2013). However, SLS feature detail is not as sharp as produced by

stereolithography (SLA). Although SLS technology has been mainly used for bone tissue engineering applications (Xia et al., 2013; Mazzoli et al., 2015; Gayer et al., 2019), there are a few studies for the peripheral nerve regeneration (Mori et al., 2008).
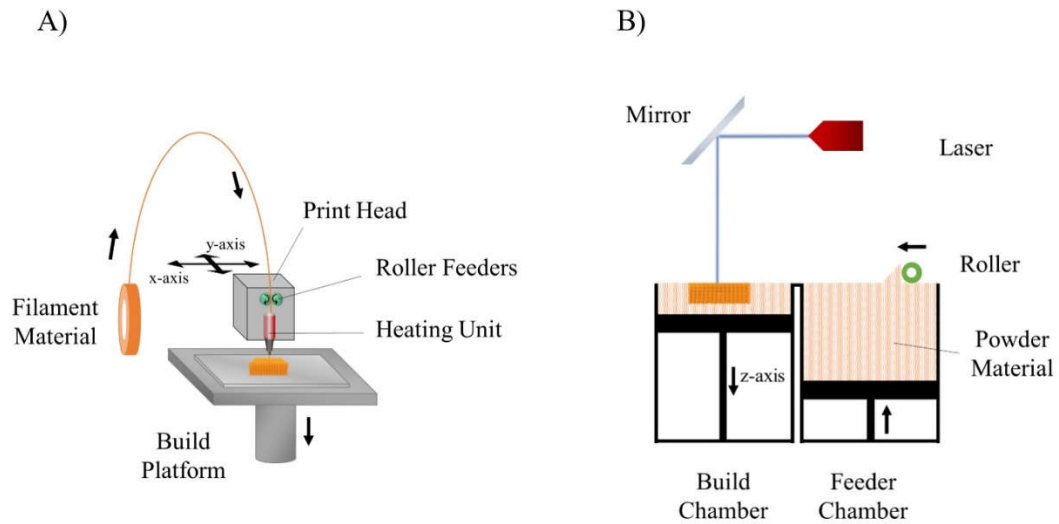
Figure 1.13. Schemes of A) fused deposition modeling (FDM) and B) selective laser sintering (SLS) techniques (Tamay et al., 2019).

1.3.2.2.3. Stereolithography (SLA)

In the stereolithography (SLA) method, UV light is irradiated on the photosensitive liquid resin surface in a precise pattern determined by CAD files (Skoog et al., 2014). The first layer of photopolymerized polymer adheres to a build platform. The platform is moved a defined step height for polymerization of the subsequent layer. This process is repeated until the 3D structure is formed. SLA can produce scaffolds with well-defined pore sizes, porosities, pore distributions, and pore interconnectivity (Gu et al., 2016). These scaffolds show similar structural and mechanical properties of the native tissue and permit cellular ingrowth and vascularization. Therefore, SLA is used in scaffold production for peripheral nerve tissue regeneration (Lee et al., 2017a; Zhu et al., 2017; Lee et al., 2018; Heo et al., 2019).

1.3.2.2.4. Solvent-Based Extrusion Freeforming (SEF)

Solvent-based extrusion freeforming (SEF) is one of the most commonly used additive manufacturing (AM) technique without material melting (Vaezi et al., 2018). Phase change is based on solvent evaporation in the SEF process. It has three main steps; preparation of bioceramic paste, 3D printing of the paste, and drying, debinding, and sintering of the 3D printed scaffold. Different types of bioceramic scaffolds have been produced using the SEF method with various compositions (different HA/β-TCP ratios) and sintered from 1100 to 1300 °C (Yang et al., 2008). Therefore, the SEF process is mainly used for the fabrication of scaffolds for bone tissue engineering (Srivas et al., 2017; Thomas et al., 2017).

1.3.2.2.5. Bioprinting

Bioprinting uses a computer controlled 3D printing device to deposit cells accurately and in precise geometries with the goal being the creation of anatomically correct structures. Computer design of the target structure is used to guide the placement of specific types of cells in precise locations that mimic the actual tissue. 3D printing and bioprinting are promising technologies to fabricate nerve conduits which closely resembles the features of the native peripheral nerve (Dixon et al., 2018). They offer the advantage of rapidly producing composite peripheral nerve matrices from micron-scaled units, using an assortment of synthetic and biological materials. 3D printing technologies allow researchers to change designs or to produce more complex nerve guides which mimic the original shape of the nerve to be replaced (Petcu et al., 2018). Many of the recent studies have focused on the production of a bioprinted nerve guide with improved properties to enhance peripheral nerve regeneration (Owens et al., 2013a; Gu et al., 2016; England et al., 2017; Dixon et al., 2018; Naghieh et al., 2019).

1.3.3. Materials in Nerve Guides for Peripheral Nerve Tissue Engineering

Both natural polymers such as gelatin, silk fibroin, chitosan and synthetic polymers such as poly(L-lactic acid) (PLLA), polycaprolactone (PCL), poly(hydroxybutyric

acid) (PHB) are used in nerve tissue engineering applications to improve surface properties, physicochemical characteristics and biological activity of the corresponding scaffolds (Goonoo et al., 2017). Natural and synthetic polymers used in the nerve conduit production are shown in Figure 1.14.
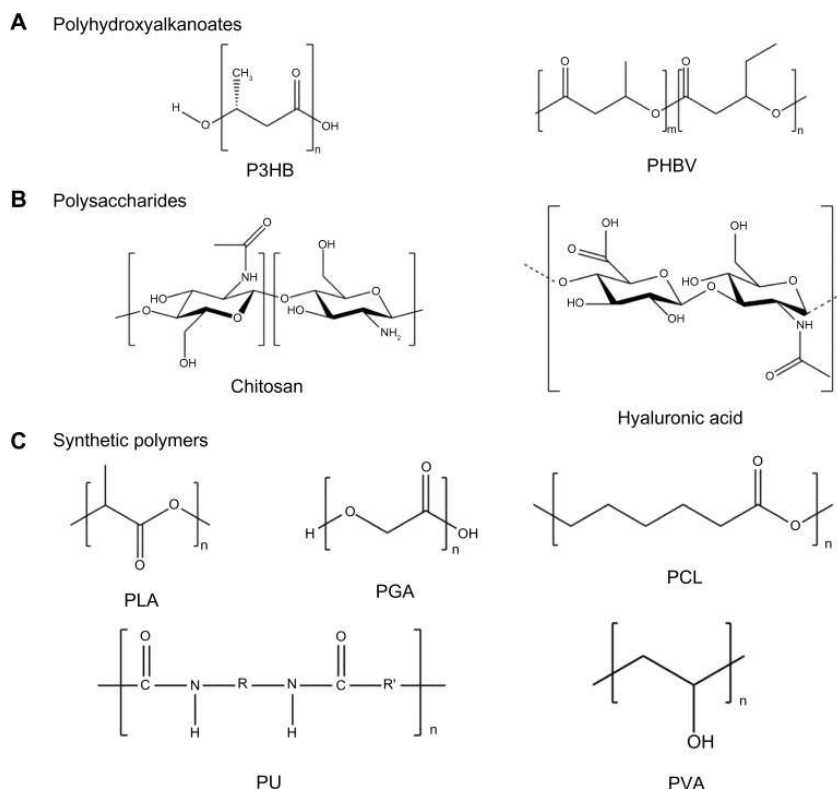
Figure 1.14. Natural and synthetic polymers used in the structure of nerve conduits (Arslantunali et al., 2014a).

1.3.3.1. Natural Polymers

Natural polymers are biocompatible, nontoxic, biodegradable, non-immunogenic, hydrophilic and do not provoke inflammatory responses in the host body (Sarker et al., 2018). The frequently used natural polymers in nerve guide or scaffold design in neural tissue engineering are collagen, gelatin, chitosan, chitin, elastin, alginate, and hyaluronic acid (HA).

1.3.3.1.1. Collagen

Collagen is one of the most studied biomolecules of the extracellular matrix (ECM) due to its presence in all connective tissue (Parenteau-Bareil et al., 2010). Collagen, a major constituent of skin and bone, represents approximately 25% of the total dry weight of mammals. 29 distinct collagen types have been characterized until now and all display a typical triple helix structure. Collagen types I, II, III, V, and XI are known to form collagen fibers (Dong, 2016). Collagen can be extracted and purified from a variety of sources such as rat tail and bovine. It has low immunogenicity, a porous structure, good permeability, biocompatibility, and biodegradability. However, the poor mechanical property of collagen scaffolds limits their applications. Collagen scaffolds can be crosslinked by chemical or physical methods or modified with natural/synthetic polymers or inorganic materials to improve its mechanical properties. Moreover, biochemical factors can be incorporated into the scaffold to enhance its biological activity. Collagen-based biomaterials have been extensively used for the production of nerve guides (Toba et al., 2001; Keilhoff et al., 2003; Alluin et al., 2009; Kemp et al., 2009; Bozkurt et al., 2016; Saltzman et al., 2018).

1.3.3.1.2. Gelatin

Among the natural polymers, gelatin can be obtained by denaturing collagen. It has almost identical composition and biological properties as those of the parent collagen (Meng et al., 2008). Therefore, much attention has been focused on the use of gelatin as a nerve tissue engineering material due to its low cost (Chen et al., 2005; Chen et al., 2006; Chang et al., 2007; Liu, 2008; Chang et al., 2009; Yang et al., 2010; Ko et al., 2017; Liu et al., 2018; Salehi et al., 2019). Gelatin is used for the production of nanoparticles, microparticles, 3D scaffolds, electrospun nanofibers and *in situ* gelling formulations (Echave et al., 2017).

1.3.3.1.3. Elastin

Elastin is a vital extracellular matrix (ECM) protein which is critical to the elasticity and resilience of many vertebrate tissues such as large arteries, lung, ligament, tendon, skin, and elastic cartilage (Mithieux and Weiss, 2005). Persistence and insolubility of elastin prevent to produce functional biomaterials in the beginning. However, the adapted use of solubilized elastin, elastin-based peptides and the increasing availability of recombinant forms of the natural soluble elastin precursor, tropoelastin make it possible to fabricate elastin-based biomaterials (Almine et al., 2010). Elastin and tropoelastin have been used as biomaterials in the structure of the nerve guides (Hsueh et al., 2014; Kakinoki et al., 2014; White et al., 2015).

1.3.3.1.4. Poly(3-hydroxybutyric acid) (P3HB)

Poly(3-hydroxybutyrate) (P3HB) is one of the most studied microbial biopolymers from the polyhydroxyalkanoates (PHAs) family (Alves et al., 2017). It is biodegradable and biocompatible. P3HB can be processed as a thermoplastic because it resists a wide temperature range (from 30 °C to 120 °C). P3HB is nontoxic, and its degradation product 3-hydroxybutyric acid is a normal constituent of human blood even at high concentrations, however, it is reported that it binds to HCA_2 receptors and might have some effects in addition to decrease in local pH (Asrar and Hill, 2002). Therefore, it can be used in bone (Coskun et al., 2005; Bakhtiyari et al., 2016; Toloue et al., 2019), nerve (Hinüber et al., 2014; Lizarraga-Valderrama et al., 2015; Lizarraga-Valderrama et al., 2019), and skin (Vigneswari et al., 2016; Volova et al., 2019) tissue engineering applications.

1.3.3.1.5. Poly(3-hydroxybutyrate-co-3-hydroxyvalerate) (PHBV)

Poly(3-hydroxybutyrate-co-3-hydroxyvalerate) (PHBV) is produced by the insertion of 3-hydroxyvalerate (HV) units into the PHB biopolymer. PHBV is an aliphatic polyester, and its chemical structure is shown in Figure 1.14A. It is a microbial biopolymer with excellent biocompatible and biodegradable properties (Rivera-Briso

and Serrano-Aroca, 2018). Its absorption capacity, biological origin, low cytotoxicity, piezoelectricity, and thermoplasticity make it a very promising biomaterial for a variety of applications. In the tissue engineering field, PHBV is used for the fabrication of the porous scaffolds which treat bone defects (Alagoz et al., 2018; Kouhi et al., 2019), and nerve injuries (Prabhakaran et al., 2013; Demirbilek et al., 2015; Hu et al., 2017; Dursun Usal et al., 2018).

1.3.3.1.6. Chitin and Chitosan

Chitin, a linear polysaccharide composed of (1-4)-linked 2-acetamido-2-deoxy-β-D-glucopyranose units, is the second prevalent form of polymerized carbon in nature after starch (Zargar et al., 2015). Chitosan is a natural polymer derived from chitin. Chitin and chitosan are used in the delivery of therapeutic agents, tissue engineering, and wound healing due to their biocompatibility and biodegradability (Marpu and Benton, 2018). Both of these polysaccharides are utilized in the production of nerve guides to provide peripheral nerve regeneration (Ao et al., 2011; Gu et al., 2012; Ruini et al., 2016; Jiang et al., 2019).

1.3.3.1.7. Hyaluronic Acid (HA)

Hyaluronic acid (HA) is a non-sulfated glycosaminoglycan which is composed of repeating polymeric disaccharides of D-glucuronic acid and *N*-acetyl-D-glucosamine linked via glycoside bond in the arrangement of alternating β-(1 → 4) and β-(1 → 3) bonds (Figure 1.14B) (Bukhari et al., 2018). HA plays important roles in skin repairment, wound healing, and tissue regeneration. Hyaluronic acid is a naturally occurring biopolymer and found in most connective tissues (Necas et al., 2008). It is synthesized by hyaluronan synthases and degraded by hyaluronidases. Hyaluronic acid based scaffolds have been used for soft tissue regeneration such as nerve (Agenor et al., 2017; Runxin Li et al., 2018), skin (Monteiro et al., 2015; Eke et al., 2017; Yang et al., 2019), and cornea (Lai et al., 2015; Fiorica et al., 2017; Xu et al., 2018).

1.3.3.1.8. Other Natural Polymers

There are also other biopolymers such as silk fibroin (SF), fibronectin, and keratin used in the fabrication of nervous scaffolds. SF has mechanical stability, slow degradation rate, biocompatibility (Teuschl et al., 2015). Therefore, silk fibroin is able to support peripheral nerve regeneration, and used as a biomaterial for the production of nerve guidance conduits (Dinis et al., 2015; Xu et al., 2016; Farokhi et al., 2017; Ebrahimi et al., 2018; Afjeh-Dana et al., 2019; Zhang et al., 2019). Another biopolymer fibronectin has a significant role in modulating Schwann cell migration and neurite outgrowth (Mukhatyar et al., 2011). Thus, it has been used as the nerve guide material in some studies (Ahmed et al., 2003; Ding et al., 2011; Mottaghitalab et al., 2013). Keratin is a fibrous protein which forms protective tissues such as hair, fur, feathers, nails, and hooves. Keratin extracted from human hair has been prepared as hydrogels, and used as nerve guide fillers (Lin et al., 2012; Pace et al., 2013).

1.3.3.2. Synthetic Polymers

Some widely used synthetic polymers for the fabrication of nervous scaffolds include biodegradable polyesters poly(lactic acid) (PLA), poly(glycolic acid) (PGA), poly(lactic acid-co-glycolic acid) (PLGA), poly(ε-caprolactone) (PCL), polyurethanes (PUs), poly(D,L-lactide-co-ε-caprolactone), and nonbiodegradable polymers such as polyvinyl alcohol (PVA), methacrylate-based hydrogels, polystyrene, silicone, and poly(tetrafluoroethylene). Conductive polymers such as polypyrrole (PPy) and polyaniline (PANI) are also gaining popularity in nerve tissue engineering by their ability to conduct electrical signals (Sensharma et al., 2017).

1.3.3.2.1. Poly(lactic acid) (PLA)

Poly(lactic acid) (PLA) is a linear aliphatic polyester derived from renewable resources such as corn, sugar, potato, and other agricultural products (Kuang et al., 2016). Water and carbon dioxide are the degradation products of PLA and do not cause any harm to the body. Therefore, PLA is more commonly used in the biomedical field

among other synthetic polymers due to its biocompatibility, absorbability, and degradation behavior (Sha et al., 2016). There are three different kinds of PLA, poly(D-lactic acid) (PDLA), poly(L-lactic acid) (PLLA), and the racemic blend D,L-PLA (PDLLA), based on their microstructures. PLA based scaffolds are used in nerve tissue engineering in the form of film (Goulart et al., 2016; Pestana et al., 2018), and fibers (Zhou et al., 2016; Naseri-Nosar et al., 2017; Martin et al., 2019).

1.3.3.2.2. Poly(glycolic acid) (PGA)

Poly(glycolic acid) (PGA) is produced by the carbonylation of formaldehyde in the presence of sulfuric acid (Storti and Lattuada, 2017). Its chemical structure is shown in Figure 1.14C. It is a biodegradable, rigid, thermoplastic, and highly crystalline polyester which has 30% ultimate strain (Manavitehrani et al., 2016). PGA has been commonly combined with collagen (Suzuki et al., 2016; Tsujimoto et al., 2017; Oatari et al., 2018; Shimizu et al., 2018) for the fabrication of the nerve guides.

1.3.3.2.3. Poly(lactic acid-co-glycolic acid) (PLGA)

PLGA is a linear copolymer which can be prepared by using different ratios of its constituent monomers, lactic (LA) and glycolic acid (GA) (Gentile et al., 2014). It can also be obtained from lactide monomer and polyglycolic acid (PGA) by ring-opening polymerization. PLGA can be dissolved in chlorinated solvents, tetrahydrofuran, acetone or ethyl acetate unlike pure polylactic and polyglycolic acid. Its tailored biodegradation rate, biocompatibility, and FDA approval for clinical use make PLGA a promising material in the tissue engineering applications. Therefore, PLGA has been utilized in the production of nerve guides to enhance peripheral nerve regeneration (Wang et al., 2015; Li et al., 2016; Zhan et al., 2016; Li and Wang, 2017; Rao et al., 2017; Nakamura et al., 2017; Wang et al., 2018).

1.3.3.2.4. Poly(ε-caprolactone) (PCL)

Polycaprolactone (PCL) is synthesized by ring opening polymerization of ε-caprolactone and its structure is shown in Figure 1.14C. Its degradation takes several

months to several years and depends on the molecular weight, degree of crystallinity, and degradation conditions (Labet and Thielemans, 2009). PCL can be used as both hard tissue and soft tissue compatible material in tissue engineering applications due to its adaptability to different production strategies (Mondal et al., 2016). Therefore, it has been used in many different studies to produce nerve tissue engineering scaffolds (Jang et al., 2016; Panahi-Joo et al., 2016; Pan et al., 2018; Passipieri et al., 2019; Sun et al., 2019).

1.3.3.2.5. Polyurethane (PU)

Polyurethane (PU) contains repeating urethane groups in its structure (Figure 1.14C). Polyurethanes have been widely used in the preparation of all kinds of medical devices due to its excellent mechanical properties and biocompatibility (Wang and Wang, 2012). Many scientists are involved in research on optimization of the properties PU for specific applications. Biodegradable polyurethanes (PU), consisting of soft and hard segments, are suitable candidate for nerve tissue engineering due to its flexibility and other mechanical properties (Houshyar et al., 2019). *In situ* extrusion, dip coating, and solvent casting are the main fabrication techniques for PU. Polyurethane based biomaterials were also used with Schwann cells to enhance peripheral nerve regeneration (Wu et al., 2016; Salehi et al., 2018; Wu et al., 2018; Salehi et al., 2019).

1.3.3.2.6. Poly(vinyl alcohol) (PVA)

Poly(vinyl alcohol) (PVA) can be prepared by the hydrolysis of polyvinylacetate (Ben Halima, 2016). It is a water soluble and biodegradable synthetic polymer. PVA is an ideal material for tissue engineering because it is biocompatible, highly hydrophilic and easily processable (Aslam et al., 2018). It can be modified chemically through the use of hydroxyl groups. PVA has been used in fibrous (Naghavi Alhosseini et al., 2015; Ghasemi Hamidabadi et al., 2017) or oxidized (Stocco et al., 2018; Porzionato et al., 2019) forms to produce nerve conduits.

1.3.3.2.7. Polypyrrole (PPy)

Polypyrrole (PPy), a conductive polymer, is synthesized by oxidative polymerization of pyrrole monomer in aqueous solution for 4 h at room temperature (Yussuf et al., 2018). It is a polycationic electrical conductor which is able to incorporate anionic biomolecules (dopants) to improve biocompatibility (Houshyar et al., 2019). Doping of PPy with polymeric or biologically active anions and buffer salts has been studied to make the PPy more attractive for tissue engineering applications due to its conductivity, antigenicity, and nontoxicity. PPy based nerve guides have been fabricated to promote peripheral nerve regeneration under electrical stimulation (Zhou et al., 2016; Jing et al., 2018; Su et al., 2019; Xu et al., 2019).

1.3.3.2.8. Polyaniline (PANI)

Polyaniline (PANI) is composed of the repeating units of the aniline monomer. The nitrogen atom in the phenyl rings allows the formation of different oxidation states (Abd Razak et al., 2015). Its ease of synthesis, the feasibility of electrical conductivity control, and the low cost of the aniline monomer make it an attractive conducting polymer for tissue engineering applications. Electrical stimulation is commonly used to enhance functional recovery of the muscle and nerve tissue (Anderson et al., 2015). PANI has been widely used to produce conductive nerve guides which show enhanced nerve tissue regeneration under electrical stimulation (Xu et al., 2016; Das et al., 2017; Abasi et al., 2019; Shrestha et al., 2019; Wang et al., 2019; Zheng et al., 2019).

1.3.4. Neurotrophic Factors Used in Peripheral Nerve Tissue Engineering

Neurotrophic factors are released endogenously by peripheral nerve tissues following lesions. Therefore, these molecules are used to improve peripheral nerve regeneration (Belanger et al., 2016). The most common compounds are nerve growth factor (NGF), brain-derived neurotrophic factor (BDNF), and glial cell-line derived neurotrophic factor (GDNF). These growth factors we loaded into the NG by physical and chemical bonds and explored frequently (Figure 1.15).
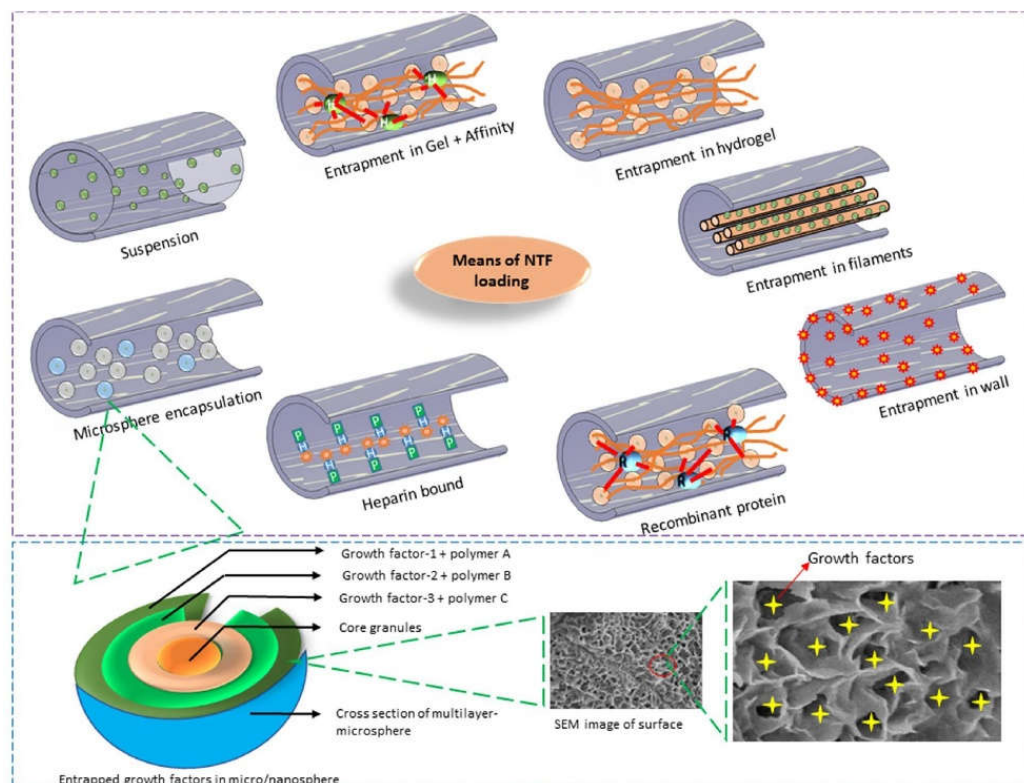
Figure 1.15. Various approaches to incorporate nerve growth factor in the nerve guidance conduits. (Sarker et al., 2018) 2018 Elsevier Ltd.

1.3.4.1. Nerve Growth Factor (NGF)

Nerve growth factor (NGF) is the first discovered (1956) and best characterized neurotrophic factor (Aloe et al., 2015). It plays a protective role in the development and survival of sympathetic, sensory and forebrain cholinergic neurons. NGF promotes neurite outgrowth both *in vivo* and *in vitro* and nerve cell recovery after injuries. Therefore, NGF has been commonly incorporated into the nerve guide structure to promote nerve regeneration at the injured site (Xu et al., 2003; Madduri et al., 2010; Xu et al., 2011; Yan et al., 2012; Zhang et al., 2017; Labroo et al., 2017; Allbright et al., 2018; Wood et al., 2018). 50 ng/mL NGF is used for the differentiation of PC12 cells *in vitro* (Hu et al., 2018).

1.3.4.2. Brain-derived Neurotrophic Factor (BDNF)

Brain-derived neurotrophic factor (BDNF) has an important role in neuronal survival, differentiation, and synapse formation during development and throughout adulthood (Garraway and Huie, 2016). It promotes motor neuron survival and supports axonal growth of motor and sensory neurons. Endogenous BDNF is required for peripheral nerve regeneration and remyelination after a nerve injury (Zhang et al., 2000). BDNF was loaded into the nerve guide structure to enhance nerve regeneration (Wang et al., 2016; Obermeyer et al., 2019). It has also been showed that BDNF could be regulated endogenously by a microRNA molecule (Yi et al., 2016).

1.3.4.3. Glial Cell Line-derived Neurotrophic Factor (GDNF)

Glial cell line-derived neurotrophic factor (GDNF) is a potent survival factor for midbrain dopaminergic neurons and many other types of neuronal populations (Gu et al., 2015). Local delivery of glial cell line-derived neurotrophic factor (GDNF) has been found to improve peripheral nerve regeneration at damage sites (Liu et al., 2018). Therefore, the release of GDNF from nerve guides has been studied to promote peripheral nerve regeneration at the injury site (Bliley et al., 2015; Hsu et al., 2017; Sarhane et al., 2019). GDNF has been combined with chondroitinase ABC to foster axonal regeneration to repair peripheral nerve gaps (Sivak et al., 2017).

1.3.4.4. Other Neurotrophic Factors

Some other neurotrophic factors such as neurotrophin-3, ciliary neurotrophic factor (CNTF), fibroblast growth factor (FGF) and granulocyte colony-stimulating factor (G-CSF) are also used to promote peripheral nerve regeneration. Neurotrophin-3 (NT-3) is the third neurotrophic factor in the family of neurotrophins. NT-3 supports the survival and differentiation of existing neurons. It also promotes the growth and differentiation of new neurons and synapses (Rangasamy et al., 2010). NT-3 (Bloch et al., 2001; Francis et al., 2017), CNTF (Lu et al., 2015; Barbon et al., 2016; Yin et

al., 2016), and FGF (Fujimaki et al., 2017; Lu et al., 2019) has been utilized to promote peripheral nerve regeneration. Granulocyte colony-stimulating factor (G-CSF) can inhibit inflammation and apoptosis (Jia et al., 2019). This provides a suitable microenvironment for axonal regeneration.

1.4. Approach, Aim, and Novelty of the Study

The aim of this study was to contruct a tubular nerve guide with inner guidance elements to create a microenvironment appropriate for peripheral nerve regeneration and then test the guide *in vitro* and *in vivo* for functionality. The construct consisted of an exterior tube and the interior guidance elements. The tube was made of polycaprolactone (PCL) and was manufactured using the fused deposition modeling (FDM) of additive manufacturing approach. The inner part of the nerve guide consisted of aligned electrospun fibers made of gelatin-PHBV5 to achieve the alignment of PC12 cells along the nerve guide when the system was tested *in vitro*. A laser-based microstereolithography setup was reported to be used in the fabrication of a guidance conduit using a photocurable liquid prepolymer based on poly(ethylene glycol) (PEG) (Haycock et al., 2015). However, this nerve guide is not biodegradable. Until now no 3D printed biodegradable nerve guide that acted as a substrate for cell migration and proliferation and actively promotes regeneration was developed for peripheral nerve injury purposes. The main novelty is in the materials (PCL, gelatin and PHBV) due to their degradability. When testing in *in vitro*, the gelatin fibers are expected to increase the cell attachment and proliferation at the site of injury because gelatin has cell attractive properties. The combination of these factors makes the nerve guidance tube a novel tool to be used in the treatment of peripheral nerve injuries. PC12 cells were only used in *in vitro* studies, and seeded on the inner gelatin-PHBV aligned fibrous mats to mimic the regeneration of the injured nerve tissue. However, Schwann cells were used in both *in vitro* and *in vivo* studies. Presence of Schwann cells on the exterior 3D printed PCL tube mimics normal nerve tissue to provide the necessary factors for differentiation of the PC12 into neurons. Moreover, these nerve guides were tested in a rat sciatic nerve injury to assess their efficiency. The

combination of these ingredients and processes allows us to produce a novel nerve guidance tube to be used in the treatment of peripheral nerve injuries.

CHAPTER 2

MATERIALS AND METHODS

2.1. Materials

Hydroxyethyl methacrylate (HEMA) monomer, ethylene glycol dimethacrylate (EGDMA), poly(3-hydroxybutyrate-*co*-3-hydroxyvalerate) (PHBV5) (with 5% HV), gelatin from porcine skin, methacrylic anhydride, chloroform, 1,1,1,3,3,3-hexafluoroisopropanol (HFIP), collagen type I, paraformaldehyde (37%), N,N,N′,N′-Tetramethylethane-1,2-diamine (TEMED), FITC-labeled phalloidin, 4,6-diamidino-2-phenylindole dihydrochloride (DAPI), NGF-β from rat, mouse anti-human collagen Type I, and Alexa Fluor 532-conjugated anti-mouse Ig antibody were purchased from Sigma (USA and Germany).

Sodium dihydrogen phosphate (NaH_2PO_4), disodium hydrogen phosphate (Na_2HPO_4), sodium chloride (NaCl), ethanol, acetic acid (HAc), acetone, 1,4-dioxane, and Tween-20 were purchased from Merck Millipore (Germany). DMEM-High glucose, DMEM-High glucose colorless, fetal bovine serum (FBS), trypsin-EDTA (0.25%) (HyClone), and SnakeSkin pleated dialysis tubing were purchased from Thermo Scientific (USA).

Alamar Blue was purchased from Invitrogen Inc. (USA). Newborn calf serum was from Lonza (Sweden). NucleoCasette was obtained from ChemoMetec (Denmark). Penicillin/streptomycin (Pen/Strep) (100 units/mL - 100 μg/mL), and bovine serum albumin (BSA) were purchased from Fluka (Switzerland). Ammonium persulfate (APS), dimethyl sulfoxide (DMSO) and Triton-X 100 were obtained from AppliChem (Germany). Anti-neuron specific beta-III tubulin antibody, anti-myelin basic protein, anti-NeuN, Donkey anti-Rabbit IgG H&L (DyLight®488) secondary antibody were purchased from Abcam (USA).

2.2. Methods

2.2.1. Synthesis of Methacrylated Gelatin (GelMA)

Methacrylated gelatin was synthesized according to protocol adapted from literature (Nichol et al., 2010). Type A porcine skin gelatin (100 bloom, Sigma, USA) was dissolved in PBS to form a 10% (w/v) solution at 60 °C and stirred until completely dissolved. Methacrylic anhydride (MA) (94%, Sigma, USA) was added into this solution to obtain 20% (v/v) solution (Figure 2.1). After 1 h reaction at 50 °C, it was diluted 5 times with warm (40°C) PBS and the resulted solution was dialyzed in a dialysis tubing (CO 10,000) against distilled water for 1 week at 40 °C to remove excess methacrylic acid and salts and then lyophilized for 1 week until a white foam was obtained. It was stored at +4 °C until further use.
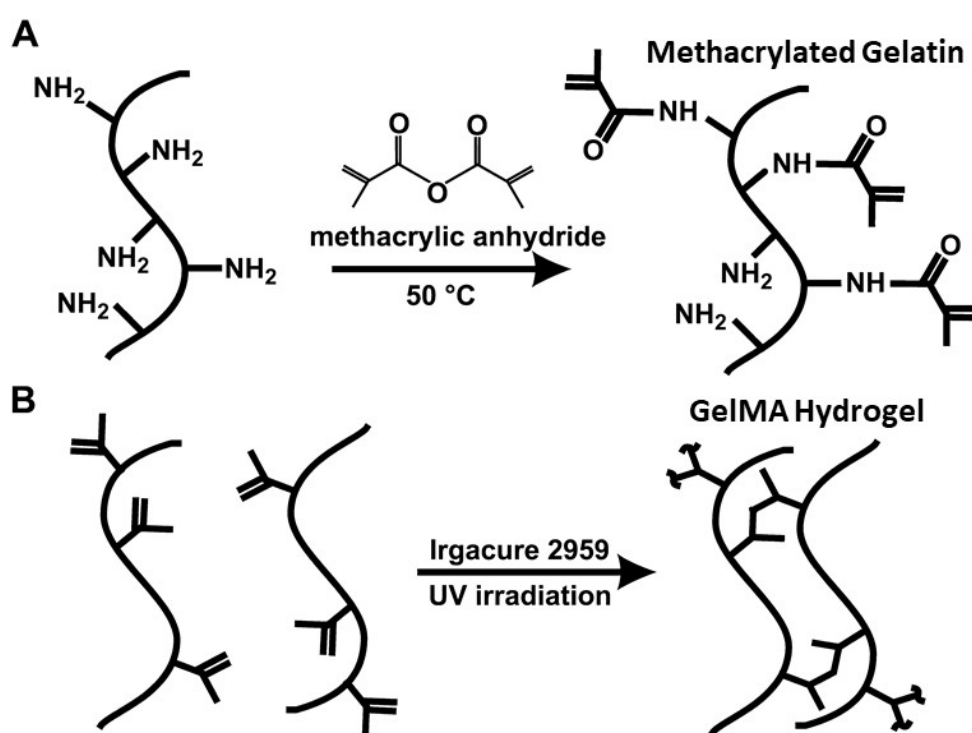
Figure 2.1. Methacrylation of gelatin. A) Methacrylation of gelatin with methacrylic anhydride, B) Crosslinking of GelMA with UV. (Nichol et al., 2010) 2010 Elsevier Ltd.

2.2.1.1. Determination of Methacrylic Acid Content of GelMA with NMR

Methacrylation of gelatin was verified using H^1 NMR. Gelatin and GelMA polymers were dissolved in D_2O at 30 mg/mL at 40 ºC. ^1H NMR spectra were obtained at room temperature on a Bruker DPX 400 spectrometer operating at a ^1H resonance frequency of 400 MHz, and sixteen scans were acquired for signal-to-noise averaging.

2.2.2. Preparation of GelMA-pHEMA Hydrogels

GelMA (15%, w/v) was dissolved in PBS in the presence of photoinitiator (2-(hydroxyl)-4-(2-hydroxyethoxy)-2-methylpropiophenone) (Sigma, USA) (0.5%, w/v). This solution was poured into a PDMS template and placed in the UV cabin (BIO-LINKTM UV Crosslinker DLX-365, Germany) and crosslinked with UV for 1 min. The final product had pHEMA in various proportions (9:1, 8:2, 7:3, 6:4, 5:5, v/v) to obtain an optimum hydrogel formation.

2.2.3. Characterization of GelMA-pHEMA Hydrogels

2.2.3.1. FTIR Analysis

The hydrogel surfaces were analyzed with FTIR-ATR spectroscopy (Perkin Elmer Spectrum, Frontier, Massachusetts, USA) to show the methacrylation of the gelatin and the homogeneity of the GelMA-pHEMA blends. All samples were scanned 4 times in the range 400-4000 cm^{-1} with a resolution of 4 cm^{-1}.

2.2.3.2. SEM and ImageJ Analysis

Scaffolds were coated with gold-palladium (Au-Pd) under vacuum and examined with SEM (Quanta 400F Field Emission SEM, Netherlands). Surface and the cross-section porosity and pore size of GelMA-pHEMA hydrogels were determined with ImageJ (NIH, USA) analysis.

2.2.3.3. Water Content (WC) Determination

The swelling behavior of the hydrogels was studied by measuring the changes in their weights and diameters. Samples were incubated at 37 °C for 12 h in a water bath, wiped with filter paper to remove the excess water and weighed. Diameters were also measured. Water content was calculated according to the following equation:

$$WC\ (\%) = ((W_w - W_d)/W_w)\ x100 \tag{1}$$

where WC (%) is water content (%, w/w), W_w is the weight of wet samples, and W_d is the weight of dry samples.

2.2.3.4. Degradation of Hydrogels

Scaffolds were weighed to a sensitivity of 0.1 mg and incubated in PBS (10 mM, pH 7.4) at 37 °C for 4 weeks to study the degradation behavior in PBS. The samples were removed from PBS, rinsed with distilled water 3 times, lyophilized and weighed. Weight loss was determined weekly for 4 weeks (n=3). The extent of degradation was determined gravimetrically as the percent weight loss according to the following equation:

$$Remaining\ weight\ (\%) = ((W_0 - W_d)/W_d)\ x\ 100 \tag{2}$$

where W_o is the original dry weight and W_d is the dry weight after incubation.

2.2.3.5. Mechanical Tests

Tensile mechanical tests were conducted on a Shimadzu AGS-X Universal Testing Machine (Japan) at a displacement rate of 2 mm/min at RT. The pHEMA and GelMA-pHEMA hydrogels were brought to equilibrium swelling in distilled water (24 h, RT) and rectangular test samples (30 mm x 10 mm) were cut and tensile modulus of the scaffolds was calculated. Compression tests were conducted on a Univert, CellScale mechanical test system (Canada) at a displacement rate of 1 mm/min in the vertical direction and compressive modulus of the scaffolds was calculated. Stress (σ), strain

(ε), tensile and compressive modulus of the samples were calculated as in equations (3), (4), and (5).

$$\text{Stress } (\sigma) = F/A \tag{3}$$

$$\text{Strain } (\varepsilon) = \Delta l/l \tag{4}$$

$$\text{Tensile/Compressive modulus} = \sigma/\varepsilon \tag{5}$$

where F is the applied force, A is the cross-sectional area, l is the initial sample length, and Δl is the displacement.

2.2.4. Preparation of Gelatin-PHBV Fiber Mats

Gelatin-PHBV5 solutions (5, 10, 15, %, w/v) were prepared in hexafluoroisopropanol (HFIP) and transferred into a syringe. The positive pole of the power supply was connected to the metal syringe tip, and the negative pole was connected to the collector. In order to obtain aligned fibers, a rectangular plate with parallel grids was used as the collector as was previously described (Yucel et al., 2010). 11 kV potential was applied. Distance between the syringe needle and the collector was 11 cm, and the flow rate was 4 µL/min. Three different polymer concentrations were used to achieve a very high degree of alignment (Table 2.1).

Table 2.1. *Conditions for electrospinning of Gelatin-PHBV5 polymer solutions in HFIP.*

Potential (kV)	Distance (cm)	Flow rate (µL/min)	Concentration (%, w/v)
11	11	4	5
11	11	4	10
11	11	4	15

2.2.4.1. SEM

Fiber diameters of gelatin-PHBV fibers were determined by using scanning electron microscopy (Quanta FEI, United States). Scaffolds were coated with gold and examined under SEM.

2.2.4.2. Degradation of Electrospun Fibrous Mats

In order to study the degradation behavior of the mats, they were weighed to a sensitivity of 0.1 mg and incubated in distilled water at 37 °C for 4 weeks. Weekly, the samples were removed from the water, lyophilized and weighed. Weight loss was determined for 4 weeks. The degradation rate was determined gravimetrically as the percent weight loss according to the following equation:

$$\text{Remaining weight (\%)} = ((W_0 - W_t)/W_t) \times 100 \tag{6}$$

where W_o is the original (dry) weight and W_t is the dry weight after incubation at time t.

2.2.5. Incorporation of the Inner Elements into the Nerve Guide

Aligned gelatin-PHBV5 fibers were produced as 2Ds mat by electrospinning. In order to introduce them into the 3D printed PCL tube, the fibrous mats were rolled into a tube (Figure 2.2).
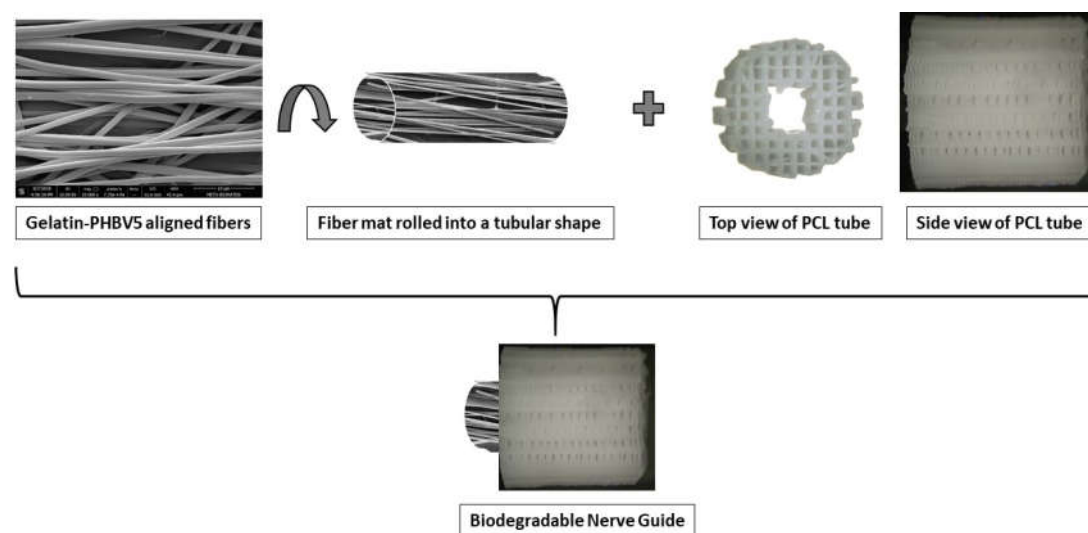
Figure 2.2. Production of a biodegradable nerve guide.

2.2.6. 3D Printing of PCL Tube

A hollow cylindrical nerve guide model (10 mm width x 10 mm height) was drawn with SketchUp 3D modeling program (Trimble Inc., USA) and it was converted to STereoLithography (.STL) files with CURA (3D printing slicing software) to make them printable with the Bioscaffolder® (SYS+ENG, Germany). Polycaprolactone (MW 50,000 daltons, Polysciences Inc., USA) was printed at 130 °C on the cold table (4 °C) at 20 °C room temperature with a 1 mm strand distance. Velocity in xy and z-directions (F_{xy}, F_z) is 300 mm/s.

2.2.6.1. SEM of 3D printed PCL Tube

Fiber diameters of PCL tubes were measured by using scanning electron microscopy (SEM) (Quanta FEI, United States). Scaffolds were coated with gold before examining under SEM.

2.2.6.2. Micro CT (µCT)

Microcomputed tomography (µCT) is an X-ray based imaging technique. In µCT, X-rays emitted from an X-ray generator travel through a sample, and are recorded by a detector on the other side to produce a radiograph. The sample is then rotated by a fraction of a degree and another projection image is obtained. This procedure is repeated until the sample is scanned throughout 360 degrees and a 3D image is obtained. In this study, micro CT studies were carried out to record and study the porous structure and the distribution of pores in the 3D printed PCL tube. Conditions applied were 10 µm/Pixel, 59 kV voltage and without any filter.

2.2.6.3. Water Contact Angle

The contact angle is a measure of surface free energy and as a result wettability of biomaterials *in situ*. It is important for cell attachment and growth for any scaffold because it influences protein adsorption and cell adhesion (Menzies and Jones, 2010). The water contact angle of the PCL tubes was determined with contact angle goniometer One Attension (Biolin Scientific, Finland). Distilled water (5 µL) was

placed at 5 different locations on the scaffolds, contact angles were measured and averaged. Contact angle θ was found according to Young's equation (Equation 7):

$$\sigma_{sg} = \sigma_{sl} + \sigma_{lg} \cdot \cos\theta \qquad (7)$$

where σ_{lg} is the surface tension of the liquid, σ_{sl} is the interfacial tension between liquid and solid and the surface free energy σ_{sg} of the solid (Figure 2.3).
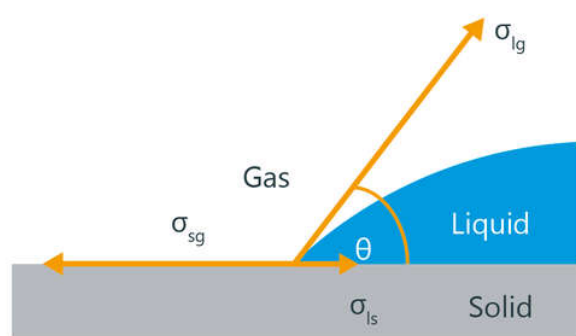
Figure 2.3. Schematic diagram of the components of a three-phase system.

2.2.6.4. Mechanical Test

It is important for a nerve conduit to have sufficient mechanical properties, especially tensile strength and toughness, to withstand the forces *in vivo* and to protect the regenerating nerve tissue (Borschel et al., 2003). All tensile tests were conducted using a Shimadzu AGS-X Universal Testing Machine (Japan). The thickness of rectangular PCL test samples (30 mm x 10 mm) was measured with a micrometer (Erste Qualited, Germany) with a sensitivity of 10 μm. Tensile properties were determined in dry state at room temperature (n=6). In order to prevent slippage, the ends of the samples were stabilized with clamps, with a gauge length of 10 mm. The crosshead speed of the load cells was 2 mm/min. Stress (σ), strain (ε), and ultimate tensile strength (UTS) of the samples were calculated according to equations (3) and (4) as stated in 2.2.3.5.

2.2.7. *In Vitro* Studies

2.2.7.1. *In Vitro* Studies with GelMA and pHEMA Hydrogels

In vitro studies were carried out to assess the cytocompatibility of the hydrogels with the Schwann cells (SCs) (SW 10, ATCC CRL-2766). These hydrogels are served as the exterior part of the nerve guide.

2.2.7.1.1. Schwann Cell Seeding on GelMA-pHEMA Hydrogels

Schwann cells (SCs) that served as the support cells for proliferating PC12 cells were seeded on the GelMA, GelMA-pHEMA (5:5), and pHEMA hydrogels. Cells were grown in DMEM high glucose tissue culture medium containing penicillin (100 U/mL), streptomycin (100 µg/mL), and 10% FBS. Aliquots of the cell suspension were seeded on scaffolds to achieve a cell density of 5×10^4 cells/scaffold. The cell-seeded hydrogels were incubated at 37 °C and 5% CO_2 for 2 h to allow for the attachment of the cells. Then, fresh medium was added, and incubation continued for three more weeks with the medium being refreshed every 2 days.

2.2.7.1.2. Determination of Cell Attachment and Proliferation

Alamar Blue cell viability assay was performed to determine cell attachment and proliferation on the hydrogels. Alamar Blue is a water soluble dye in its oxidized form and is reduced in the cytosol by mitochondrial enzyme activity upon accepting electrons from NADPH, FADH, and NADH (O'Brien et al., 2000). This redox reaction is accompanied by a color change of the culture medium from Indigo Blue (resazurin) to fluorescent pink (resorufin); the reduced state. The UV-Vis absorbances or fluorescence intensity was measured with a UV-Vis spectrophotometer at 570 and 595 nm. Reductions were calculated according to the protocol of the producer (Invitrogen Inc., USA) in Appendix B.

A calibration curve was constructed using known cell densities (SCs) to correlate the cell numbers with the extent of dye reduction (%) (shown in Appendix B).

2.2.7.1.3. Confocal Laser Scanning Microscopy (CLSM) Studies

At the end of the culture period, the growth media of the cell-seeded GelMA-pHEMA hydrogels and gelatin-PHBV mats were discarded, and cells fixed with 4% (w/v) paraformaldehyde at RT for 15 min. Cell membranes were permeabilized with Triton X-100 (1% v/v in PBS pH 7.4) at RT for 5 min. After washing, samples were incubated in BSA (1% w/v in PBS) at 37 °C for 30 min. The stain Alexa Fluor 488-Phalloidin (1:200 w/v, prepared in 0.1% BSA, w/v in PBS), was added to the samples and stored at RT for 1 h to stain the actin fibers of the cytoskeleton. After two washes with PBS, samples were incubated with DRAQ5 (Sigma, USA) for 30 min at RT to stain the cell nuclei. Samples were washed twice with PBS and stored in PBS solution until examination using a Confocal Laser Scanning Microscope (Leica, Germany).

2.2.7.2. *In Vitro* Studies with Gelatin-PHBV Fibrous Mats

2.2.7.2.1. PC12 Cell Seeding on Aligned Gelatin-PHBV Mats

PC12 cells (pheochromocytoma cells derived from the adrenal gland of Rattus norvegicus) (ATCC CRL-1721.Adh) were grown in Ham's F12 tissue culture medium containing penicillin (100 U/mL), streptomycin (100 μg/mL), 2.5% FBS, and 15% horse serum, 50 ng/mL NGF. Aliquots of the cell suspension were added on the scaffolds to create a cell density of 5×10^4 cells/scaffold. The cell-seeded mats were incubated at 37 °C and 5% CO_2 for 2 h to ensure attachment of the cells. Then, fresh medium was added onto the scaffolds, and incubation continued for three weeks.

2.2.7.2.2. Cytoskeleton and Nucleus Staining

Cell-material interactions were studied using both SCs and PC12 with confocal laser scanning microscopy (CLSM). Cells were fixed with 4% (w/v) paraformaldehyde (Sigma, USA) at room temperature (RT) for 15 min. Cell membrane was permeabilized by treating with Triton X-100 (1% v/v in PBS pH 7.4) for 5 min. Samples were incubated in BSA (1% w/v in PBS) at 37 °C for 30 min and then stained with Alexa Fluor 488-Phalloidin (Abcam, USA), (1:200 w/v, prepared in 0.1% BSA,

w/v in PBS) (1 h, RT). After two washes with PBS, the samples were incubated with DRAQ5 (Sigma, USA) (30 min, RT) to stain the cell nuclei red. Samples were washed and stored in PBS solution until examination with a CLSM (Leica, Germany).

2.2.7.2.3. Live-Dead Cell Viability Test

In order to study the viability of PC12 cells in the Gelatin-PHBV fiber mats. PC12 seeded mats were stained with Live-Dead assay dye mixture (250 µL) for 15 min at RT. Dye mixture was removed, mats washed with PBS, and scaffolds were examined with CLSM.

2.2.7.2.4. Beta-III Tubulin and NeuN Antibody Staining

PC12 cells on the aligned gelatin-PHBV mats were stained with beta-III tubulin and NeuN antibody to study their differentiation into neurons. The scaffolds were fixed as above, and were incubated in the blocking solution (1% BSA, 10% goat serum, 0.1% Tween 20 and 0.3 M glycine in PBS), and then anti-beta III tubulin and NeuN antibodies (1:100 and 1:20 dilution in 0.1% PBS/BSA solution, respectively) were added onto the specimens and incubated overnight at 4 °C. After washing with 0.1% PBS-BSA solution, they were incubated in both Alexa Fluor 488-labelled anti-mouse antibody produced in goat (1:100 dilution in 0.1% BSA-PBS) and Alexa Fluor 647-labelled anti-rabbit antibody produced in donkey (1:100 dilution in 0.1% BSA-PBS) at 37 °C for 1 h and washed with 0.1% PBS-BSA. Samples were examined with CLSM.

2.2.7.2.5. SEM of PC12 Cell Seeded Mats

PC12 cells on gelatin-PHBV fibrous mats were studied by using scanning electron microscopy (SEM). Mats were coated with gold before examining under SEM from the top (Quanta FEG 650, Quanta FEI, United States).

2.2.7.3. *In Vitro* Studies with 3D Printed PCL Tube

2.2.7.3.1. Schwann Cell Culture

Schwann cells (SCs) were seeded on the PCL tubes as support cells. SCs were grown in DMEM high glucose tissue culture medium containing penicillin (100 U/mL), streptomycin (100 µg/mL), and 10% FBS. Aliquots of the Schwann cell (SW10, ATCC CRL-2766) suspension were seeded on scaffolds to achieve a cell density of 5×10^4 cells/scaffold. The cell seeded scaffolds were incubated at 37 °C and 5% CO_2 for 2 h to allow for attachment of the cells. Then, fresh medium was added and incubation continued for four weeks with the medium being refreshed every 2 days.

2.2.7.3.2. Cell Attachment and Proliferation

Alamar Blue Cell Viability Assay was performed to quantify the cell attachment and proliferation on the PCL tubes. Reductions were calculated according to the protocol of the producer (Invitrogen Inc., USA, Appendix B).

2.2.7.3.3. CLSM

Surface properties of PCL tubes and their interactions with cells were studied with confocal laser scanning microscopy (CLSM). Cells were fixed with 4% (w/v) paraformaldehyde (Sigma, USA) (15 min, RT), and membranes were permeabilized with Triton X-100 (1% v/v in PBS pH 7.4) for 5 min. Samples were then incubated in BSA (1% w/v in PBS) at 37 °C for 30 min. Alexa Fluor 488-Phalloidin (Abcam, USA), (1:200 w/v, prepared in 0.1% BSA, w/v in PBS), was added directly onto the samples and stored at RT for 1 h to stain the actin fibers of the cytoskeleton. After washing with PBS, the samples were incubated with DRAQ5 (Sigma, USA) (30 min, RT) to stain the cell nuclei red. Samples were washed twice with PBS and stored in PBS solution until examination using a Confocal Laser Scanning Microscope (Leica, Germany).

2.2.7.3.4. Myelin Basic Protein (MBP) Antibody Staining

Schwann cells were stained with myelin basic protein (MBP) to study its expression level on the PCL tubes. The scaffolds were fixed with 4% paraformaldehyde for 15 min. Then they were incubated in the blocking solution (1% BSA, 10% goat serum, 0.1% Tween 20 and 0.3 M glycine in PBS). Anti-Myelin Basic Protein antibody (1:20 dilution in 0.1% PBS/BSA solution, respectively) was then added onto the specimens and incubated overnight at 4 °C. After washing with 0.1% PBS-BSA solution they were incubated in both Alexa Fluor 488-labelled anti-mouse antibody produced in goat (1:100 dilution in 0.1% BSA-PBS) and Alexa Fluor 647-labelled anti-rabbit antibody produced in donkey (1:100 dilution in 0.1% BSA-PBS) at 37 °C for 1 h and then washed with 0.1% PBS-BSA solution. Samples were studied using a confocal laser scanning microscope (Zeiss LSM 9100, Germany).

2.2.7.3.5. SEM of Schwann Cell Seeded PCL Tubes

Schwann cells seeded on PCL tubes were coated with gold, and examined under scanning electron microscopy (SEM) (Quanta FEG 650, Quanta FEI, United States).

2.2.8. 3D Printing of PCL Tube for *In Vivo* Studies

A hollow cylindrical nerve guide model (5 mm width x 10 mm height) was drawn with SketchUp 3D modeling program, and then converted to STereoLithography (.STL) files with CURA (3D printing slicing software) in order to make them printable with the Bioscaffolder® (SYS+ENG, Germany). Polycaprolactone (MW 50,000 daltons, Polysciences Inc., USA) was printed at 120 °C on the cold table (4 °C) at 20 °C with a 1 mm strand distance. Velocity in xy and z-direction (F_{xy}, F_z) is 300 mm/s.

2.2.9. *In Vivo* Studies

This part of the studies was performed at Department of Medical Pharmacology, Hacettepe University. *In vivo* studies were conducted with male Wistar rats weighing between 200-220 g. There were four experimental groups. The first group consisted of rats, the sciatic nerve of which were cut and a 10 mm long section was removed.

This group was used as a negative control. 10 mm x 5 mm (length x width) hollow cylindrical 3D printed PCL tube was implanted in the damaged area in the second group. The third group had 3D printed PCL tube like the second group, also gelatin-PHBV fibers were integrated inside of this PCL tube. The last group of animals had the complete set of nerve guide including a 3D printed PCL tube, gelatin-PHBV fibers, and Schwann cells (SW10 cell line) seeded on the PCL tube.
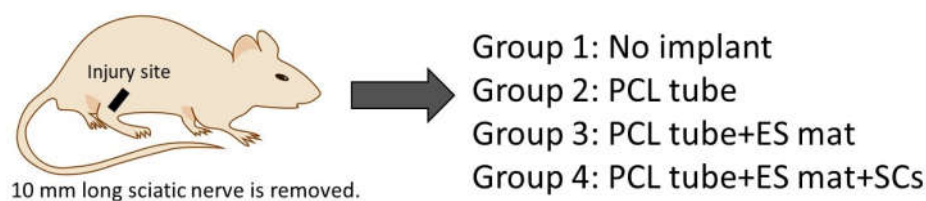
Figure 2.4. Schematic representation of the *in vivo* groups.
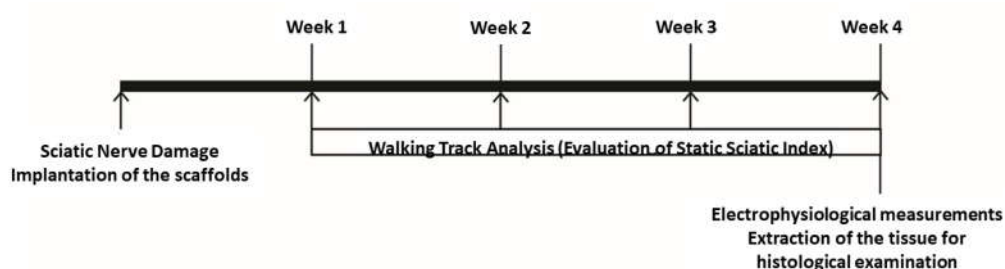
Figure 2.5. Time course of the *in vivo* studies.

2.2.9.1. Implantation of the Nerve Guides

Rats anesthetized with intraperitoneal xylazine (90 mg/kg) + ketamine (10 mg/kg) were shaved from the right hind leg surface. The skin was disinfected with a 10% polyvinylpyrrolidone-iodine solution. 2 cm long skin incision was made to reveal the sciatic nerve on the right side of the right leg. A portion of 10 mm from the right sciatic nerve was cut out, and tubes prepared in the other groups were placed, and the left

sciatic nerve was opened in the same way, and sham surgery was performed without damaging the sciatic nerve. 1 mg/mL paracetamol was given to the animals in drinking water for 24 h. Schwann cell group was cultured 10 days before implantation, and they reached $2,39 \times 10^4 \pm 23 \times 10^3$ cells when the cell seeded scaffolds were implanted.

2.2.9.2. Walking Track Analysis

The rats were taken into a transparent 20 x 12 x 9 cm cage and illuminated by the cold light source from the bottom. The camera was placed under the cage and with the help of the Image J Software, the width of the toes was measured on a weekly basis. 50 photographs are taken in 10 minutes per animal. 5 of these photographs were selected and used for the calculation of the static sciatic index (SSI). Criteria for selection of photographs were: 1) rat body was flat, and 2) the 4 paws of the rat were on the transparent platform. For each rat, the 5 measurements were averaged. The measurements were compared with both nerve damaged and sham-operated paws and nerve healing is evaluated functionally.

The parameters of 1–5 toe spread (TS) and 2–4 intermediate toe spread (ITS) of injured and non-injured hind footprints were measured on the basis of the digital images using the Visual-SSI setup (Bozkurt et al., 2008). After image acquisition, digital images were exported to the available image editing program for quantification of the toe spreading. The measurements from these footprints were averaged to determine the parameter values and their standard deviations. Ratios of hindfoot parameters (1–5 toe spread factor [TSF], and intermediate toe spread factor [ITF]) were determined as described by Bervar (2000) for both injured and uninjured paws, all measurements being made by a single observer:

$$TSF = (OTS - NTS) / NTS \qquad (8)$$

$$ITSF = (OITS - NITS) / NITS \qquad (9)$$

$$SSI \; index = (108.44 \times TSF) + (31.85 \times ITSF) - 5.49 \qquad (10)$$

TSF: toe spread factor, OTS: operated side toe spread, NTS: non-operated side toe spread, ITSF: intermediate toe spread factor, OITS: operated side intermediate toe spread, NITS: nonoperated side intermediate toe spread, SSI: static sciatic index.

2.2.9.3. Electrophysiological Measurements

The sciatic nerves of rats were anesthetized with the injection of intraperitoneal xylazine (90 mg/kg) + ketamine (10 mg/kg) on day 28. Once the right leg of the rat was well fixed, the sciatic nerve was isolated from the surrounding tissues starting from the distal. Bipolar stimulation electrode was placed on the proximal side of the sciatic nerve to introduce monophasic stimuli (stimulation frequency 0.1 Hz; pulse duration 0.1 millisecond; pulse intensity 1-12 V). The recordings were obtained from the distal with bipolar platinum hook electrodes. The signals for the recordings were digitized with Powerlab (AD Instruments, Australia) with a differential amplifier. The threshold and maximum amplitude were determined by increasing the intensity of the stimulation pulses, and the results were evaluated electrophysiologically by comparing the left sciatic nerve with sham surgery.

2.2.9.4. Histological Analysis

Histological assessments were conducted to observe the scaffold integration into the nervous tissue. They gave information about the immunological response, repair and regeneration of the tissue after implantation.

2.2.9.4.1. Embedding of the Scaffolds

Scaffolds were removed on Day 28 after the electrophysiology recordings were completed. They were fixed in 4% paraformaldehyde (PFA) solution overnight. Then, they were washed twice with PBS. Scaffolds were put in 15% sucrose solution for 30 min on a shaking incubator. After then, 15% sucrose solution was removed and the scaffolds were put into 30% sucrose solution for 30 min. After taking out a 30% sucrose solution, 30% sucrose-optimal cutting temperature (OCT) (1:1) solution was added onto the scaffolds for 30 min. Lastly, scaffolds were removed from that solution

and put onto freezing molds. OCT medium was added onto them to cover all of their surfaces, then they were stored at -80 °C freezer.

2.2.9.4.2. Sectioning with Cryotome

OCT blocks including scaffolds were taken out from -80 °C freezer and put onto the cryotome holder for sectioning. 10 μm thick tissue slices were taken onto glass slides. Sections were taken from the upper, middle and lower part of the scaffolds. They were stored at +4 °C until they were stained.

2.2.9.4.3. Hematoxylin and Eosin (HE) Staining

The tissue sections were washed with distilled water for 15 min to remove OCT medium. Then, sections were incubated in alcohol series (100%, 96%, 70%) for 3 min each. Sections were incubated in Hematoxylin stain for 5 min. Slides were washed with tap water for 7 min to remove the excess stain. Then, slides were incubated in eosin stain for 5 min. After staining, slides were kept in 96% alcohol for 2 min and then in 100% absolute ethanol for 3 min. Slides were dried and mounted with Entallan. Micrographs of the tissue sections were taken under light microscope.

2.2.9.4.4. Masson's Trichrome Staining

Masson's trichrome staining procedure was performed according to the HT15 Trichrome Stains (Masson) Kit (Sigma Aldrich, USA). The tissue sections were washed with distilled water for 15 min to remove OCT medium. Then, slides were incubated in Working Weigert's Iron Hematoxylin solution for 5 min. Slides were washed with running tap water for 5 min, and rinsed with deionized water. After then, slides were incubated in Biebrich Scarlet-Acid Fuchsin for 5 min, and rinsed with deionized water. Slides were incubated in working phosphotungstic/phosphomolybdic acid solution for 5 min. Then, slides were incubated in aniline blue solution for 5 min. After then, slides were kept in 1% (v/v) acetic acid for 2 min and rinsed. Slides were dehydrated through 96% and 100% alcohol respectively, and mounted. Micrographs of the tissue sections were taken under light microscope.

2.3. Statistical Analysis

Statistical analyses were performed using a two-way analysis of variance (ANOVA) with Tukey's post hoc test or Student's t-test with a minimum confidence level of 95%, $p \leq 0.05$ were considered statistically significant. All values were reported as the mean ± standard deviation.

CHAPTER 3

RESULTS AND DISCUSSION

3.1. Methacrylic Acid (MA) Content of GelMA

Gelatin was methacrylated as presented in section 2.2.1. Proton NMR was used to determine the degree of methacrylation. Degree of methacrylation (DM) is found by dividing the number of methacrylated groups attached to gelatin into the number of amine groups of unreacted gelatin (Brinkman et al., 2003). In this study, DM was determined by dividing the integrated peaks at 5.3 ppm and 5.5 ppm due to double bond hydrogens of methacrylate groups to integrated peaks at 7.2 ppm due to aromatic residues of gelatin (Nichol et al., 2010). DM of 65% was calculated according to the NMR results. Figure 3.1 shows the NMR spectra of both gelatin and methacrylated gelatin. Formation of 5.3 ppm and 5.5 ppm peaks after methacrylation indicates the incorporation of double bonds into the gelatin structure.
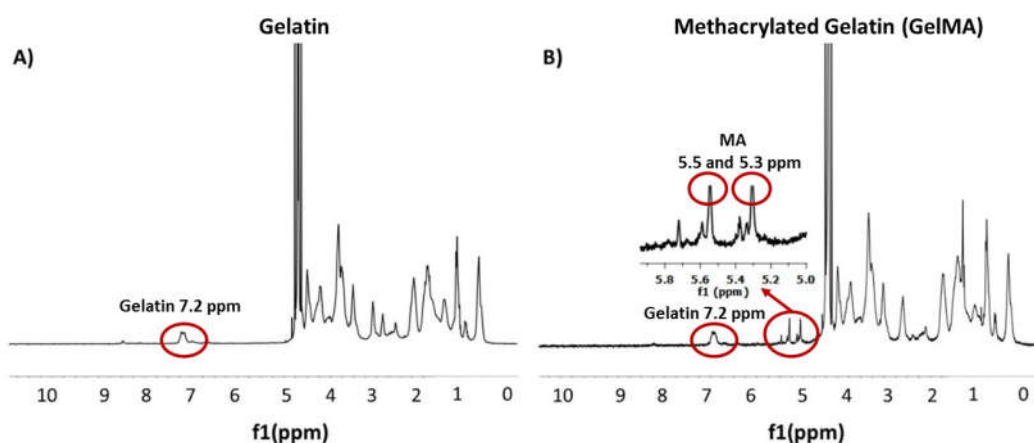
Figure 3.1. ^{1}H NMR spectra of A) Gelatin and B) Methacrylated gelatin (GelMA). The expanded region between 5 and 6 ppm in the GelMA spectrum is shown at the inset.

3.2. Characterization of GelMA-pHEMA Hydrogels

3.2.1. FTIR Analysis

3300 cm^{-1} (O–H stretching vibrations), 2922 cm^{-1} (C–H stretching), 1640 cm^{-1} (O–H bonding), and 1525 cm^{-1} (C–N stretching and N–H bending) bands are seen in Figure 3.2 which shows the FTIR spectrum of gelatin, GelMA and uncrosslinked GelMA (Li et al., 2005). A decrease around 3300 cm^{-1} peak can be related to the decrease in the total number of –OH groups in the polysaccharide structure because of UV crosslinking (Ciardelli et al., 2005). Moreover, the decrease of the 3010 cm^{-1} peak related to the C-C bond shows the success of the photopolymerization and the consequent introduction of GelMA in the final structure of the hydrogel (Almeida et al., 2011). There are typical amide I and II bands at 1640 cm^{-1} and 1540 cm^{-1} in this spectrum due to C=O stretching and N–H bending, respectively. There are also differences in the C–H stretching and bending areas between gelatin and GelMA spectra due to the addition of the methacrylate groups into the lysine groups of gelatin.
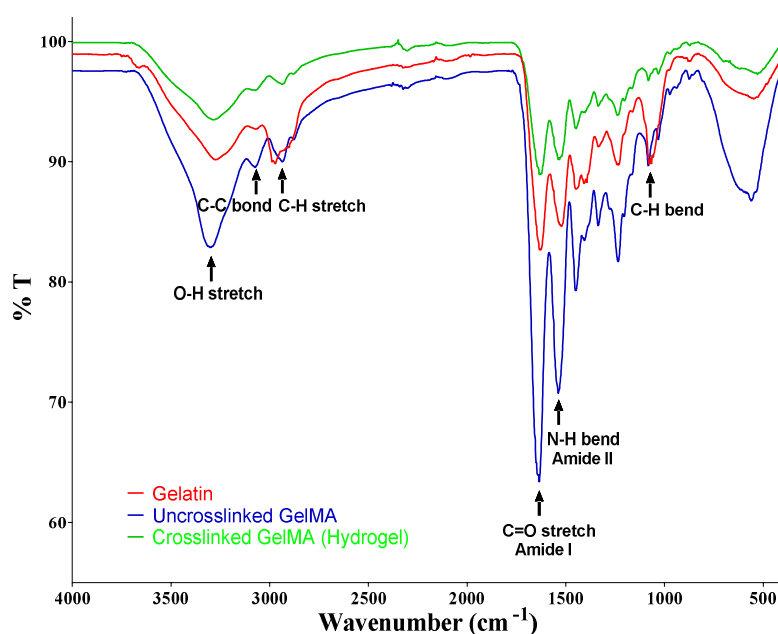
Figure 3.2. FTIR spectra of gelatin, uncrosslinked and crosslinked GelMA.

Figure 3.3 shows the FTIR spectra of GelMA, pHEMA, and GelMA-pHEMA (6:4) hydrogels. The blend of GelMA-pHEMA contains the peaks of both GelMA and pHEMA (1700 cm^{-1}, 1630 cm^{-1}, 1545 cm^{-1} and 1154 cm^{-1}). This confirms the homogeneous nature of the blend hydrogel.
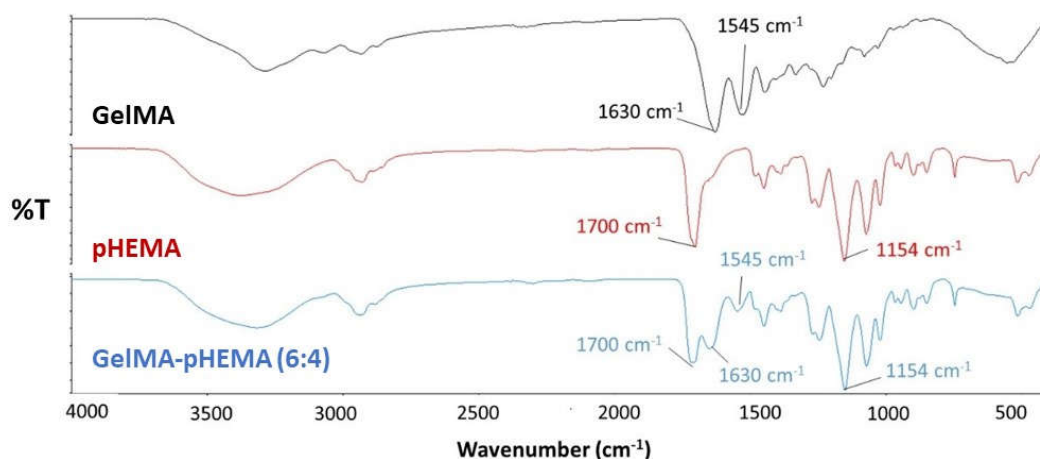
Figure 3.3. FTIR spectra of GelMA, pHEMA, GelMA-pHEMA (6:4).

3.2.2. SEM Analysis

Porosity, pore size distribution and the average pore size of the scaffolds are very critical for cell migration, nutrient diffusion, and waste removal (Hasirci et al., 2010). Therefore, structures with interconnected pores are considered to be suitable for the survival of the cells. SEM micrographs GelMA, GelMA-pHEMA blend (9:1, 8:2, 7:3, 6:4, 5:5), pHEMA hydrogel surfaces and cross-sections are shown in Figure 3.4 and 3.5. Porosity and pore size of the hydrogels decreased when the amount of pHEMA is increased in the hydrogel structure. Figure 3.6 shows the porosity and the pore sizes calculated by Image J program. While pHEMA has the lowest (15%) porosity, GelMA has the highest (70%). Other hydrogels with different GelMA and pHEMA compositions (9:1, 8:2, 7:3, 6:4, 5:5) had porosity between these values (20-65%).

This is also similar for the pore sizes (15-40 µm). It was observed that as the concentration of pHEMA increased, pore sizes of the hydrogel decreased.
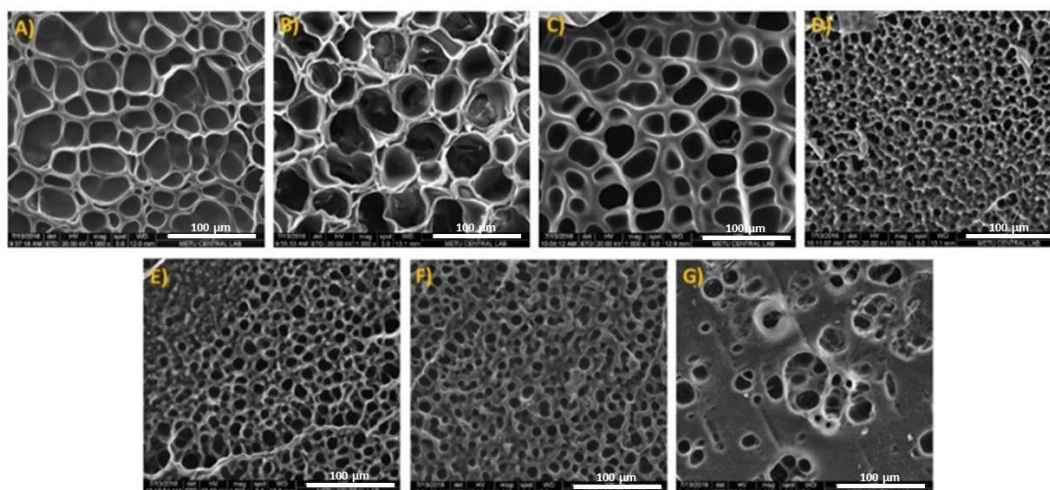
Figure 3.4. SEM micrographs of surfaces of A) GelMA, B) GelMA-pHEMA (9:1), C) GelMA-pHEMA (8:2), D) GelMA-pHEMA (7:3), E) GelMA-pHEMA (6:4), F) GelMA-pHEMA (5:5), G) pHEMA hydrogels.
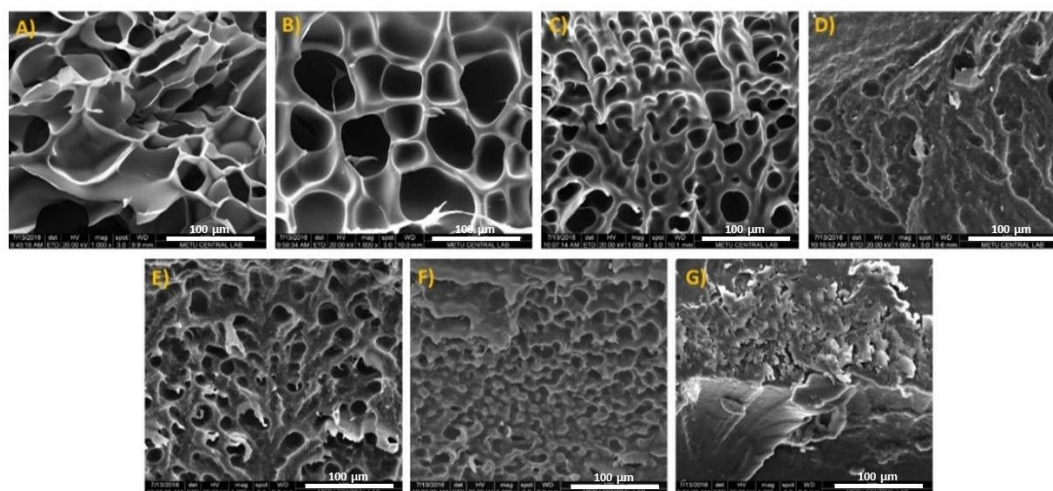
Figure 3.5. SEM micrographs of cross-sections of A) GelMA, B) GelMA-pHEMA (9:1), C) GelMA-pHEMA (8:2), D) GelMA-pHEMA (7:3), E) GelMA-pHEMA (6:4), F) GelMA-pHEMA (5:5), G) pHEMA hydrogels.
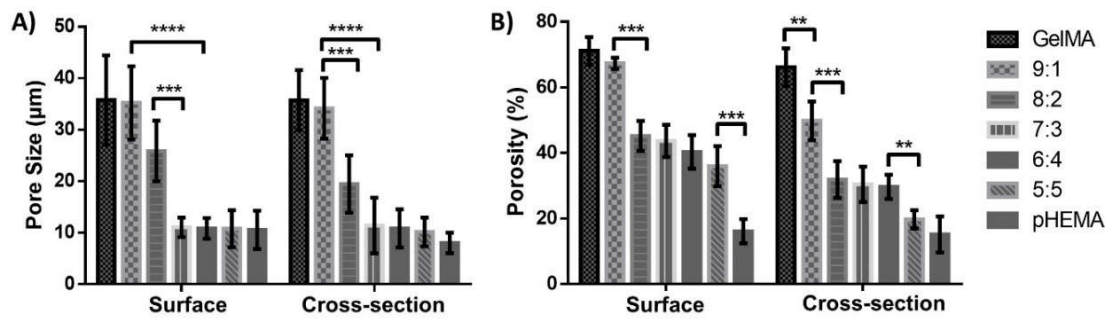
Figure 3.6. Characterization of the GelMA-pHEMA the hydrogels. A) Porosity, B) Pore size (ImageJ). Statistical differences (* $p \leq 0.05$, **$p \leq 0.01$, ***$p \leq 0.001$, ****$p \leq 0.0001$) are indicated.

3.2.3. Water Contents

The water contents of different types of GelMA, GelMA-pHEMA blend (9:1, 8:2, 7:3, 6:4, 5:5), pHEMA hydrogels were ingestigated in PBS and presented in Figure 3.7. Water contents of GelMA and pHEMA were calculated as 92% and 21%, respectively. Similar values of water content (91% and 30%) were reported for GelMA and pHEMA hydrogels in the literature (Wang et al., 2016). The water content of the hydrogels decreased, as the amount of pHEMA in the hydrogel structure increased. This suggests that the pHEMA amount in the hydrogel decreases the water content of the hydrogel significantly. In a study, the influence of pHEMA content in the gel on its swelling behavior has been explored (Bajpai and Kankane, 2007). Their results indicate an important decrease in the water sorption capacity with increasing pHEMA content like in this study. This situation may be explained by increasing synthetic polymer fraction in the gel. Another reason could be that the intermolecular forces between the functional groups of chains become stronger and the gel becomes compact with reduced sizes with an increasing number of pHEMA chains in the gel. This causes a significant fall in the water content of the hydrogels.
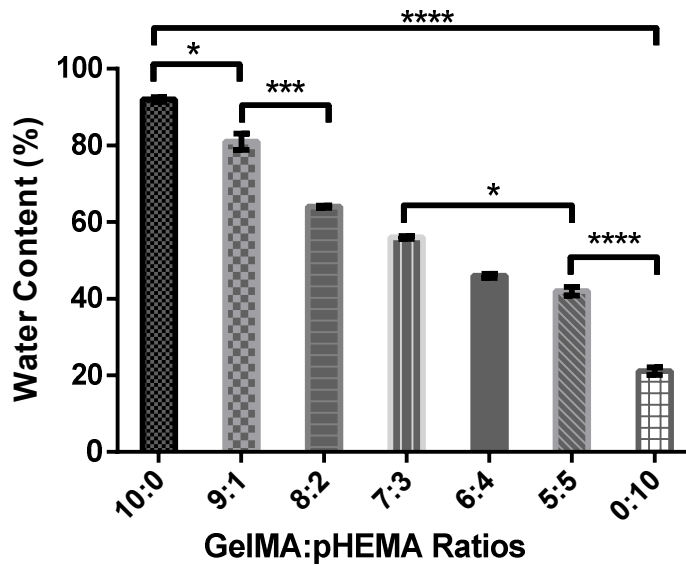
Figure 3.7. Water content of the GelMA:pHEMA the hydrogels. Statistical differences (* p ≤ 0.05, **p ≤ 0.01, ***p ≤ 0.001, ****p ≤ 0.0001) are indicated.

3.2.4. Mechanical Tests

Only pHEMA and GelMA-pHEMA (5:5) blend hydrogels were tested since other blend hydrogels (9:1, 8:2, 7:3, 6:4) were very soft, and could not withstand the pressure during the tensile test. Tensile modulus and the UTS of the pHEMA hydrogels were found as 710±150 kPa and 200±70 kPa. These values are 320±60 kPa and 140±50 kPa for GelMA-pHEMA (5:5) hydrogels (Table 3.1). The compressive modulus of pHEMA (163±29 kPa) is significantly higher than that of GelMA-pHEMA (5:5) (65±10 kPa), and GelMA (1.73±0.15 kPa) hydrogels. Compression values of GelMA-pHEMA (5:5) hydrogels are almost half of pHEMA hydrogels. This reveals that pHEMA contributes to the mechanical strength of the nerve guide significantly. In another study, a gradual increase in compression modulus was observed with increased HEMA/AAc ratio (from 3/7 to 7/3) of the hydrogels (Jaiswal and Koul, 2013). This could be the result of the reduced water content of hydrogels with higher pHEMA contents. Decreased displacement values with increasing HEMA content

may be caused by the lesser amount of water present in the hydrogel for displacement during the compression test.

Table 3.1. *Mechanical properties of GelMA and pHEMA based hydrogels.*

Samples	Tensile Modulus (kPa)	Tensile Strength (kPa)	Compressive Modulus (kPa)
pHEMA	710±150	200±70	163±29
GelMA-pHEMA (5:5)	320±60	140±50	65±10
GelMA	-	-	1.73±0.15

Borschel et al. (2003) found the ultimate tensile strength (UTS) and tensile modulus (Young's modulus) of a rat sciatic nerve tissue as 2720 kPa and 580 kPa, respectively. Moreover, decellularized nerve tissue had a UTS of 1400 kPa and an elastic modulus of 576 kPa (Borschel et al., 2003). Since the conduit constructed in this study is initially free of cells, it is more appropriate to compare it with the decellularized nerve. Although the UTS is lower than the expected value, tensile modulus of the pHEMA and GelMA-pHEMA (5:5) hydrogel are very close to the decellularized nerve guide. Thus, both GelMA-pHEMA (5:5) and pHEMA hydrogels could be used in the outer part of the nerve guide. After cell growth, the mechanical strength is expected to increase significantly (Frantz et al., 2010).

3.2.5. Weight Loss Test in PBS

Biodegradable scaffolds are widely used in tissue engineering applications. Cells are initially grown on the scaffolds in the tissue construction process, and they gradually penetrate into the structure. Meanwhile, polymer degradation creates space for cell growth, and the cells deposit new extracellular matrix (ECM) which eventually replace the scaffold (Salih, 2009). In the end of this degradation process, the scaffold is expected to disappear completely. Rate of ECM deposition should match the rate of scaffold degradation for the appropriate healing of the tissue. In this study, both PHBV, a biopolymer, and gelatin, another natural polymer, were biodegradable, with different rates of degradability.

Weight loss of GelMA, GelMA-pHEMA (5:5), and pHEMA hydrogels are presented in Figure 3.8. Degradation of pHEMA product is not detected as it is a nondegradable polymer (Slaughter et al., 2009). GelMA hydrogels, however, lose half of their content over four weeks. This degradation rate is suitable for cell growth because it creates extra space for cell growth. In a different study, comparatively a loose network was formed by incorporation of gelatin, where gelatin was leached in a time-dependent manner (Jaiswal and Koul, 2013).
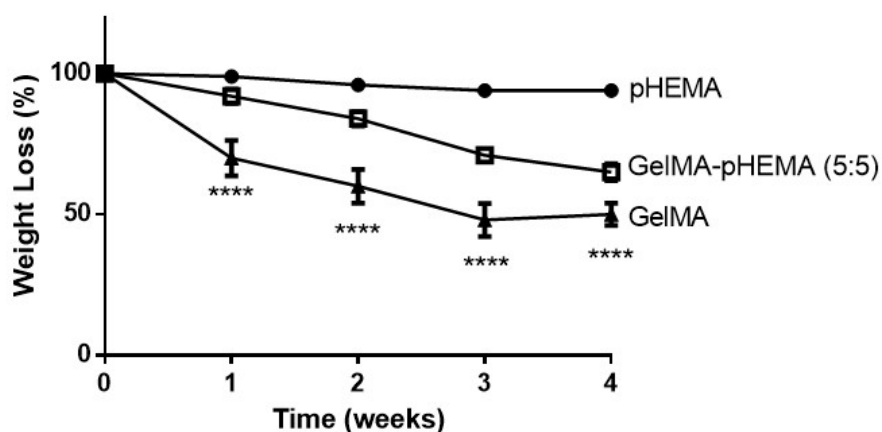
Figure 3.8. Weight loss of the GelMA and pHEMA based hydrogels over 4 weeks. Statistical differences (* $p \leq 0.05$, **$p \leq 0.01$, ***$p \leq 0.001$, ****$p \leq 0.0001$) are indicated.

3.3. Characterization of Gelatin-PHBV5 Fiber Mats

Gelatin and PHBV were designed as a partially sacrificial fiber system. Different polymer concentrations (5, 10, 15, %, w/v) were prepared to achieve the highest degree of alignment (Figure 3.9). Alignment is very important for a nerve guide since cells need topographical cues for their migration. Therefore, it is critical to align the nerve cells along the nerve guide to provide successful nerve regeneration since nerve tissue is anisotropic.
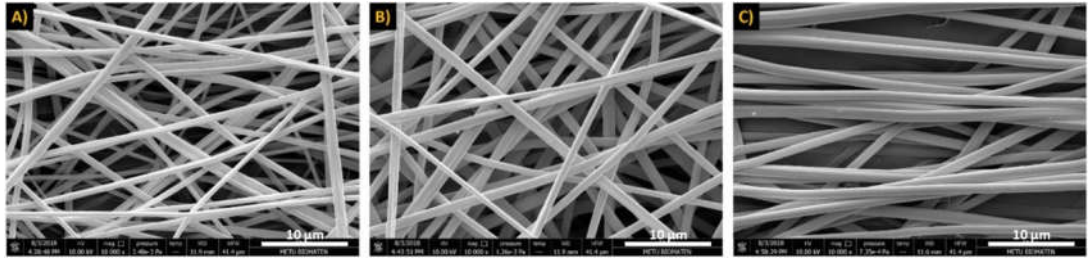
Figure 3.9. SEM micrographs of Gelatin-PHBV fiber mats. A) 5%, B) 10%, and C) 15% polymer concentration.

In this study, the degree of alignment is increased with the increasing polymer concentration which may be attributed to the increasing fiber diameter (Table 3.2). The highest degree of alignment (7°), calculated by using NIH, ImageJ program, was achieved with 15% polymer concentration. This situation is also observed in another study (Bashur et al., 2009). As the concentration of poly(ester urethane) urea solution increased from 8 to 12%, the alignment of the fibers also increased. The fiber diameters were also increased with the increasing concentration of the polymer.

Table 3.2. *Characteristics of gelatin-PHBV fiber mats.*

Concentration of gelatin-PHBV solution in HFIP (%, w/v)	Degree of Alignment (°)	Porosity (%)	Fiber diameter (μm)
5	46	44±3	0.3±0.2
10	21	51±2	1.2±0.5
15	7	44±3	3.2±2.1

3.3.1. Dissolution Profile of Electrospun Mats

Figure 3.10 shows the dissolution profile of gelatin-PHBV mats. On Day 1, 31% of the weight of gelatin-PHBV5 fibrous mats was lost. This high loss rate is probably due to the high dissolution rate of gelatin, since it was not stabilized by crosslinking. Gelatin was introduced as a sacrificial material to be removed rapidly to create some

space for the cells to grow on which would not be possible if the fibers filled the inner volume without leaving room for the cells to adhere and extent on. By Day 7, the weight loss was 44%, practically half the mat material which is roughly equal to the gelatin content. After losing the gelation content on the first week, the weight loss rate was lower.
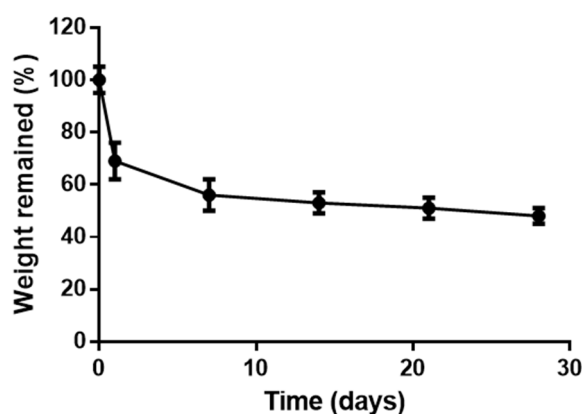
Figure 3.10. Dissolution profile of Gelatin-PHBV ES fibrous mats in PBS at 37 °C shaking incubator over 28 days.

3.3.2. Thickness of Electrospun Mats

Aligned mats were cut into 1 cm x 1.5 cm rectangles, rolled into a cylindrical shape, and inserted into the PCL tubes. However, the rolling process of the thin mats is very difficult. The collector used was rectangular, and fibers which have the highest alignment were found at the center of the collector, however, these mats were very thin and difficult to roll. Mats from the edge of the collector (36.2 ± 6.57 μm) were thicker than the mats from the center of the collector (10.2 ± 2.17 μm). Thickness, fiber diameter, and degree of alignment of gelatin-PHBV mats from the center and the edge of the collector are summarized in Table 3.3. Both of them had the similar degree of alignment and fiber diameter. The only significant difference was found in their

66

thickness. Therefore, mats from the edge of the collector were used for the rest of this study.

Table 3.3. *Physical properties of gelatin-PHBV ES mats at the center and the edge of the electrospin system collector.*

Sample	Thickness (μm)	Fiber Diameter (μm)	Degree of Alignment (°)
Center of the collector (thin)	10.2 ± 2.17	1.8 ± 0.60	7 ± 7
Edge of the collector (thick)	36.2 ± 6.57	1.5 ± 0.40	8 ± 6

3.4. 3D Printing of the Nerve Guides

Different types of nerve guide models were drawn with SketchUp 3D modeling program and they were converted to STereoLithography (.STL) files with CURA (3D printing slicing software) in order to be able to print with the Bioscaffolder® (SYS+ENG, Germany) (Figure 3.11).

Figure 3.11. Bioscaffolder® 3D printing system.

Figure 3.12 shows three different cylindrical models designed and printed by using PCL. The first model was a hollow PCL tube (20 mm diameter). Then, channels were

added along the axis of the cylinder to provide guidance of the cells. However, in our studies, we tried to decrease the size of our model to mimic the natural nerve issue. When the diameter of the model is decreased, it becomes almost impossible to provide guidance channels due to the fiber diameter set by the inner diameter of the needle. Still, due to the nature of fuse deposition of the polymer, Figure 3.11C has aligned surface inside. Therefore, this model was used for further experiments.
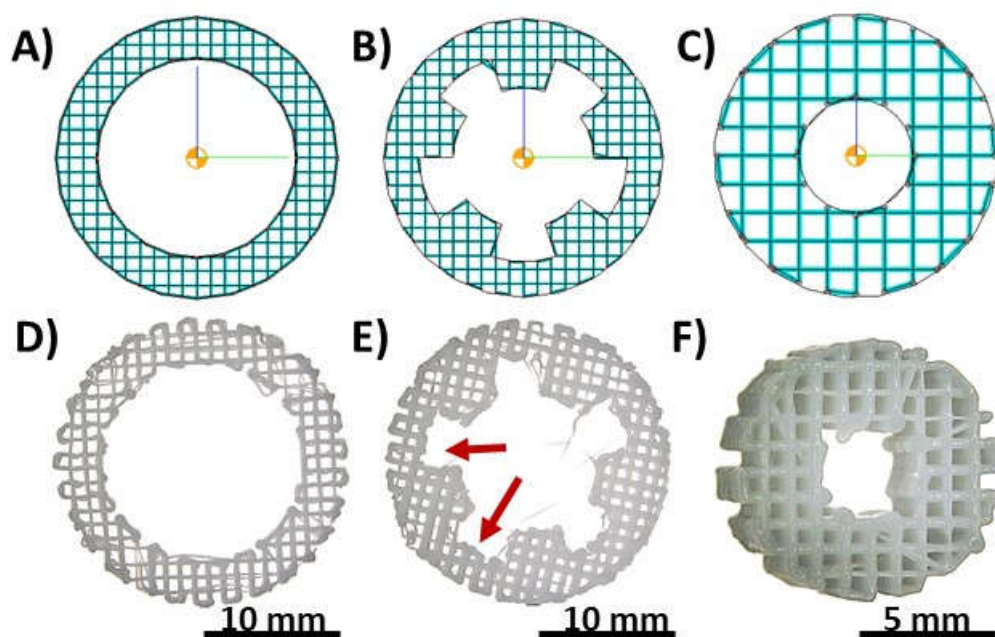
Figure 3.12. STereoLithography (.STL) files and stereomicrographs of FDM printed PCL scaffolds. A, D) w/o guidance elements (diameter 20 mm, 4 layers), B, E) w/ guidance elements (diameter 20 mm, 4 layers), C, F) w/o guidance elements (diameter 10 mm, 75 layers).

After deciding about the model, PCL was printed at different temperatures (110 °C, 120 °C, 130 °C) to optimize the printing conditions. Even though the melting point of PCL is around 60 °C, PCL could not be printed at 110 °C. At 130 °C, polymer melted excessively forming some extra fibers (Figure 3.13A). Printing at 120 °C was possible and thus 120 °C was the optimum temperature for 3D printing. Cold table (4 °C) was used to cool the printing platform on which the layers are deposited. The shapes of the

tubes became irregular rather than straight (Figure 3.13B). Distorted shapes become more apparent when the side views of the scaffolds were compared (Figure 3.13E). The best scaffold printing was achieved by using a cold table and 120 °C (Figure 3.13F). After this point, 120 °C and cold table were used as the printing conditions for the rest of the study.
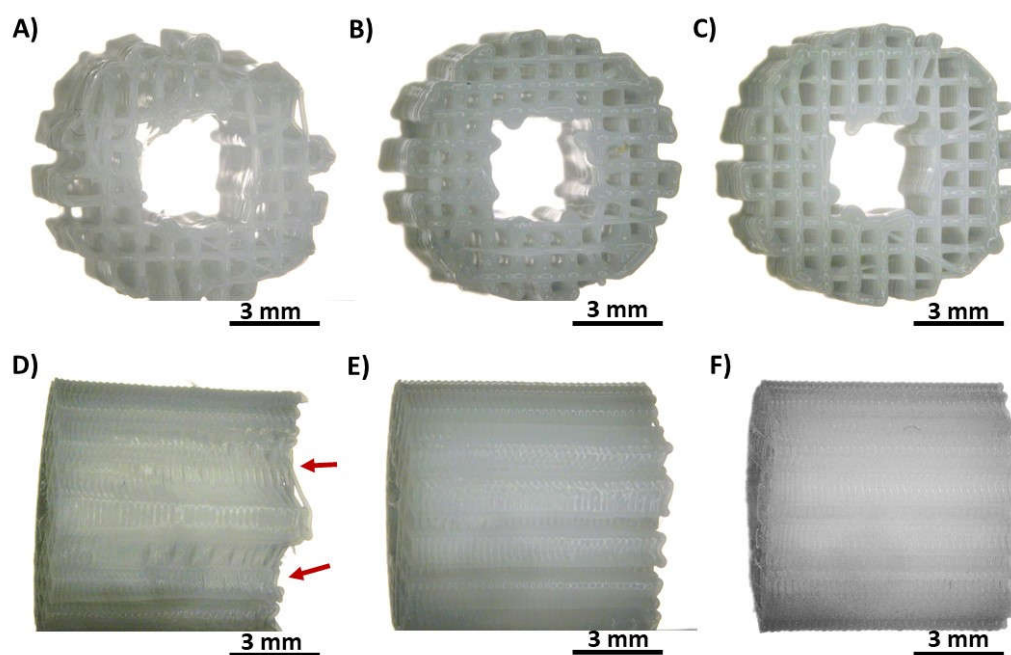
Figure 3.13. 3D printed PCL tubes (10 mm x10 mm) under different temperatures, and with and without cold table. Top views A) at 130 °C, B) at 120 °C, C) at 120 °C on a cold table, Side views D) at 130 °C, E) at 120 °C, F) at 120 °C on a cold table.

3.4.1. SEM of PCL tube

The SEM results of the PCL tubes show that the gap sizes are 675 ± 40 µm and the fiber diameters are 382 ± 25 µm. These sizes are quite suitable for cell growth and penetration. The side view shows that both the pore sizes and fiber diameters are significantly smaller than from the top view; 47 ± 16 µm and 231 ± 8 µm, respectively. It is mostly caused by the long height (10 mm) of the tubular structure since 75 layers

of PCL was printed for each scaffold and some fibers collapse into each other. However, it is an advantage for cell seeding because Schwann cells (SCs) were seeded from the outside of the tube and small pore sizes may increase the chance of cell attachment and retention on this surface. Figure 3.14 also shows the smooth surface of deposited PCL fibers which is an indicator of successful 3D printing.
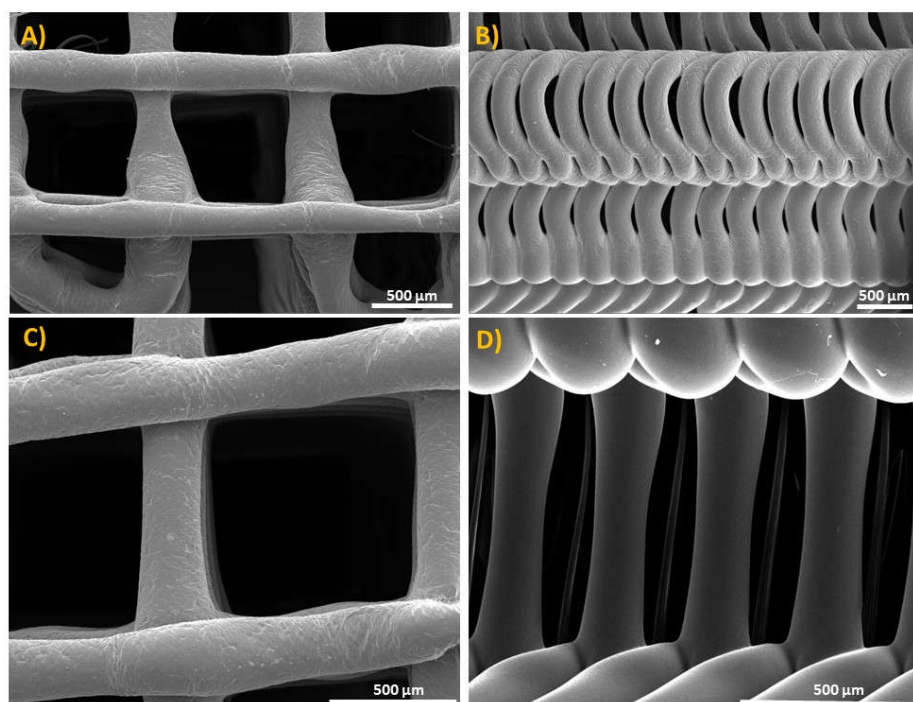
Figure 3.14. SEM micrographs of PCL tube from A, C) Top and B, D) Side view.

3.4.2. Micro CT

Micro CT (μCT) is an advanced method which enables imaging in three dimensions on a small scale with a very high resolution. Using a μCT scanner, the internal structure of tissue can be visualized without destroying the sample tissue. Micro CT was used to provide an insight about 3D printed PCL tubes. Figure 3.14A shows the 3D computer model of the nerve guide prepared by CURA, and its structure is very

similar to the μCT image of the 3D printed PCL tube (Figure 3.14B). This fidelity between them indicates the success of 3D printing. Micro CT image of the 3D printed PCL conduit shows the precisely mimicked inner architecture of the tube and homogeneous nature of the fibers and the pores. Total porosity of the tube walls was measured as 55%. This is expected because the structure was designed to have fibers 380 μm thick and the lateral gaps between the fibers were 675 μm wide. The center of the tubular scaffold is hollow in order to incorporate the electrospun fibers.
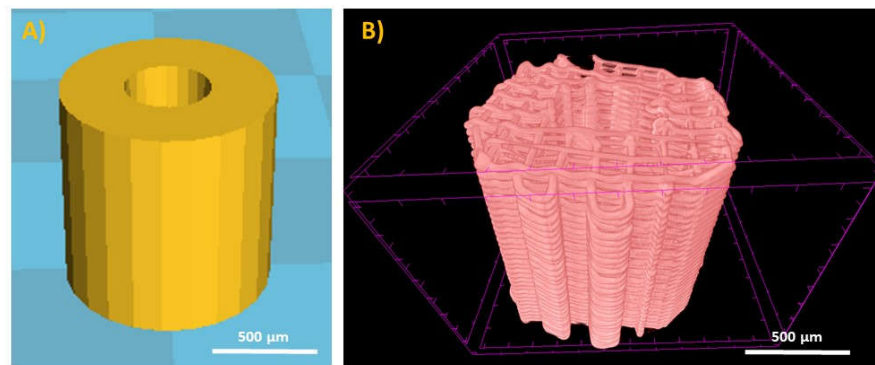
Figure 3.15. Nerve guide structures. A) 3D model of the nerve guide, B) Micro CT micrograph of PCL tube.

3.4.3. Water Contact Angle

Wettability is the ability of a liquid to maintain contact with a solid surface which results from intermolecular interactions. The degree of wettability is determined by a balance between adhesive and cohesive forces (Menzies and Jones, 2010). Wettability of biomaterials *in vitro* is assessed by measuring the water contact angle (WCA) at the liquid-solid interface. When a liquid comes into contact with a solid surface, there is a relationship between the contact angle θ, the surface tension of the liquid σ_{lg}, the interfacial tension σ_{sl} between liquid and solid and the surface free energy σ_{sg} of the solid according to Young's equation:

$$\sigma_{sg} = \sigma_{sl} + \sigma_{lg} \cdot \cos\theta \qquad (11)$$

71
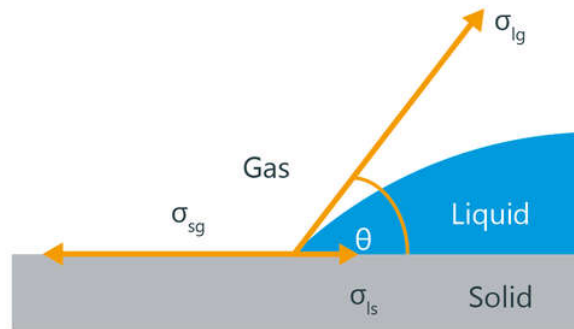
Figure 3.16. Schematic diagram of the components of a three-phase system.

According to the Young equation, a solid surface with low energy shows a high contact angle, whereas a high energy surface displays a low contact angle (Huhtamäki et al., 2018). In the measurement, the sessile drop technique used in this study involves placing a droplet of distilled water from a syringe onto the surface of the test material and the CA is measured with a goniometer. The water contact angle on the 3D printed PCL surface was found as $77 \pm 7°$ which corresponds to the high wettability category (Rupp et al., 2014). Cell attachment is generally high on moderately hydrophilic surfaces (González-Carrasco et al., 2019). Therefore, Schwann cells were expected to attach to the PCL tube surface effectively.

3.4.4. Tensile Testing

Stress (σ) is the force (F) exerted on the area (A) of the tested sample, the highest values of which is the ultimate tensile strength (UTS). In the elastic region, the slope of the initial linear region of the stress-strain curve gives the elastic modulus (Young's modulus, E), and the maximum value of the stress is the ultimate tensile strength (UTS) (Figure 3.17).

$$\text{Stress } (\sigma) = F/A \qquad\qquad (12)$$

72
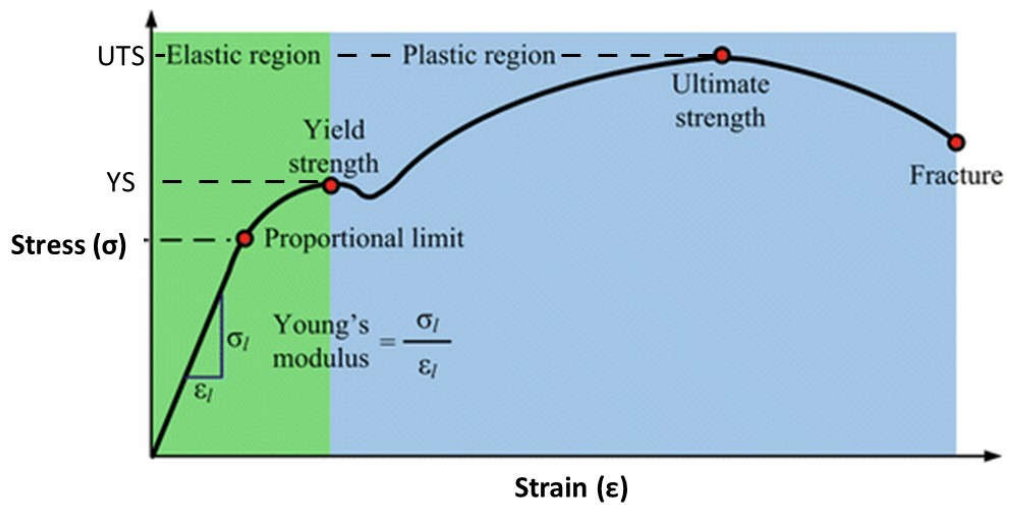
Figure 3.17. Stress-strain curve of a ductile material. (Teo et al., 2014) Springer-Verlag London 2014.

Young's modulus and the UTS of PCL films were found as 150±20 kPa and 12,000±800 kPa, respectively. Appropriate flexibility and rigidity of nerve guide tubes are necessary for the migration of Schwann cells and endothelial cells as well as long term support for regenerated nerves (Niu et al., 2014). Damaged nerve ends can come together with the excellent mechanical properties of PCL (Qian et al., 2018).

Young's modulus and the UTS of the pHEMA hydrogels were found as 570±80 kPa and 200±70 kPa, respectively. These values are 260±40 kPa and 140±50 kPa for GelMA-pHEMA (5:5) hydrogels (Table 3.4). When compared with the values of pHEMA and GelMA-pHEMA (5:5) hydrogel, these are very improved results. In a study by Borschel et al. (2003), the elastic modulus and UTS of a rat sciatic nerve tissue were found to be 570 kPa and 2700 kPa, respectively. PCL films have higher UTS, but lower elastic modulus than the rat sciatic nerve. After cell growth, the mechanical strength is expected to increase significantly.

Table 3.4. *Mechanical properties of PCL, pHEMA, and pHEMA-GelMA (5:5).*

Sample	PCL	pHEMA	pHEMA-GelMA (5:5)
Young's modulus (kPa)	150±20	570±80	260±40
UTS (kPa)	12,000±800	200±70	140±50

3.5. *In Vitro* Studies

3.5.1. *In Vitro* Studies with GelMA and pHEMA Hydrogels

3.5.1.1. Schwann Cell Proliferation

Alamar Blue assay was conducted to study the proliferation of Schwann cells (SCs) seeded on GelMA, GelMA-pHEMA (5:5) and pHEMA hydrogels (Figure 3.18). SCs attached on all of these hydrogel surfaces and proliferated significantly as the culture duration increased. Schwann cell number was higher on GelMA, GelMA-pHEMA (5:5) than pHEMA alone on Day 14. This may be attributed to the cell attractive properties of gelatin because it has inherent peptide sequences (Arg-Gly-Asp (RGD) motif) which facilitate cell adhesion (Koshy et al., 2014). However, all hydrogels supported cell growth which shows that any of them could be used as a nerve guide material in the treatment of peripheral nerve injuries.
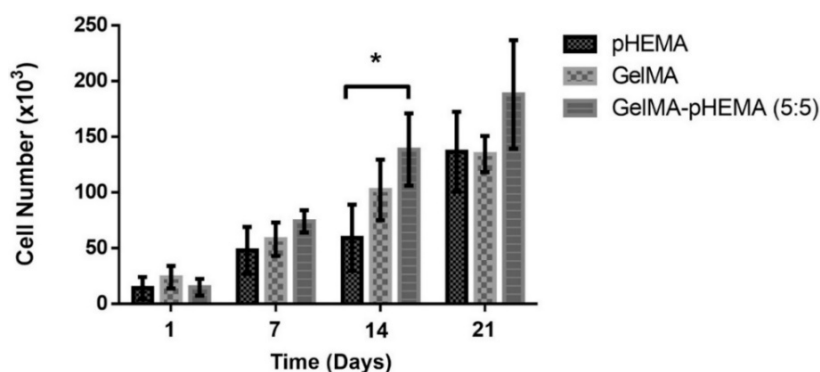
Figure 3.18. Schwann cell proliferation on pHEMA, GelMA and GelMA-pHEMA (5:5) hydrogels over 3 weeks. Initial cell seeding density: 10^5 cells/cm^2. Statistical differences (*p $\leq$ 0.05) are indicated.

3.5.1.2. CLSM

Cell-material interactions were studied with CLSM. The cytoskeleton (green) and the nuclei (red) were stained with Alexa Fluor 488-Phalloidin and DRAQ5, respectively. Schwann cell (SC) proliferation on GelMA-pHEMA (5:5) and pHEMA hydrogels was shown in Figure 3.19. Cellular connections were apparent on Day 14. Cell number seemed higher on GelMA-pHEMA (5:5) hydrogel which was also confirmed with Alamar Blue assay. This may be attributed to the cell attractive properties of the gelatin. Another study revealed that the covalently bound gelatin sequences significantly improve the biocompatibility of pHEMA based hydrogels (Dragusin et al., 2012). SCs covered most of the hydrogel surface and formed cellular networks on Day 21. These results suggest that both pHEMA and GelMA-pHEMA hydrogel were suitable for Schwann cell proliferation.
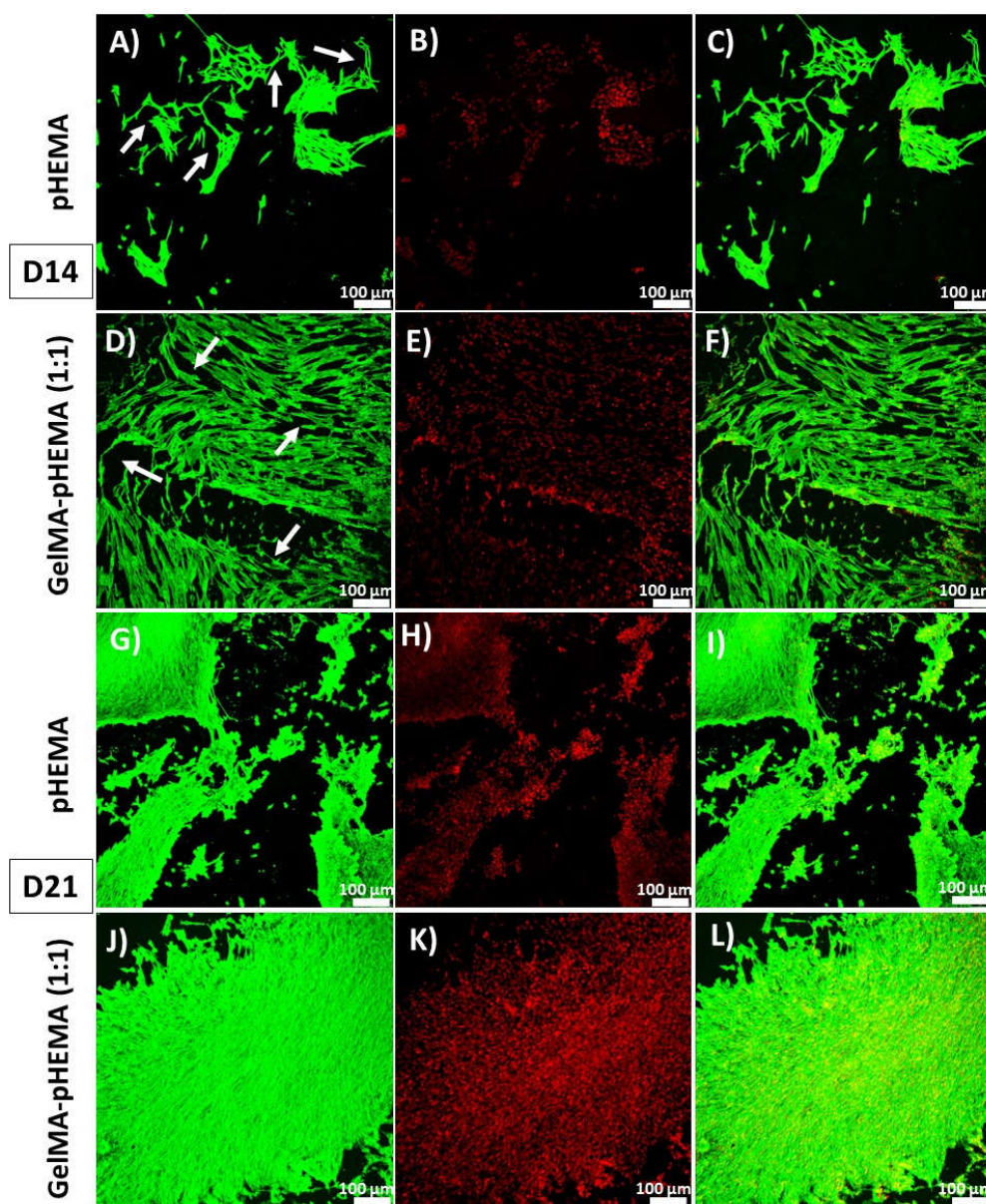
Figure 3.19. CLSM images of cytoskeleton (green), nucleus (red), and merged Schwann cells on A-C) pHEMA, D14, D-F) GelMA-pHEMA (5:5), D14, G-I) pHEMA, D21, J-L) GelMA-pHEMA (5:5), D21.

3.5.2. *In Vitro* Studies with Gelatin-PHBV Fibrous Mats

3.5.2.1. PC12 Cell Proliferation

Attachment and proliferation of PC12 cells on gelatin-PHBV mats from the center and the edge of the collector were studied with Alamar Blue assay (Figure 3.20). Initial

cell seeding density was 5×10^4 cells/scaffold. Cell attachment was better on the mats from the edge of the collector. It can be due to the thickness of the mats. Samples from the edge of the collector are thicker than the ones taken from the middle part. Therefore, cell number is higher on the mats from the side of the collector. However, cell proliferation is higher on the mats from the center of the collector as the incubation time increased. This can be explained by cell penetration to those mats. These mats are thinner, so there is more space for cell penetration. Although there is a significant difference between the two mats statistically, both of them seem suitable for cell attachment and proliferation.
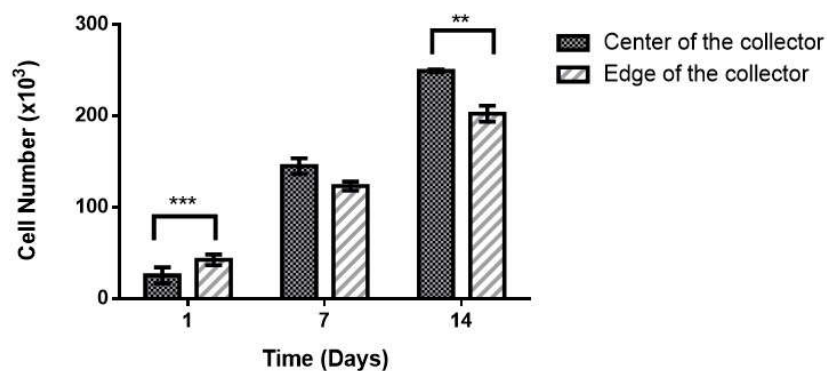
Figure 3.20. PC12 proliferation on thick and thin gelatin-PHBV electrospun mats. Initial cell seeding density: 5×10^4 cells/scaffold.

3.5.2.2. PC12 Cell Alignment

PC12 cells were seeded on both plain glass slide and aligned gelatin-PHBV fibers in order to study the PC12 cell alignment throughout the fibers (Figure 3.21). PC12 cells had a random cell distribution on the glass slide because there are not any guidance cues on them. However, PC12 cells are aligned in the direction of the fibers since aligned fibers provided attachment places throughout their uniaxial direction. This

directional cell alignment is necessary for the formation of uniaxial nerve tissue formation.
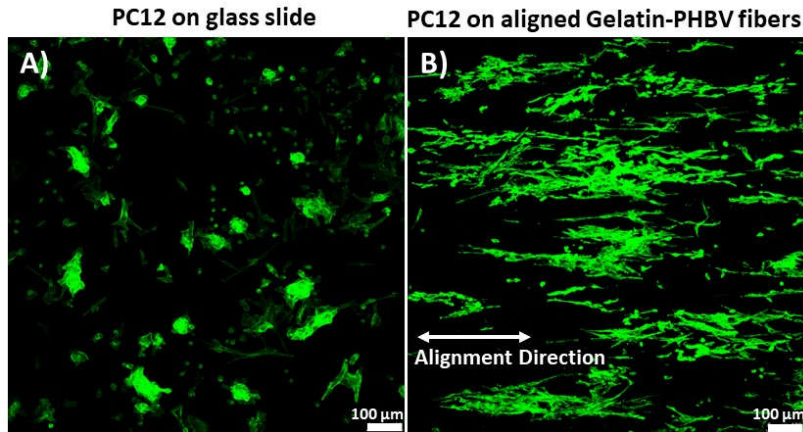
Figure 3.21. CLSM images of cytoskeleton staining of PC12 cells on A) Glass slide, and B) Aligned gelatin-PHBV fibers on Day 7, 10x.

Figure 3.22 shows the PC12 cells on gelatin-PHBV (5:5) aligned fibrous mats over three weeks. Even on Day 1, cells were aligned along the fibers. Cellular connections and neurite outgrowth were observed on Day 7. Surfaces of the mats were covered with PC12 cells on both D14 an D21. Like cell growth, neurite extensions showing the differentiation of PC12 cells into neurons were more apparent with increasing incubation time. This shows the suitability of gelatin-PHBV mat surface for cell attachment, proliferation, and alignment. Integration of this mat inside the nerve guide as inner guidance element would provide attachment and alignment of the damaged neurons at the injured site. By this way, damaged neurons could be rejoined through the use of gelatin-PHBV aligned fibrous mats to provide peripheral nerve regeneration. Z-section micrographs of these mats also show the increased penetration and the growth of PC12 cells on these mats with increasing incubation duration. It also shows the migration of these cells into the mat structure.
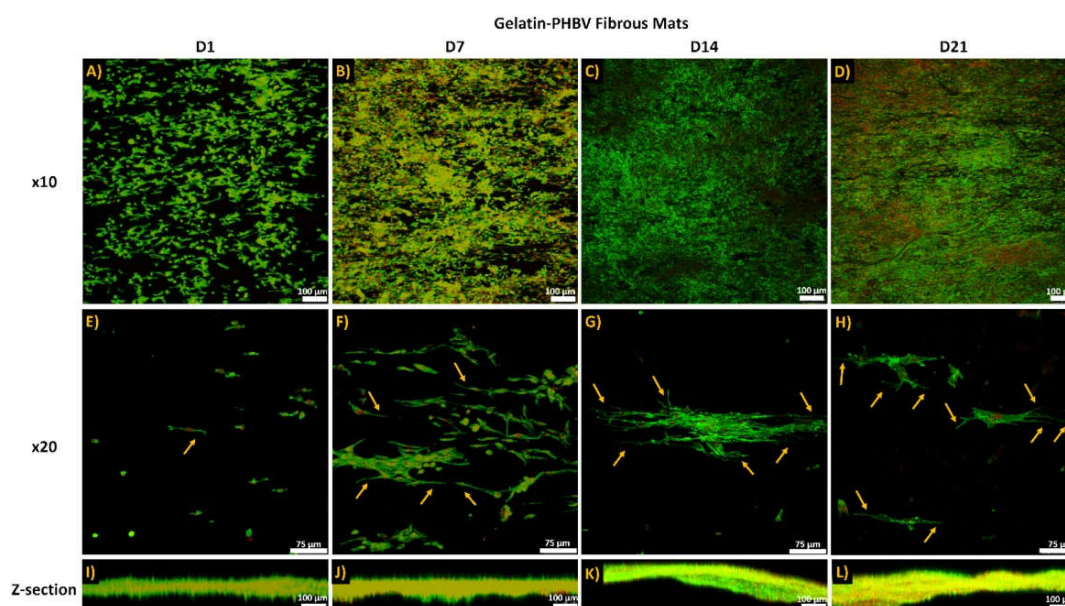
Figure 3.22. CLSM images of PC12 cells on gelatin-PHBV aligned fibrous mats. A) Day 1, B) Day 7, C) Day 14, D) Day 21, E) Day 1, F) Day 7, G) Day 14, H) Day 21, I) Day 1, z-section, J) Day 7, z-section, K) Day 14, z-section, L) Day 21, z-section. Cytoskeleton (green) and nucleus (red) staining. Arrows show the neurite outgrowth.

3.5.3. *In Vitro* Studies with 3D Printed PCL Tube

3D printed PCL tubes were served as the exterior of the nerve guide and Schwann cells (SCs) were seeded on this part as support cells to mimic the peripheral nerve and support nerve regeneration.

3.5.3.1. Schwann Cell Proliferation

The proliferation of Schwann cells seeded on PCL tubes was studied with Alamar Blue assay over 3 weeks. Cell attachment was successful and Schwann cells proliferated very well on PCL tubes (Figure 3.23). Although cell proliferation rate was higher on TCP surface (TCPS), the proliferation rate of SCs on PCL tube was close to the TCPS surface. More space (surface area of Sarstedt 6-well plate=8,87 cm^2) is available for the cells on the TCPS, however, PCL tube has smaller areas (surface area of the scaffold=3,14 cm^2) for the cell growth and proliferation due to the limited size

of the scaffolds. Besides, Schwann cells were seeded on the top of the tubular scaffolds, even smaller surface area was available for the cell attachment on Day 1.
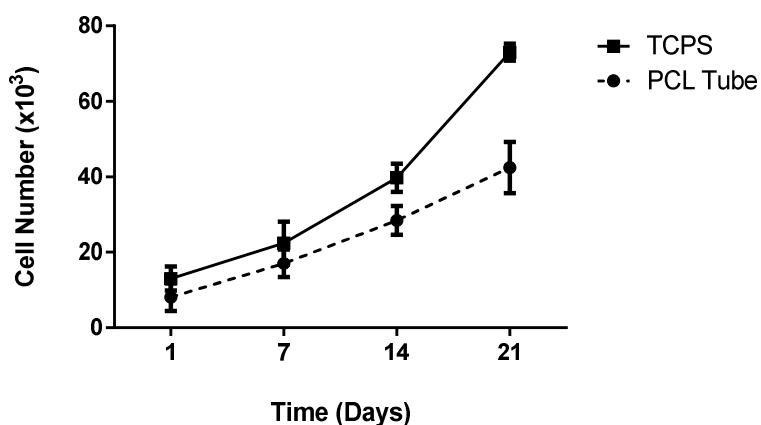
Figure 3.23. Schwann cell proliferation on PCL tubes over 3 weeks. Initial cell seeding density: 2.5×10^4 cells/scaffold.

3.5.3.2. Confocal Microscopy of SCs on the PCL Tubes

CLSM studies were carried out to study the cell-material interaction. Alexa Fluor 488-Phalloidin was used to stain the cytoskeleton (green) and DRAQ5 to stain the nuclei (red) of SCs. Figure 3.24 shows the Schwann cell (SC) proliferation on 3D printed PCL tubes. In the beginning of the incubation, there are less number of cells because the initial cell seeding density is low. However, as the incubation duration increased, SC number increased, too. This is also confirmed with Alamar Blue assay. The highest number of cells was found on PCL tubes at the end of the incubation time (Day 21). They even migrated into the sides of the PCL tubes.
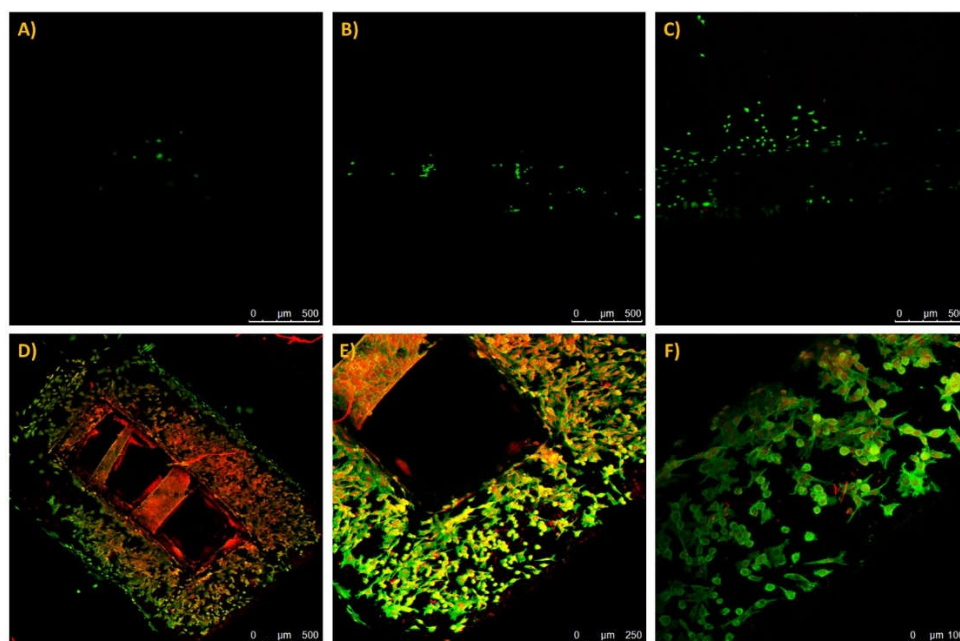
Figure 3.24. CLSM images of Schwann cells seeded on 3D printed PCL tubes. A) D1, B) D7, C) D14, D-F) D21. Cytoskeleton (green) and nucleus (red) staining.

3.5.4. *In vitro* Studies with Nerve Guide (Coculture of SCs and PC12)

The positive effect of SCs on the myelination and differentiation of PC12 cells has been shown in other studies (Watabe et al., 1995; Keilhoff et al., 2006; Sango et al., 2012). Therefore, SCs were seeded on the exterior of the 3D printed PCL tubes. Gelatin-PHBV5 (5:5) mats were produced by electrospinning and incorporated into the 3D printed PCL tube as inner guidance elements to provide the alignment of the nerve cells. PC12 cells were seeded on one side of these mats which is considered as the proximal part of the damaged nerve. Migration of these cells into the other part of the mat (distal part) was studied to create an *in vitro* model of peripheral nerve regeneration.

3.5.4.1. SCs and PC12 Cell Proliferation on the Whole Nerve Guide

The cell proliferation on the nerve guide was studied with Alamar Blue assay. The proliferation rate on TCPS was higher than that on the nerve guide (Figure 3.25). The

cell number increase on TCPS and nerve guide continued for 3 weeks. When compared with TCPS, less number of cells attached to the nerve guide on Day 1, but their proliferation rate was very high. Although cell proliferation rate was 4-fold higher on TCPS, the proliferation rate of SCs and PC12 on the nerve guide was also good. TCPS has larger surface area for cell growth, and the cells on TCPS has easier nutrient and oxygen access because of its 2D structure. On the 3D nerve guides, cells must have migrated into the pores of the tube and the mat, therefore they may not have sufficient nutrient and oxygen flow as on TCPS. However, when different time points were compared, a successful cell proliferation rate was also observed with the nerve guide structure.
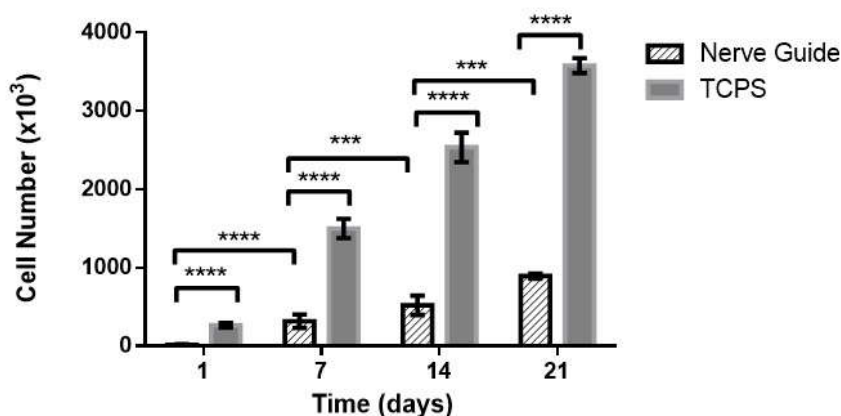
Figure 3.25. Proliferation of PC12 and Schwann cells on nerve guide and tissue culture plate surface (TCPS control) over 21 days. Initial cell seeding density: 2×10^5 cells/scaffold. Cell number is the total of SCs and PC12 cells as Alamar Blue assay cannot distinguish the two.

3.5.4.2. Confocal Microscopy of SCs on PCL Tube and PC12 on ES Mats

Figure 3.26 and 3.27 show Schwann cell (SC) proliferation on PCL tubes over three weeks. SC proliferation was higher on PCL tubes with a higher incubation duration. This was also confirmed with Alamar Blue assay. They showed cluster-like formations on the PCL tube which is more apparent on D21. SCs were seeded on the

exterior side of the PCL tube. However, SCs were not only found on the side of the tubes, but they were also seen on the top of the PCL tube at the end of the incubation. Figure 3.27 shows SCs on the top of the PCL tube. This indicates that SCs migrated along the PCL tube, and proliferated. This is very promising for the mimicking of the nerve tissue in which SCs are found on the outer side of the peripheral nerve trunk.
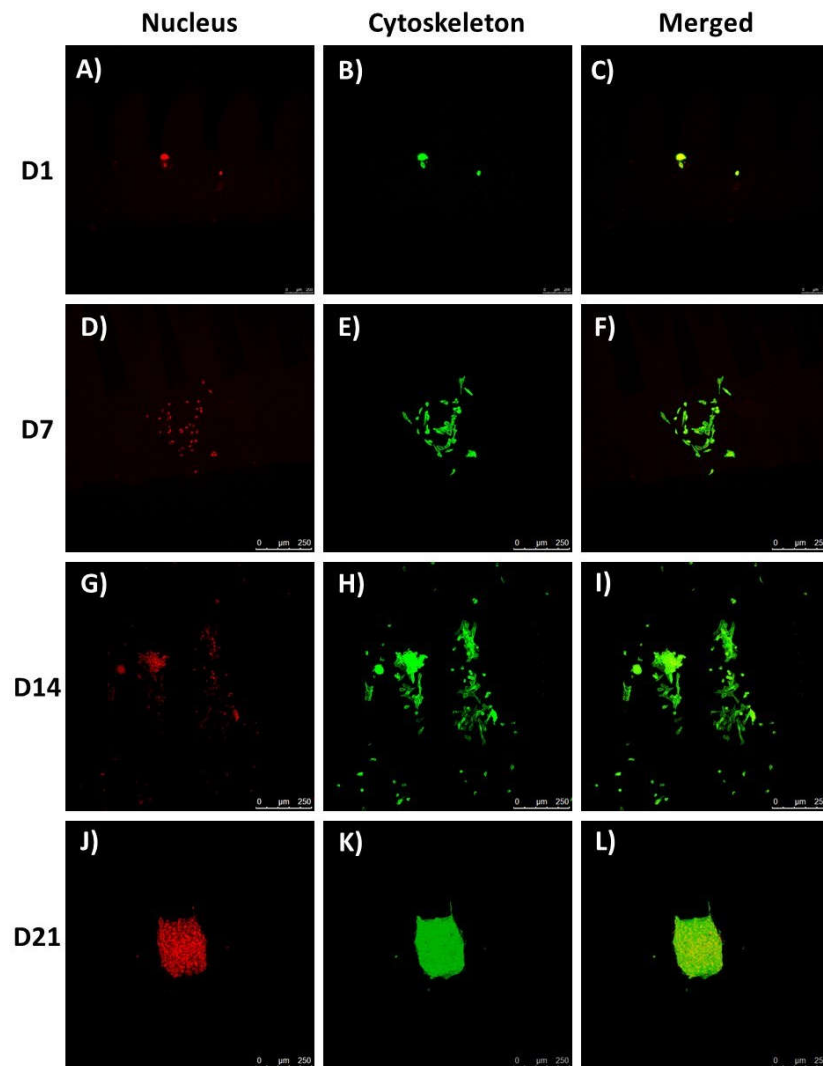
Figure 3.26. CLSM images of SCs cells on 3D printed PCL tubes over 3 weeks view from the side, 10x. A) Nucleus, B) Cytoskeleton, C) Merged image (Day 1), D) Nucleus, E) Cytoskeleton, F) Merged image (Day 7), G) Nucleus, H) Cytoskeleton, I) Merged image on Day 14, G) Nucleus, H) Cytoskeleton, I) Merged image (Day 14), G) Nucleus, H) Cytoskeleton, I) Merged image on Day 14, G) Nucleus, H) Cytoskeleton, I) Merged image (Day 21).
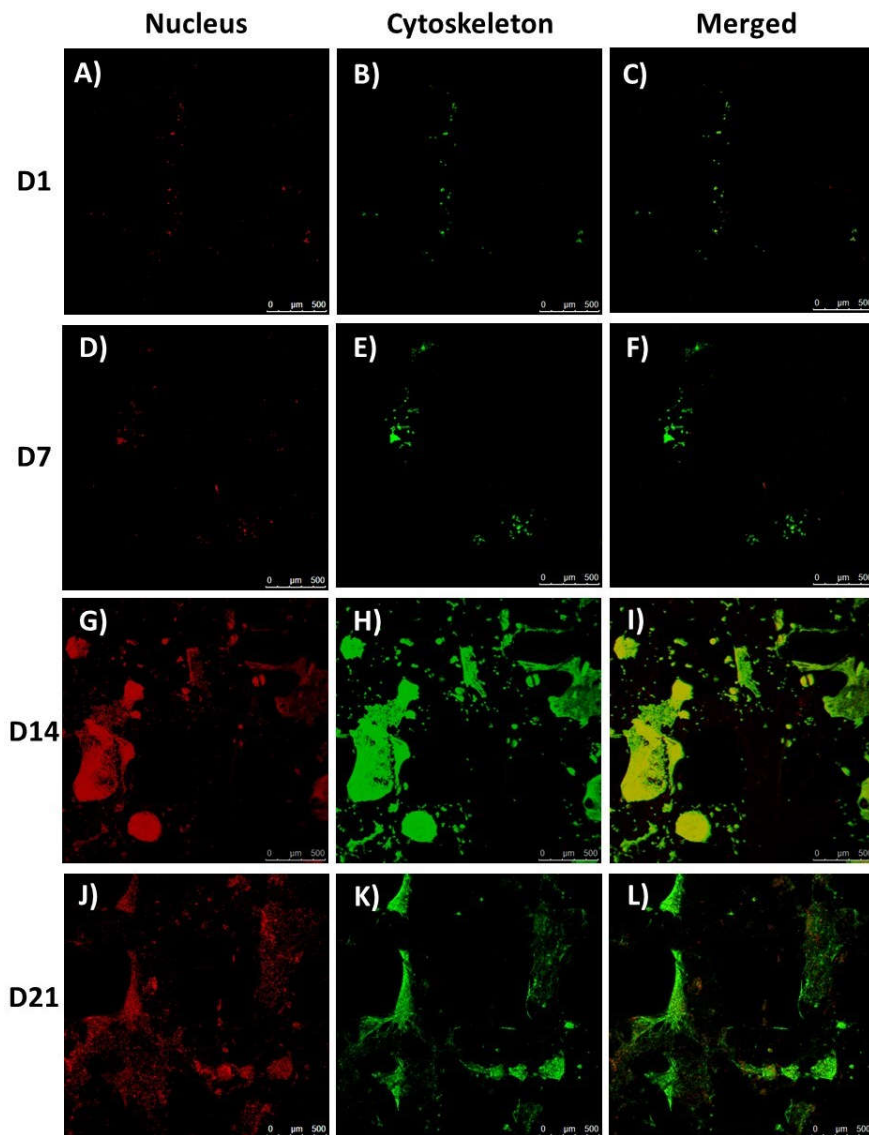
Figure 3.27. CLSM images of SCs cells on 3D printed PCL tubes over 3 weeks view from the top, 5x. A) Nucleus, B) Cytoskeleton, C) Merged image (Day 1), D) Nucleus, E) Cytoskeleton, F) Merged image (Day 7), G) Nucleus, H) Cytoskeleton, I) Merged image (Day 14), G) Nucleus, H) Cytoskeleton, I) Merged image on Day 14, G) Nucleus, H) Cytoskeleton, I) Merged image (Day 21).

Figure 3.28 shows the PC12 cells on the gelatin-PHBV (5:5) aligned fibrous mats removed from the inside of the nerve guide. Cells were attracted to this surface very well and proliferated admirably over three weeks. Alignment of these cells was apparent on Day 1, and most of the mat surfaces were covered with PC12 cells at the

end of the incubation period. This was also confirmed with the cell proliferation assay. Cell attractive properties of gelatin-PHBV mats make them very suitable for tissue engineering applications.
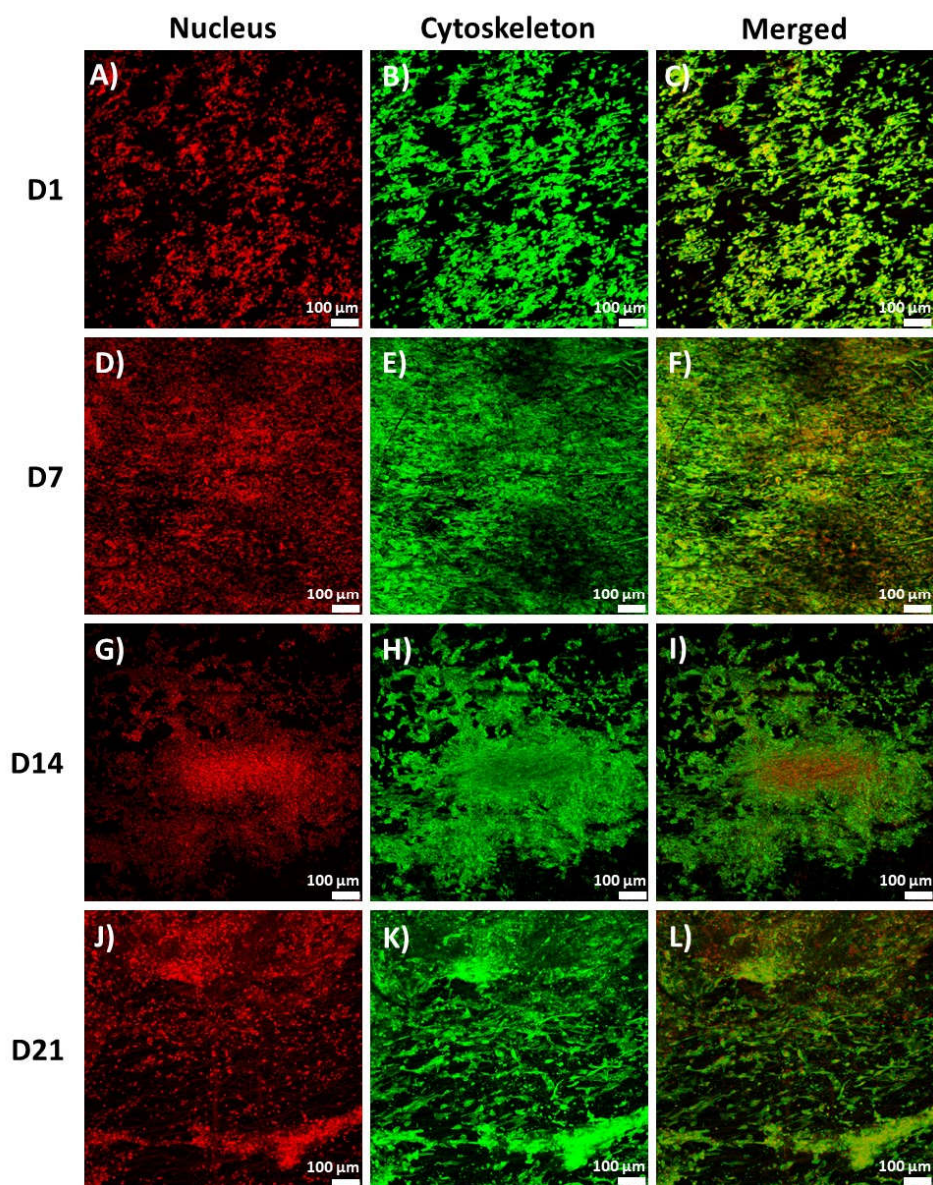
Figure 3.28. CLSM images of PC12 cells on 3D printed gelatin-PHBV mats over 3 weeks, 10x. A) Nucleus, B) Cytoskeleton, C) Merged image (Day 1), D) Nucleus, E) Cytoskeleton, F) Merged image (Day 7), G) Nucleus, H) Cytoskeleton, I) Merged image (Day 14), G) Nucleus, H) Cytoskeleton, I) Merged image (Day 14), G) Nucleus, H) Cytoskeleton, I) Merged image (Day 21).

3.5.4.3. Live-Dead Assay of PC12 Cells on ES Mats

Gelatin-PHBV aligned fibrous mats were rolled and placed into the hollow 3D printed PCL tube to form the nerve guide structure. PC12 cells were seeded on one side of these mats to mimic the proximal region of the damaged peripheral nerves. In half of the samples, Schwann cells (SCs) were seeded on the PCL exterior of the nerve guide while PC12 were on the mat to study the effect of SCs on PC12 cell migration. Live-Dead assay was conducted to study the viability of PC12 cells in the mats. PC12 cells were seen to cover the mats completely (proximal, middle, and distal) with SCs group even from D14, however, no cells were observed on the distal part of the mats without SCs group (Figure 3.29). On D21, PC12 cells had covered the mats fully with both SCs and without SCs group having less number of cells on the distal part. At the end of the incubation, all parts of the mats were covered with PC12 cells on both groups. A large fraction of cells (>95%) was alive on the gelatin-PHBV fibrous mats (Figure 3.30A). It is an indicator that inner guidance elements composed of gelatin-PHBV aligned fibrous mats can provide space for the growing neurons for the neuronal regeneration in the case of peripheral nerve injury. One significant difference was observed on D28 samples; a higher number of cells were alive in the SCs group. Figure 3.30B shows the cell number analysis on the different parts of the nerve guide in with (w SCs) or without (wo SCs) Schwann cells group. As the incubation duration was increased, the cell number increased, too. However, this analysis was made by using the CLSM micrographs of the PC12 cells, and may not represent the whole nerve guide structure. Still, it gives an idea about the general distribution of the PC12 cells on the gelatin-PHBV mats. For example, there are not any cells found on the distal part of the nerve guide on Day 14.
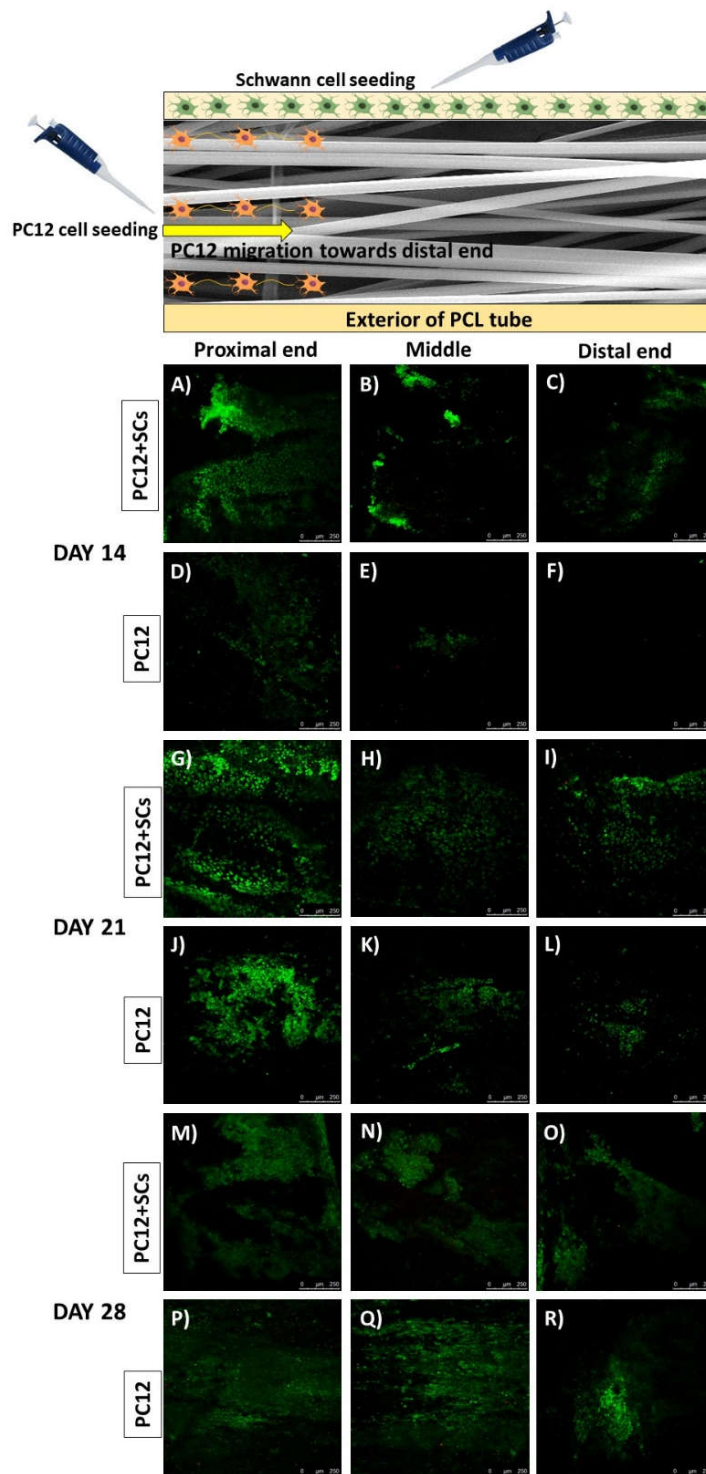
Figure 3.29. Live-Dead and Migration analysis of PC12 cells on gelatin-PHBV aligned fibrous mats. A-C) Proximal, Middle, Distal, Day 14, with SCs, D-F) Proximal, Middle, Distal, Day 14, w/o SCs, G-I) Proximal, Middle, Distal, Day 21, with SCs, J-L) Proximal, Middle, Distal, Day 21, w/o SCs, M-O) Proximal, Middle, Distal, Day 28, with SCs, P-R) Proximal, Middle, Distal, Day 28, w/o SCs.
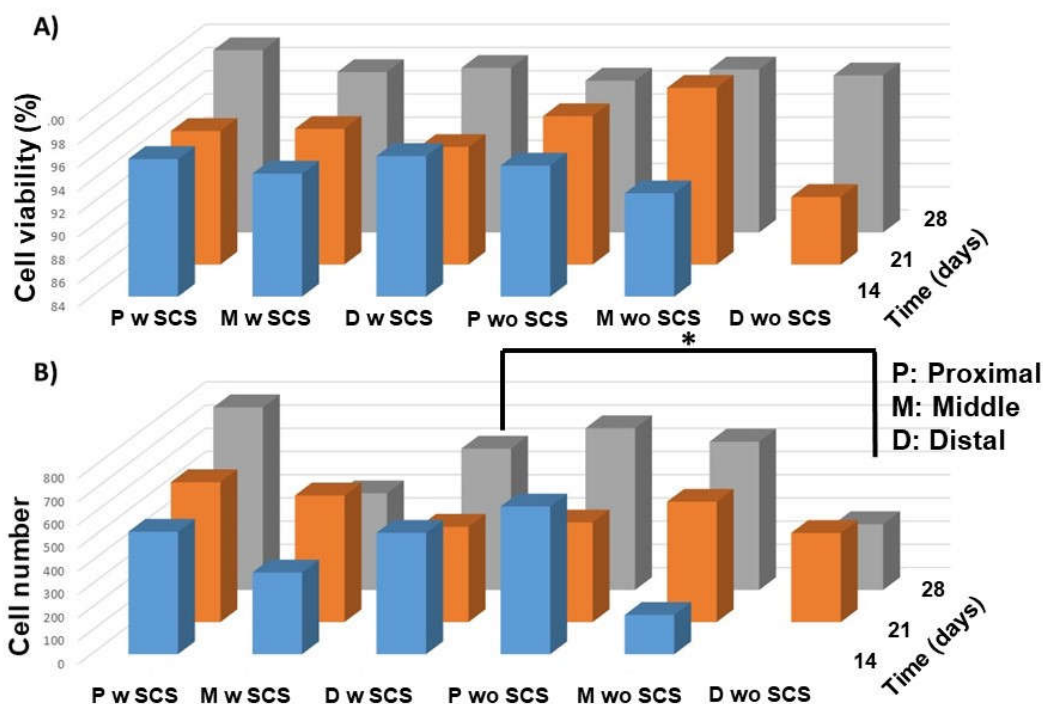
Figure 3.30. Cell viability and cell number analysis of PC12 cells by NIH, ImageJ. A) Cell viability (%) analysis of PC12 cells on D14, D21 and D28 micrographs, B) Cell number analysis of PC12 cells on D14, D21, and D28 micrographs.

3.5.4.4. Neuron-Specific Antibody Staining

Class III β-tubulin (β-III tubulin) is a microtubule element expressed in neurons and it is used as an early neuronal marker (Brat, 2010). NeuN is a neuronal nuclear antigen which is used as a late neuronal marker (Gusel'nikova and Korzhevskiy, 2015). In this study, PC12 cells (derived from a pheochromocytoma of the rat adrenal medulla) are used to represent the peripheral nerve cells. PC12 cells have the potential to differentiate into neurons in the presence of the nerve growth factor (NGF). PC12 cells were stained with both an early (β-III tubulin) and a late (NeuN) neuronal marker to study their differentiation into neurons.

As in the earlier tests, scaffolds seeded with PC12 alone and with Schwann cells (SCs) were used. Figure 3.31 (A-H) shows the beta-tubulin, cytoskeleton, and nucleus

staining of the D28 PC12 cells on gelatin-PHBV aligned mats. Analysis of antibody expression levels was studied with NIH, ImageJ program. Expression of beta-tubulin is higher with SCs group. Figure 3.31 (I-P) shows the NeuN, cytoskeleton, and nucleus staining of the D28 PC12 cells on gelatin-PHBV aligned mats. NeuN expression is 10-fold lower when compared with beta-tubulin expression, however, no difference was observed between the groups. Their difference may be more apparent as the incubation time increased since NeuN is a late neuronal marker.
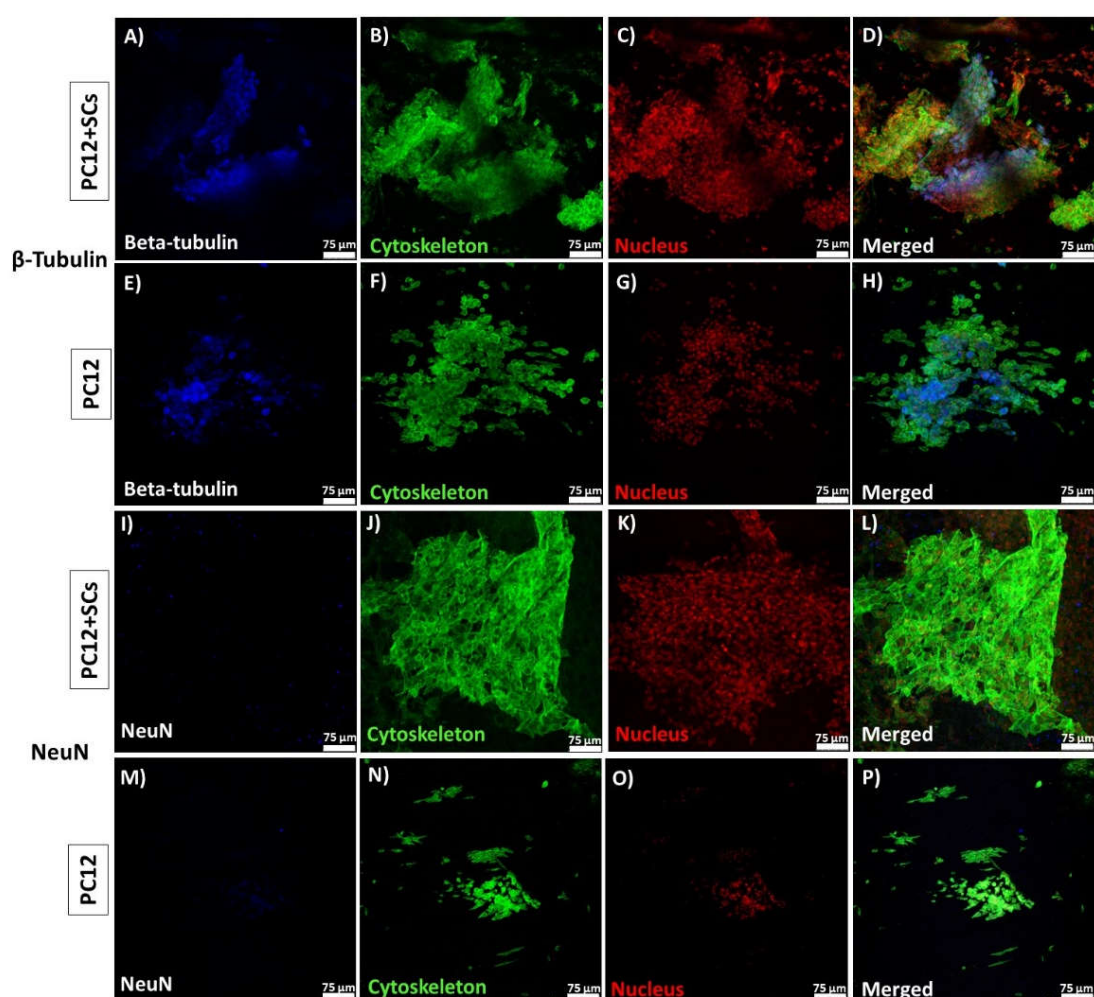
Figure 3.31. Beta-tubulin (blue), NeuN (blue), cytoskeleton (green) and nucleus (red) merged CLSM images of PC12 cells on gelatin-PHBV aligned fibrous mats on D28.

3.5.4.5. SEM of PC12-Seeded on Gelatin-PHBV Fibrous Mats

Gelatin-PHBV (1:1) aligned fiber mats were produced as inner guidance elements for the nerve guide. By this way, anisotropic nature of the nerve tissue can be mimicked. To make a complete nerve guide, these aligned structures were incorporated into the 3D printed PCL tube. PC12 cells were seeded on these mats to mimic the nerve cells. Figure 3.32 shows the PC12 cell attachment and cell-to-cell contact throughout the fibers on Day 28. Most of the mat surface is covered with PC12 cells, and neurites of these cells make connections with each other which is a good sign for neural transmission. Relatively loose network of fibers was observed most probably due to the dissolution of the gelatin from the mats which provided more space for cell growth. In another study, neurites of PC12 cells showed the parallel growth on aligned PCL fibers (Yao et al., 2009).
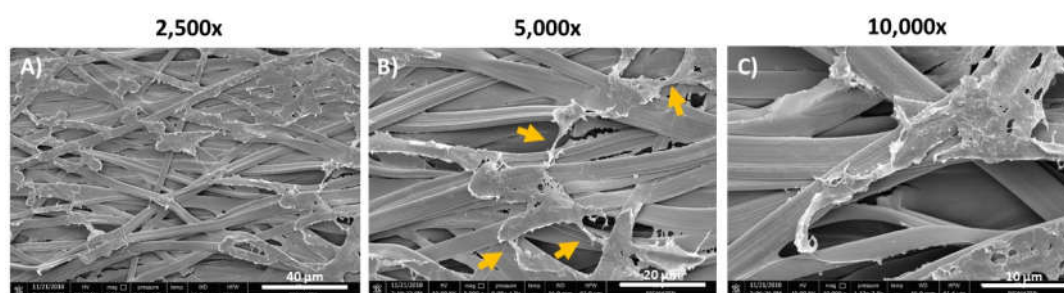
Figure 3.32. SEM micrographs of D28 PC12 cells on gelatin-PHBV mats. A) 2,500x, B) 5,000x, C) 10,000x. Arrows show cell-to-cell contact points.

3.5.4.6. Expression of Myelin Basic Protein (MBP) by Schwann Cells

In this study, Schwann cells (SCs) were seeded on the exterior of the nerve guide, a 3D printed PCL tube, to serve as support cells for neuronal regeneration. The myelin sheath functions as an insulator to greatly increase the velocity of axonal impulse conduction. MBP maintains the correct structure of myelin, interacting with the lipids in the myelin membrane and the expression of the MBP by the SCs shows the

myelination of the SCs which is an indicator of the functionalization of these cells. Myelin basic protein (MBP) is an important protein in the myelination process of the nerves (Boggs, 2006). Figure 3.33 shows the MBP, cytoskeleton, and nucleus staining of the D28 SCs on PCL tube. SCs formed colony-like formations on the fibers of the PCL tube. High expression level of MBP on the 3D printed PCL tube indicated the functionalization of SCs. The negative controls of both 3D printed PCL tube and gelatin-PHBV fibers are presented in Figure 3.34. This figure shows that there is no signal coming from the scaffolds which causes the autofluorescence. Therefore, it can be concluded that all the signals are coming from the cells.
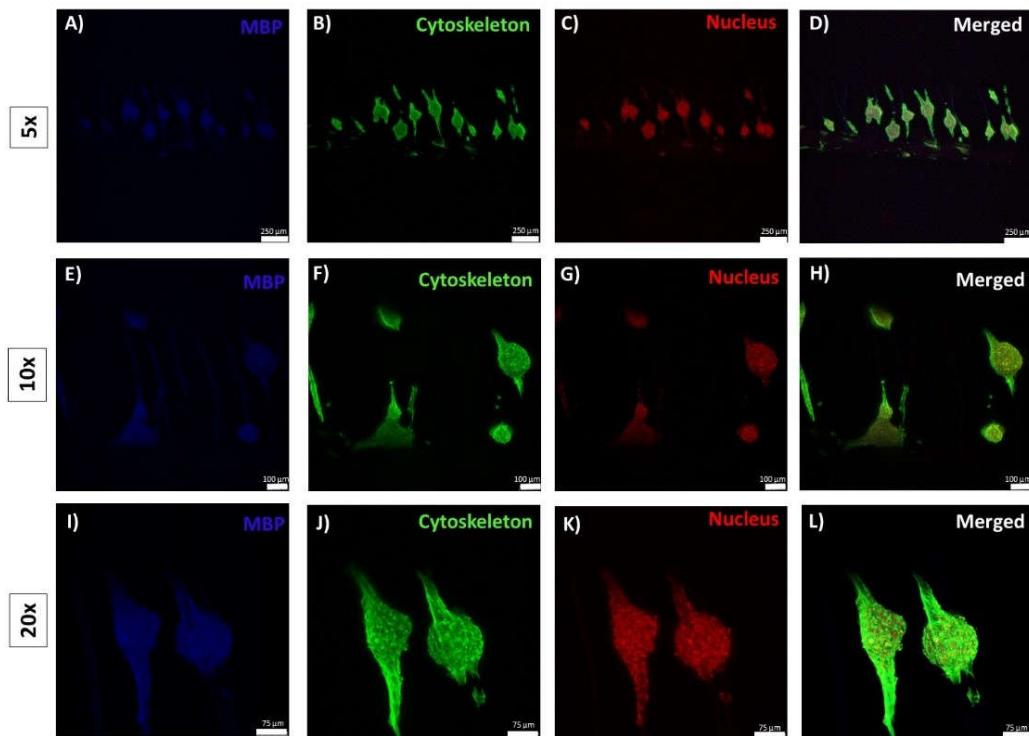
Figure 3.33. Myelin Basic Protein (MBP) (blue), cytoskeleton (green), nucleus (red), and merged CLSM images of Schwann cells seeded on PCL exterior of the nerve guide (D28).
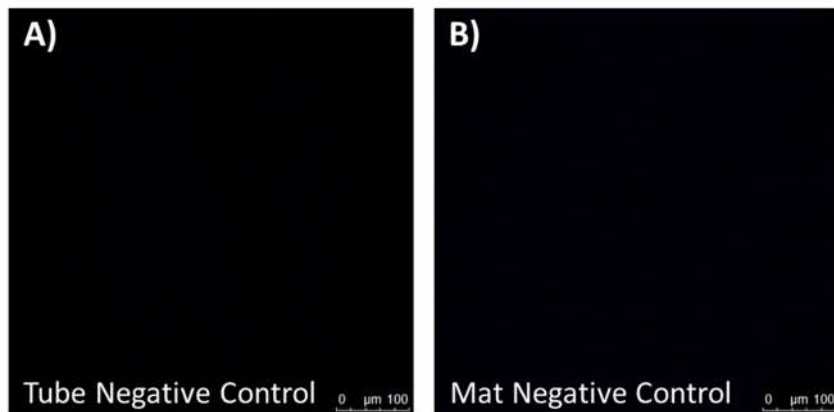
Figure 3.34. CLSM images of unstained A) PCL tube and B) Gelatin-PHBV mat from 488 channel which is used for the antibody staining.

3.5.4.7. SEM of SCs Seeded on PCL Tube

Schwann cell attachment on the 3D printed PCL surface was shown in Figure 3.35. Yellow arrows indicate the cellular connections between SCs which is very good for cell proliferation and signaling. Most of the cells protrude from one fiber into another and migrate on the surface of the PCL tube. Schwann cells interacted with the PCL fibers very nicely by forming the cellular appendages on the fiber which shows the biocompatibility of the material.
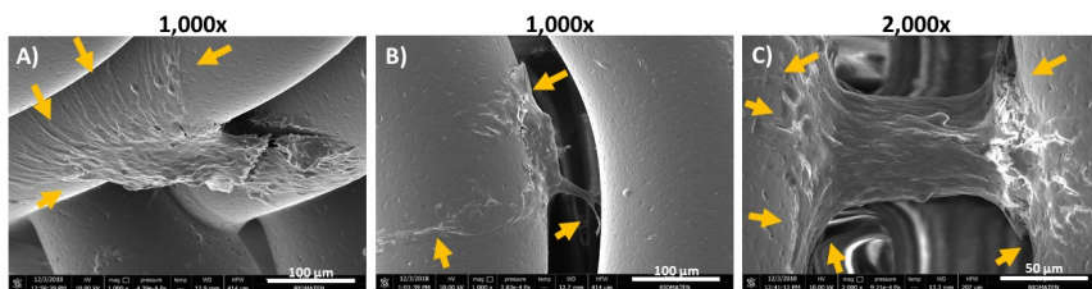
Figure 3.35. SEM micrographs of D28 Schwann cells on 3D printed PCL tube. A-B) 1,000x, C) 2,000x. Arrows show cell-to-cell contact points.

3.6. *In Vivo* Studies

The effect of the nerve guide on peripheral nerve healing was evaluated in terms of their function and also histologically in rats from whose sciatic nerves were cut. A sciatic nerve injury (10 mm long) was created in Wistar star rats and *in vivo* studies were conducted at Medical Pharmacology Department, Hacettepe University to assess the efficiency of the developed nerve guides.

3.6.1. SEM of 3D Printed PCL Nerve Guide for *In Vivo* Studies

The diameter of the PCL tubes was decreased from 5 mm to 3 mm in order to match the dimensions of the rat sciatic nerve tissue which has a diameter around of 1-2 mm. SEM shows that the average pore size of this PCL tube is 208 ± 19 μm and the average fiber diameter is 218 ± 31 μm (Figure 3.36).
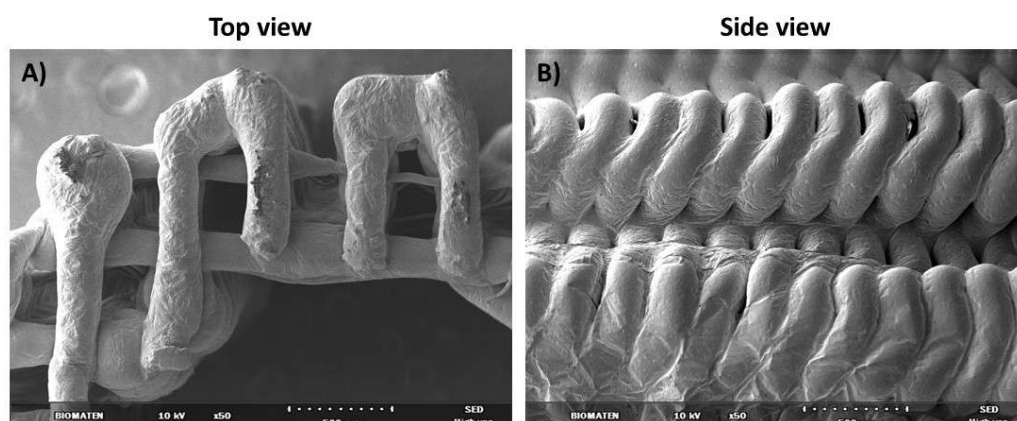
Figure 3.36. SEM micrographs of 3D printed PCL tube for *in vivo* studies, 50x. A) Top view, B) Side view.

3.6.2. Implantation of the Nerve Guides

Implantation procedure of the nerve guides to the Wistar star rats is shown in Figure 3.37. First, the surgical site is cut open, and 10 mm long sciatic nerve is dissected and the site is stiched back with 7/0 vicryl sutures. This served as the negative control

group. The other groups were 3D printed PCL tubes; 1) Hollow, 2) With gelatin-PHBV mats inserted, and 3) With gelatin-PHBV mats and seeded with Schwann cells on the exterior of the PCL tube. After the implantation of the nerve guides, the surgical site was closed with 4/0 prolene sutures. Each group had 6 animals, and they were anesthetized with intraperitoneal xylazine (90 mg/kg) + ketamine (10 mg/kg).
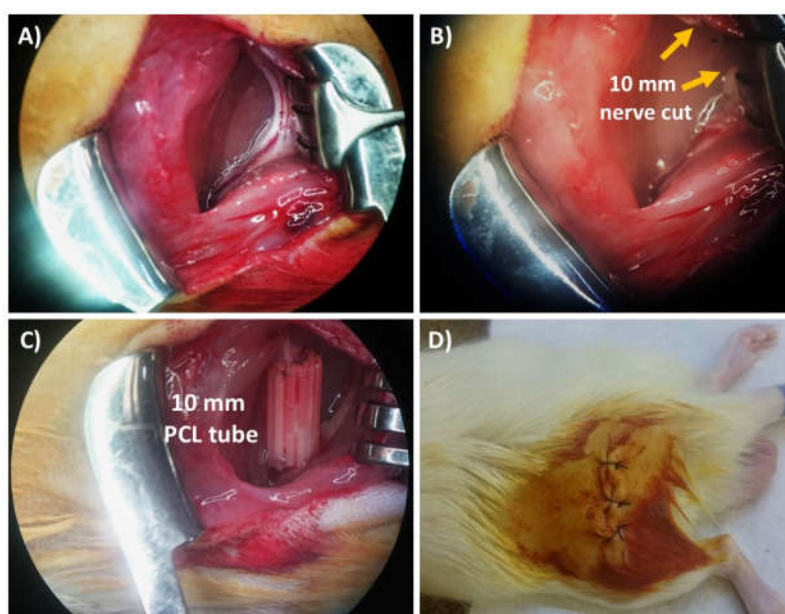
Figure 3.37. Implantation procedure of the nerve guides. A) Dissection of rat sciatic nerve, B) Removal of 10 mm sciatic nerve, C) Implantation of 10 mm hollow PCL tube, D) Closing of the surgical site. In the negative control, step C was omitted.

3.6.3. Testing of Functionality (Static Sciatic Index-Walking Track Analysis)

A footprint analysis method was developed to evaluate the degree of functional recovery in studying peripheral nerve regeneration process (de Medinaceli et al., 1982). This method was modified over the years (Bain et al., 1989). The SFI (sciatic functional index), a footprint analysis, uses three parameters of hind limb performance: Print Length (PL, heel to tip of toe 3), Intermediate Toe Spread (ITS, distance between toes 2-4) and Toe Spread (TS, distance between toes 1-5). Bervar

introduced a new parameter termed the static sciatic index (SSI) (Bervar, 2000). In this technique, both ITS and TS parameters were demonstrated to be statistically correlated with the SFI. In this study, SSI was used as an indication of the functional recovery after sciatic nerve injury. SSI index was calculated according to the following equations:

$$TSF = (OTS - NTS) / NTS \tag{13}$$

$$ITSF = (OITS - NITS) / NITS \tag{14}$$

$$SSI\ index = (108.44 \times TSF) + (31.85 \times ITSF) - 5.49 \tag{15}$$

TSF: toe spread factor, OTS: operated side toe spread, NTS: non-operated side toe spread, ITSF: intermediate toe spread factor, OITS: operated side intermediate toe spread, NITS: nonoperated side intermediate toe spread, SSI: static sciatic index.

After the implantation of the nerve guides, static sciatic index (SSI) values of the four different groups (n=4) were calculated for each time point. TSF, ITSF, and SSI values of different groups were presented in Table 3.5. Different types of groups can be summarized as Group I: empty defect, Group II: Tubular nerve guide at the defect site, Group III: Tubular nerve guide with the mat at the defect site, Group IV: Tubular nerve guide with the mat and the Schwann cells at the defect site.

Table 3.5. *SSI scores of different in vivo groups.*

Group Number	TSF				ITSF				SSI			
	D7	D14	D21	D28	D7	D14	D21	D28	D7	D14	D21	D28
I	-0,61	-0,63	-0,60	-0,64	-0,48	-0,51	-0,60	-0,45	-87	-90	-84	-91
II	-0,56	-0,60	-0,62	-0,58	-0,46	-0,51	-0,62	-0,51	-81	-87	-90	-85
III	-0,55	-0,59	-0,58	-0,60	-0,43	-0,44	-0,52	-0,48	-79	-83	-83	-86
IV	-0,57	-0,58	-0,58	-0,58	-0,48	-0,43	-0,61	-0,51	-82	-82	-90	-84

Figure 3.38 shows SSI scores of different groups over 28 days. There is a significant difference between the Group I, II and IV on Day 28. This shows that there is a functional recovery in the groups having PCL tube and PCL tube, gelatin-PHBV mat, and Schwann cells which shows the efficiency of these nerve guides to repair a sciatic nerve injury. No significant difference was found in Group III when compared with

the control (Group I). This was not expected because the mat was incorporated into the nerve conduit to guide the neurons. However, no major recovery was observed in terms of action potential propagation. This might be a result of the blockage of the cell growth inside the PCL tube.
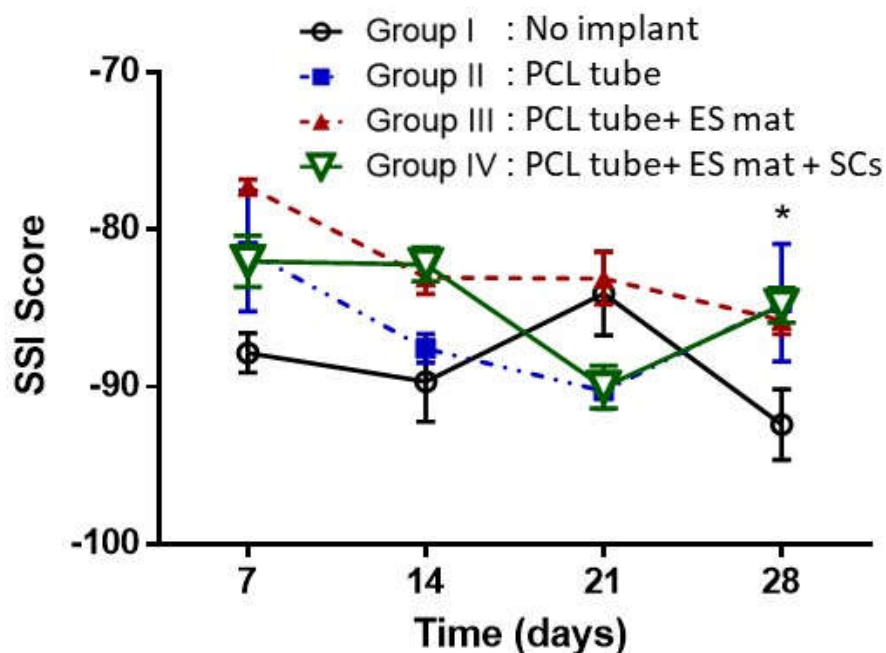
Figure 3.38. Static sciatic index (SSI) scores of *in vivo* samples over 28 days. Statistical differences (* $p \leq 0.05$, **$p \leq 0.01$, ***$p \leq 0.001$, ****$p \leq 0.0001$) are indicated.

3.6.4. Electrophysiological Measurements

Electrophysiological measurements of amplitude % and nerve conduction velocity of the different groups were conducted (Figure 3.39). Positive control was the untreated rat sciatic peripheral nerve, and its amplitude (%) was taken as 100. When compared with the negative control group, the PCL tube group presented a statistically significant improvement. However, other groups did not show any significant improvement.

This situation is the same for the nerve conduction velocity. PCL tube including mat and SCs has also improved nerve conduction velocity compared with injury. These results are consistent with static sciatic index (SSI) values. Action potential amplitudes of Group IV (PCL tube+ES mat+SCs) displayed partial recovery. And newly rejoined axons had conduction velocities almost comparable with the controls showing that SCs improved recovery despite the presence of the mat. Tubes having gelatin-PHBV mats (Group III) did not show any significant improvement. Mats may not be properly placed in the PCL tube due to their thin nature which caused this problem.
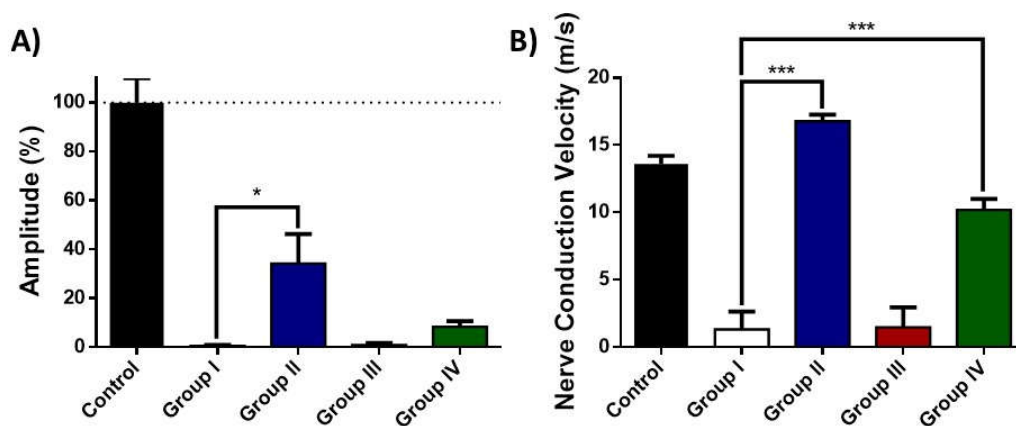
Figure 3.39. Electrophysiological measurements of *in vivo* studies on D28. A) Amplitude (%) and B) Nerve conduction velocity values of different groups. Statistical differences (* $p \leq 0.05$, **$p \leq 0.01$, ***$p \leq 0.001$, ****$p \leq 0.0001$) are indicated.

3.6.5. Histological Analyses

Histological staining with hematoxylin and eosin, and Masson's trichrome were performed to study the integration of the scaffolds into the nervous tissue and to assess the inner architecture of the nerve guides such as placement of the mats.

3.6.5.1. Hematoxylin and Eosin (HE) Staining

Hematoxylin is a dark blue stain which is basic positive. It binds to basophilic substances such as DNA and RNA, which are acidic and negatively charged (Fischer et al., 2008). Eosin is a red stain which is acidic and negative. Therefore, it binds to acidophilic substances such as positively charged amino acid side chains such as lysine, arginine. In hematoxylin and eosin staining, hematoxylin stains the nucleus (purple) and eosin stains the cytoplasm (pink) of the cells. Hematoxylin-eosin staining results in Figure 3.40 showed that tissue was distrupted and there was an irregular, improper, slight tissue formation when there is no implant. On the other hand, there was no significant tissue damage around implants and there was a significant tissue growth around and inside the PCL tube in all implanted samples. Fibrous tissue growth and blood vessel integration were observed around all implants. Blood vessels were extensively seen particularly in the presence of Schwann cells. The axonal growth was observed especially in groups of PCL tube both with and without electrospun mat. However, more specific types of staining are needed for the identification of the nerve tissue.
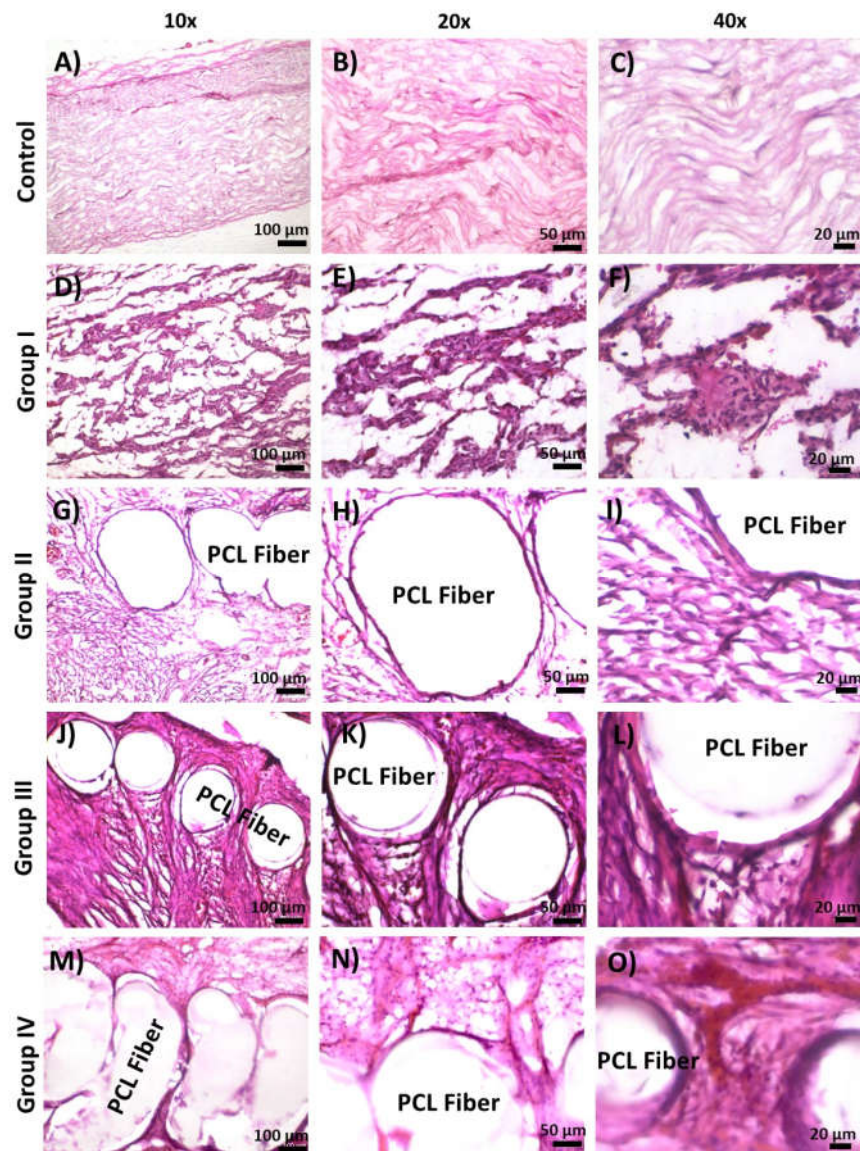
Figure 3.40. Hematoxylin and Eosin staining of the A-C) Control, D-F) Group I, G-I) Group II, J-L) Group III, and M-O) Group IV on D28.

3.6.5.2. Masson's Trichrome (MTC) Staining

Trichrome staining differentiates the collagen fibers of the ECM from the other types of structures such as epithelial tissue, muscles, parenchyma (Carriel et al., 2014). Masson's trichrome (MTC) is the most common trichrome method in pathology and muscle histology. It is occasionally used for the histological analysis of peripheral

nerve. The quality of the histology of peripheral nerve with MTC is better than HE since it also highlights the connective tissue (Raimondo et al., 2009). In this study, MTC was used to visualize myelin sheaths (purple-red). A thin membrane of fibrous tissue (blue) covered the implanted nerve guides (Figure 3.41).
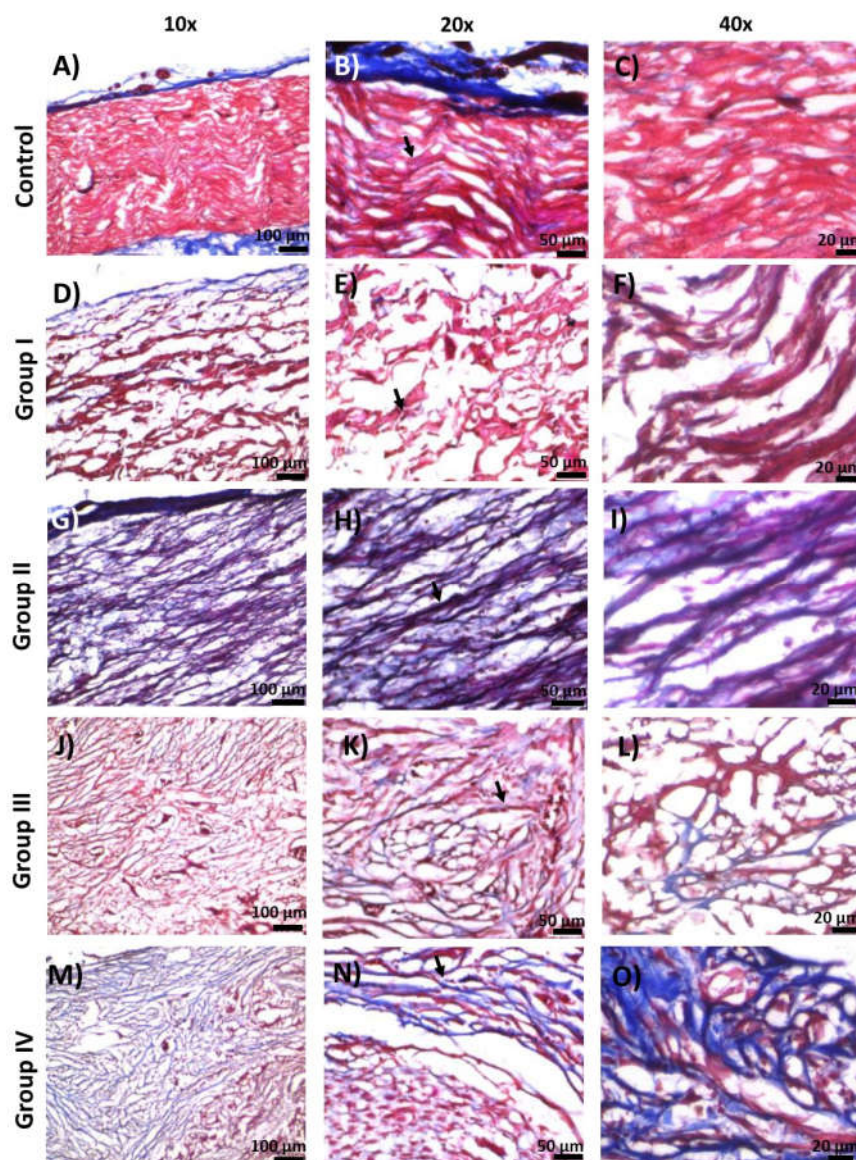
Figure 3.41. Masson's trichrome staining of the A-C) Control, D-F) Group I, G-I) Group II, J-L) Group III, and M-O) Group IV on D28 .

CHAPTER 4

CONCLUSION

In this study, it was aimed to produce a composite nerve guide which has inner guidance elements to provide peripheral nerve regeneration. For this purpose, the exterior (GelMA-pHEMA hydrogels and 3D printed PCL tube), and interior (gelatin-PHBV) part of the nerve guide were tested for their suitability for peripheral nerve tissue engineering. It was found that their properties such as porosity, pore size, water content, mechanical strength, wettability, and alignment were suitable. Both GelMA-pHEMA hydrogels and PCL tube were studied under *in vitro* conditions, and they supported Schwann cell attachment and proliferation. PC12 cells were seeded on gelatin-PHBV5 aligned fibrous mats, and cells aligned themselves along the fibers. Then, these two structures (3D printed PCL tube and gelatin-PHBV mats) were combined together to produce a whole nerve guide structure. Gelatin-PHBV aligned fibrous mats were rolled into a tubular shape and put into the 3D printed PCL tube. SCs were seeded on the outer PCL part, and PC12 cells were seeded on the inner gelatin-PHBV part. Cell attachment and proliferation on the nerve guide was quite good over three weeks. Differentiation of PC12 cells was observed on gelatin-PHBV fibers with the increased expression of neuronal markers. *In vivo* studies were conducted with different types of nerve guides. Significant improvements in terms of functionality and conductivity were observed with the groups having 3D printed PCL tube and PCL tube, gelatin-PHBV mat, Schwann cells. Histological studies showed the integration of these nerve guides into the nervous tissue which proves the biocompatibility of the guides. In conclusion, these developed nerve guides have a high potential for the treatment of peripheral nerve injuries.

REFERENCES

Abasi, S., Aggas, J. R., Guiseppi-Elie, A. (2019). Physiochemical and morphological dependent growth of NIH/3T3 and PC-12 on polyaniline-chloride/chitosan bionanocomposites. Materials Science and Engineering: C, 99, 1304-1312.

Abd Razak, S. I., Wahab, I. F., Fadil, F., Dahli, F. N., Md Khudzari, A. Z., Adeli, H. (2015). A Review of Electrospun Conductive Polyaniline Based Nanofiber Composites and Blends: Processing Features, Applications, and Future Directions. Advances in Materials Science and Engineering, 2015, 1-19.

Abzan, N., Kharaziha, M., Labbaf, S., Saeidi, N. (2018). Modulation of the mechanical, physical and chemical properties of polyvinylidene fluoride scaffold via non-solvent induced phase separation process for nerve tissue engineering applications. European Polymer Journal, 104, 115-127.

Afjeh-Dana, E., Naserzadeh, P., Nazari, H., Mottaghitalab, F., Shabani, R., Aminii, N., Mehravi, B., Rostami, F. T., Joghataei, M. T., Mousavizadeh, K., Ashtari, K. (2019). Gold nanorods reinforced silk fibroin nanocomposite for peripheral nerve tissue engineering applications. International Journal of Biological Macromolecules, 129, 1034-1039.

Agenor, A., Dvoracek, L., Leu, A., Hunter, D. A., Newton, P., Yan, Y., Johnson, P. J., Mackinnon, S. E., Moore, A. M., Wood, M. D. (2017). Hyaluronic acid/carboxymethyl cellulose directly applied to transected nerve decreases axonal outgrowth. Journal of Biomedical Materials Research Part B: Applied Biomaterials, 105(3), 568-574.

Ahmed, Z., Underwood, S., Brown, R. A. (2003). Nerve Guide Material Made from Fibronectin: Assessment of in Vitro Properties. Tissue Engineering, 9(2), 219-231.

Alagoz, A. S., Rodriguez-Cabello, J. C., Hasirci, V. (2018). PHBV wet-spun scaffold coated with ELR-REDV improves vascularization for bone tissue engineering. Biomedical Materials, 13(5), 055010.

Allbright, K. O., Bliley, J. M., Havis, E., Kim, D.-Y., Dibernardo, G. A., Grybowski, D., Waldner, M., James, I. B., Sivak, W. N., Rubin, J. P., Marra, K. G. (2018). Delivery of adipose-derived stem cells in poloxamer hydrogel improves peripheral nerve regeneration. Muscle & Nerve, 58(2), 251-260.

Alluin, O., Wittmann, C., Marqueste, T., Chabas, J.-F., Garcia, S., Lavaut, M.-N., Guinard, D., Feron, F., Decherchi, P. (2009). Functional recovery after peripheral nerve injury and implantation of a collagen guide. Biomaterials, 30(3), 363-373.

Almeida, J. F., Ferreira, P., Lopes, A., Gil, M. H. (2011). Photocrosslinkable biodegradable responsive hydrogels as drug delivery systems. International Journal of Biological Macromolecules, 49(5), 948-954.

Almine, J. F., Bax, D. V., Mithieux, S. M., Nivison-Smith, L., Rnjak, J., Waterhouse, A., Wise, S. G., Weiss, A. S. (2010). Elastin-based materials. Chemical Society Reviews, 39(9), 3371-3379.

Aloe, L., Rocco, M. L., Balzamino, B. O., Micera, A. (2015). Nerve Growth Factor: A Focus on Neuroscience and Therapy. Current Neuropharmacology, 13(3), 294-303.

Alves, M. I., Macagnan, K. L., Rodrigues, A. A., de Assis, D. A., Torres, M. M., de Oliveira, P. D., Furlan, L., Vendruscolo, C. T., Moreira, A. da S. (2017). Poly(3-hydroxybutyrate)-P(3HB): Review of Production Process Technology. Industrial Biotechnology, 13(4), 192-208.

Amoh, Y., Aki, R., Hamada, Y., Niiyama, S., Eshima, K., Kawahara, K., Sato, Y., Tani, Y., Hoffman, R. M., Katsuoka, K. (2012). Nestin-positive hair follicle pluripotent stem cells can promote regeneration of impinged peripheral nerve injury. The Journal of Dermatology, 39(1), 33-38.

Anderson, M., Shelke, N. B., Manoukian, O. S., Yu, X., McCullough, L. D., Kumbar, S. G. (2015). Peripheral Nerve Regeneration Strategies: Electrically Stimulating Polymer Based Nerve Growth Conduits. Critical Reviews in Biomedical Engineering, 43(2-3), 131-159.

Ao, Q., Fung, C.-K., Yat-Ping Tsui, A., Cai, S., Zuo, H.-C., Chan, Y.-S., Kwok-Yan Shum, D. (2011). The regeneration of transected sciatic nerves of adult rats using chitosan nerve conduits seeded with bone marrow stromal cell-derived Schwann cells. Biomaterials, 32(3), 787-796.

Arslantunali, D., Dursun, T., Yucel, D., Hasirci, N., Hasirci, V. (2014a). Peripheral nerve conduits: technology update. Medical Devices: Evidence and Research, 7, 405-424.

Arslantunali, D., Budak, G., Hasirci, V. (2014b). Multiwalled CNT-pHEMA composite conduit for peripheral nerve repair. Journal of Biomedical Materials Research. Part A, 102(3), 828–841.

Aslam, M., Kalyar, M. A., Raza, Z. A. (2018). Polyvinyl alcohol: A review of research status and use of polyvinyl alcohol based nanocomposites. Polymer Engineering & Science, 58(12), 2119-2132.

Asrar, J., Hill, J. C. (2002). Biosynthetic processes for linear polymers. Journal of Applied Polymer Science, 83(3), 457-483.

Baghaban-Eslaminejad, M., Oryan, A., Kamali, A., Moshiri, A. (2017). The role of nanomedicine, nanotechnology, and nanostructures on oral bone healing, modeling, and remodeling. Nanostructures for Oral Medicine, 777-832.

Bain, J. R., Mackinnon, S. E., Hunter, D. A. (1989). Functional evaluation of complete sciatic, peroneal, and posterior tibial nerve lesions in the rat. Plastic and Reconstructive Surgery, 83(1), 129-138.

Bajpai, A. K., Kankane, S. (2007). Preparation and characterization of macroporous poly(2-hydroxyethyl methacrylate)-based biomaterials: Water sorption property and in vitro blood compatibility. Journal of Applied Polymer Science, 104(3), 1559-1571.

Bakhtiyari, S. S. E., Karbasi, S., Monshi, A., Montazeri, M. (2016). Evaluation of the effects of nano-TiO2 on bioactivity and mechanical properties of nano bioglass-P3HB composite scaffold for bone tissue engineering. Journal of Materials Science: Materials in Medicine, 27(1), 2.

Barbon, S., Stocco, E., Negro, A., Dalzoppo, D., Borgio, L., Rajendran, S., Grandi, F., Porzionato, A., Macchi, V., De Caro, R., Parnigotto, P. P., Grandi, C. (2016). In vitro assessment of TAT — Ciliary Neurotrophic Factor therapeutic potential for peripheral nerve regeneration. Toxicology and Applied Pharmacology, 309, 121-128.

Barnes, D. W., Singh, N. N., Helmrich, A., Barnes, D. W. (2001). Neural Cell Lines Kaoru Murayama, Natalia N. Singh, Angela Helmrich. In Protocols for Neural Cell Culture (pp. 219–228). New Jersey: Humana Press.

Bashur, C. A., Shaffer, R. D., Dahlgren, L. A., Guelcher, S. A., Goldstein, A. S. (2009). Effect of Fiber Diameter and Alignment of Electrospun Polyurethane Meshes on Mesenchymal Progenitor Cells. Tissue Engineering Part A, 15(9), 2435-2445.

Bassilios Habre, S., Bond, G., Jing, X. L., Kostopoulos, E., Wallace, R. D., Konofaos, P. (2018). The Surgical Management of Nerve Gaps. Annals of Plastic Surgery, 80(3), 252-261.

Belanger, K., Dinis, T. M., Taourirt, S., Vidal, G., Kaplan, D. L., Egles, C. (2016). Recent Strategies in Tissue Engineering for Guided Peripheral Nerve Regeneration. Macromolecular Bioscience, 16(4), 472-481.

Ben Halima, N. (2016). Poly(vinyl alcohol): review of its promising applications and insights into biodegradation. RSC Advances, 6(46), 39823–39832.

Bervar, M. (2000). Video analysis of standing--an alternative footprint analysis to assess functional loss following injury to the rat sciatic nerve. Journal of Neuroscience Methods, 102(2), 109-116.

Billiet, T., Gevaert, E., De Schryver, T., Cornelissen, M., Dubruel, P. (2014). The 3D printing of gelatin methacrylamide cell-laden tissue-engineered constructs with high cell viability. Biomaterials, 35(1), 49-62.

Bliley, J. M., Sivak, W. N., Minteer, D. M., Tompkins-Rhoades, C., Day, J., Williamson, G., Liao, H. T., Marra, K. G. (2015). Ethylene Oxide Sterilization Preserves Bioactivity and Attenuates Burst Release of Encapsulated Glial Cell Line

Derived Neurotrophic Factor from Tissue Engineered Nerve Guides For Long Gap Peripheral Nerve Repair. ACS Biomaterials Science & Engineering, 1(7), 504-512.

Bloch, J., Fine, E. G., Bouche, N., Zurn, A. D., Aebischer, P. (2001). Nerve Growth Factor- and Neurotrophin-3-Releasing Guidance Channels Promote Regeneration of the Transected Rat Dorsal Root. Experimental Neurology, 172(2), 425-432.

Boggs, J. M. (2006). Myelin basic protein: a multifunctional protein. Cellular and Molecular Life Sciences, 63(17), 1945-1961.

Boriani, F., Fazio, N., Bolognesi, F., Pedrini, F. A., Marchetti, C., Baldini, N. (2019). Noncellular Modification of Acellular Nerve Allografts for Peripheral Nerve Reconstruction: A Systematic Critical Review of the Animal Literature. World Neurosurgery, 122, 692-703.

Borschel, G. H., Kia, K. F., Kuzon, W. M., Dennis, R. G. (2003). Mechanical properties of acellular peripheral nerve. Journal of Surgical Research, 114(2), 133-139.

Bozkurt, A., Boecker, A., Tank, J., Altinova, H., Deumens, R., Dabhi, C., Tolba, R., Weis, J., Brook, G. A., Pallua, N., van Neerven, S. G. A. (2016). Efficient bridging of 20 mm rat sciatic nerve lesions with a longitudinally micro-structured collagen scaffold. Biomaterials, 75, 112-122.

Bozkurt, Ahmet, Tholl, S., Wehner, S., Tank, J., Cortese, M., O'Dey, D., Deumens, R., Lassner, F., Schügner, F., Gröger, A., Smeets, R., Brook, G., Pallua, N. (2008). Evaluation of functional nerve recovery with Visual-SSI-A novel computerized approach for the assessment of the static sciatic index (SSI). Journal of Neuroscience Methods, 170(1), 117-122.

Brat, D. J. (2010). Neuronal and Glioneuronal Neoplasms. In Practical Surgical Neuropathology: A Diagnostic Approach (pp. 125–150). Churchill Livingstone.

Brinkman, W. T., Nagapudi, K., Thomas, B. S., Chaikof, E. L. (2003). Photo-Cross-Linking of Type I Collagen Gels in the Presence of Smooth Muscle Cells: Mechanical Properties, Cell Viability, and Function. Biomacromolecules, 4(4), 890-895.

Bukhari, S. N. A., Roswandi, N. L., Waqas, M., Habib, H., Hussain, F., Khan, S., Sohail, M., Ramli, N. A., Thu, H. E., Hussain, Z. (2018). Hyaluronic acid, a promising skin rejuvenating biomedicine: A review of recent updates and pre-clinical and clinical investigations on cosmetic and nutricosmetic effects. International Journal of Biological Macromolecules, 120, 1682-1695.

Caon, M. (2018). Nervous System. In Examination Questions and Answers in Basic Anatomy and Physiology (pp. 405–473). Cham: Springer International Publishing.

Carnevale, G., Pisciotta, A., Riccio, M., Bertoni, L., De Biasi, S., Gibellini, L., Zordani, A., Cavallini, G. M., La Sala, G. B., Bruzzesi, G., Ferrari, A., Cossarizza, A., de Pol, A. (2018). Human dental pulp stem cells expressing STRO-1, c-kit and CD34

markers in peripheral nerve regeneration. Journal of Tissue Engineering and Regenerative Medicine, 12(2), e774–e785.

Carriel, V., Garzón, I., Alaminos, M., Cornelissen, M. (2014). Histological assessment in peripheral nerve tissue engineering. Neural Regeneration Research, 9(18), 1657-1660.

Carroll, S. L., Worley, S. H. (2017). Wallerian Degeneration. Reference Module in Neuroscience and Biobehavioral Psychology.

Carvalho, C. R., Wrobel, S., Meyer, C., Brandenberger, C., Cengiz, I. F., López-Cebral, R., Silva-Correia, J., Ronchi, G., Reis, R. L., Grothe, C., Oliveira, J. M., Haastert-Talini, K. (2018). Gellan Gum-based luminal fillers for peripheral nerve regeneration: an in vivo study in the rat sciatic nerve repair model. Biomaterials Science, 6(5), 1059-1075.

Cattin, A.-L., Burden, J. J., Van Emmenis, L., Mackenzie, F. E., Hoving, J. J. A., Garcia Calavia, N., Guo, Y., McLaughlin, M., Rosenberg, L. H., Quereda, V., Jamecna, D., Napoli, I., Parrinello, S., Enver, T., Ruhrberg, C., Lloyd, A. C. (2015). Macrophage-Induced Blood Vessels Guide Schwann Cell-Mediated Regeneration of Peripheral Nerves. Cell, 162(5), 1127-1139.

Chang, J.-Y., Ho, T.-Y., Lee, H.-C., Lai, Y.-L., Lu, M.-C., Yao, C.-H., Chen, Y.-S. (2009). Highly Permeable Genipin-Cross-linked Gelatin Conduits Enhance Peripheral Nerve Regeneration. Artificial Organs, 33(12), 1075-1085.

Chang, J.-Y., Lin, J.-H., Yao, C.-H., Chen, J.-H., Lai, T.-Y., Chen, Y.-S. (2007). In Vivo Evaluation of a Biodegradable EDC/NHS-Cross-Linked Gelatin Peripheral Nerve Guide Conduit Material. Macromolecular Bioscience, 7(4), 500-507.

Chen, M.-H., Chen, P.-R., Chen, M.-H., Hsieh, S.-T., Huang, J.-S., Lin, F.-H. (2006). An in vivo study of tricalcium phosphate and glutaraldehyde crosslinking gelatin conduits in peripheral nerve repair. Journal of Biomedical Materials Research Part B: Applied Biomaterials, 77B(1), 89-97.

Chen, Y.-S., Chang, J.-Y., Cheng, C.-Y., Tsai, F.-J., Yao, C.-H., Liu, B.-S. (2005). An in vivo evaluation of a biodegradable genipin-cross-linked gelatin peripheral nerve guide conduit material. Biomaterials, 26(18), 3911-3918.

Chijimatsu, R., Ikeya, M., Yasui, Y., Ikeda, Y., Ebina, K., Moriguchi, Y., Shimomura, K., Hart, D. A., Hideki, Y., Nakamura, N. (2017). Characterization of Mesenchymal Stem Cell-Like Cells Derived From Human iPSCs via Neural Crest Development and Their Application for Osteochondral Repair. Stem Cells International, 2017, 1-18.

Chin Ang, K., Fai Leong, K., Kai Chua, C., Chandrasekaran, M. (2006). Investigation of the mechanical properties and porosity relationships in fused deposition modelling-fabricated porous structures. Rapid Prototyping Journal, 12(2), 100-105.

Chung, T.-W., Yang, M.-C., Tseng, C.-C., Sheu, S.-H., Wang, S.-S., Huang, Y.-Y., Chen, S.-D. (2011). Promoting regeneration of peripheral nerves in-vivo using new PCL-NGF/Tirofiban nerve conduits. Biomaterials, 32(3), 734-743.

Coskun, S., Korkusuz, F., Hasirci, V. (2005). Hydroxyapatite reinforced poly (3-hydroxybutyrate) and poly (3-hydroxybutyrate-co-3-hydroxyvalerate) based degradable composite bone plate. Journal of Biomaterials Science, Polymer Edition, 16(12), 1485-1502.

Cui, L., Jiang, J., Wei, L., Zhou, X., Fraser, J. L., Snider, B. J., Yu, S. P. (2008). Transplantation of Embryonic Stem Cells Improves Nerve Repair and Functional Recovery After Severe Sciatic Nerve Axotomy in Rats. Stem Cells, 26(5), 1356-1365.

Das, K., Srivastava, A. (2019). Nerve conduits as replacements of autografts in peripheral nerve surgery: Still a work in progress. Neurology India, 67(7), 115-117.

Das, S., Sharma, M., Saharia, D., Sarma, K. K., Muir, E. M., Bora, U. (2017). Electrospun silk-polyaniline conduits for functional nerve regeneration in rat sciatic nerve injury model. Biomedical Materials, 12(4), 045025.

de Medinaceli, L., Freed, W. J., Wyatt, R. J. (1982). An index of the functional condition of rat sciatic nerve based on measurements made from walking tracks. Experimental Neurology, 77(3), 634-643.

Deleyto, E., Lasso, J. M. (2017). An Overview of Peripheral Nerve Xenotransplantation-Present Status and Future Directions. J Dermatol Plast Surg, 2(3), 1018.

Demirbilek, M., Sakar, M., Karahaliloğlu, Z., Erdal, E., Yalçın, E., Bozkurt, G., Korkusuz, P., Bilgiç, E., Temuçin, Ç. M., Denkbaş, E. B. (2015). Aligned bacterial PHBV nanofibrous conduit for peripheral nerve regeneration. Artificial Cells, Nanomedicine, and Biotechnology, 43(4), 243-251.

Ding, T., Lu, W. W., Zheng, Y., Li, Z., Pan, H., Luo, Z. (2011). Rapid repair of rat sciatic nerve injury using a nanosilver-embedded collagen scaffold coated with laminin and fibronectin. Regenerative Medicine, 6(4), 437-447.

Dinis, T. M., Elia, R., Vidal, G., Dermigny, Q., Denoeud, C., Kaplan, D. L., Egles, C., Marin, F. (2015). 3D multi-channel bi-functionalized silk electrospun conduits for peripheral nerve regeneration. Journal of the Mechanical Behavior of Biomedical Materials, 41, 43-55.

Dixon, A. R., Jariwala, S. H., Bilis, Z., Loverde, J. R., Pasquina, P. F., Alvarez, L. M. (2018). Bridging the gap in peripheral nerve repair with 3D printed and bioprinted conduits. Biomaterials, 186, 44-63.

Dong, C., Lv, Y., Dong, C., Lv, Y. (2016). Application of Collagen Scaffold in Tissue Engineering: Recent Advances and New Perspectives. Polymers, 8(2), 42.

Dragusin, D.-M., Van Vlierberghe, S., Dubruel, P., Dierick, M., Van Hoorebeke, L., Declercq, H. A., Cornelissen, M. M., Stancu, I.-C. (2012). Novel gelatin–PHEMA porous scaffolds for tissue engineering applications. Soft Matter, 8(37), 9589-9602.

Du, J., Chen, H., Qing, L., Yang, X., Jia, X. (2018). Biomimetic neural scaffolds: a crucial step towards optimal peripheral nerve regeneration. Biomaterials Science, 6(6), 1299-1311.

Dursun Usal, T., Yucel, D., Hasirci, V. (2018). Differentiation of BMSCs into Nerve Precursor Cells on Fiber-Foam Constructs for Peripheral Nerve Tissue Engineering. Biology, 11(2), 119-130.

Dursun Usal, T., Yucel, D., Hasirci, V. (2019). A novel GelMA-pHEMA hydrogel nerve guide for the treatment of peripheral nerve damages. International Journal of Biological Macromolecules, 121, 699-706.

Ebrahimi, M., Ai, J., Biazar, E., Ebrahimi-Barough, S., Khojasteh, A., Yazdankhah, M., Sharifi, S., Ai, A., Heidari-Keshel, S. (2018). In vivo assessment of a nanofibrous silk tube as nerve guide for sciatic nerve regeneration. Artificial Cells, Nanomedicine, and Biotechnology, 46(sup1), 394-401.

Echave, M. C., Burgo, L. S., Pedraz, J. L., Orive, G. (2017). Gelatin as Biomaterial for Tissue Engineering. Current Pharmaceutical Design, 23(24), 3567-3584.

Eke, G., Mangir, N., Hasirci, N., MacNeil, S., Hasirci, V. (2017). Development of a UV crosslinked biodegradable hydrogel containing adipose derived stem cells to promote vascularization for skin wounds and tissue engineering. Biomaterials, 129, 188-198.

Eltom, A., Zhong, G., Muhammad, A. (2019). Scaffold Techniques and Designs in Tissue Engineering Functions and Purposes: A Review. Advances in Materials Science and Engineering, 2019, 1-13.

England, S., Rajaram, A., Schreyer, D. J., Chen, X. (2017). Bioprinted fibrin-factor XIII-hyaluronate hydrogel scaffolds with encapsulated Schwann cells and their in vitro characterization for use in nerve regeneration. Bioprinting, 5, 1-9.

Entekhabi, E., Haghbin Nazarpak, M., Moztarzadeh, F., Sadeghi, A. (2016). Design and manufacture of neural tissue engineering scaffolds using hyaluronic acid and polycaprolactone nanofibers with controlled porosity. Materials Science and Engineering: C, 69, 380-387.

Entekhabi, E., Nazarpak, M. H. (2018). Neural tissue engineering scaffolds fabrication technologies: peripheral nervous system. Journal of Applied Tissue Engineering, 5(3), 1-11.

Fairbairn, N. G., Meppelink, A. M., Ng-Glazier, J., Randolph, M. A., Winograd, J. M. (2015). Augmenting peripheral nerve regeneration using stem cells: A review of current opinion. World Journal of Stem Cells, 7(1), 11-26.

Farokhi, M., Mottaghitalab, F., Shokrgozar, M. A., Kaplan, D. L., Kim, H.-W., Kundu, S. C. (2017). Prospects of peripheral nerve tissue engineering using nerve guide conduits based on silk fibroin protein and other biopolymers. International Materials Reviews, 62(7), 367-391.

Faroni, A., Mobasseri, S. A., Kingham, P. J., Reid, A. J. (2015). Peripheral nerve regeneration: Experimental strategies and future perspectives. Advanced Drug Delivery Reviews, 82, 160-167.

Fiorica, C., Palumbo, F. S., Pitarresi, G., Bongiovì, F., Giammona, G. (2017). Hyaluronic acid and beta cyclodextrins films for the release of corneal epithelial cells and dexamethasone. Carbohydrate Polymers, 166, 281-290.

Fischer, A. H., Jacobson, K. A., Rose, J., Zeller, R. (2008). Hematoxylin and Eosin Staining of Tissue and Cell Sections. Cold Spring Harbor Protocols, 2008(6), pdb.prot4986-pdb.prot4986.

Francis, N. L., Hunger, P. M., Donius, A. E., Wegst, U. G. K., Wheatley, M. A. (2017). Strategies for neurotrophin-3 and chondroitinase ABC release from freeze-cast chitosan-alginate nerve-guidance scaffolds. Journal of Tissue Engineering and Regenerative Medicine, 11(1), 285-294.

Frantz, C., Stewart, K. M., Weaver, V. M. (2010). The extracellular matrix at a glance. Journal of Cell Science, 123(Pt 24), 4195-4200.

Frost, H. K., Andersson, T., Johansson, S., Englund-Johansson, U., Ekström, P., Dahlin, L. B., Johansson, F. (2018). Electrospun nerve guide conduits have the potential to bridge peripheral nerve injuries in vivo. Scientific Reports, 8(1), 16716.

Fu, K.-Y., Dai, L.-G., Chiu, I.-M., Chen, J.-R., Hsu, S. (2011). Sciatic Nerve Regeneration by Microporous Nerve Conduits Seeded With Glial Cell Line-Derived Neurotrophic Factor or Brain-Derived Neurotrophic Factor Gene Transfected Neural Stem Cells. Artificial Organs, 35(4), 363-372.

Fujimaki, H., Uchida, K., Inoue, G., Miyagi, M., Nemoto, N., Saku, T., Isobe, Y., Inage, K., Matsushita, O., Yagishita, S., Sato, J., Takano, S., Sakuma, Y., Ohtori, S., Takahashi, K., Takaso, M. (2017). Oriented collagen tubes combined with basic fibroblast growth factor promote peripheral nerve regeneration in a 15 mm sciatic nerve defect rat model. Journal of Biomedical Materials Research Part A, 105(1), 8-14.

Garraway, S. M., Huie, J. R. (2016). Spinal Plasticity and Behavior: BDNF-Induced Neuromodulation in Uninjured and Injured Spinal Cord. Neural Plasticity, 2016, 1-19.

Gayer, C., Ritter, J., Bullemer, M., Grom, S., Jauer, L., Meiners, W., Pfister, A., Reinauer, F., Vučak, M., Wissenbach, K., Fischer, H., Poprawe, R., Schleifenbaum, J. H. (2019). Development of a solvent-free polylactide/calcium carbonate composite

for selective laser sintering of bone tissue engineering scaffolds. Materials Science and Engineering: C, 101, 660-673.

Gentile, P., Chiono, V., Carmagnola, I., Hatton, P., Gentile, P., Chiono, V., Carmagnola, I., Hatton, P. V. (2014). An Overview of Poly(lactic-co-glycolic) Acid (PLGA)-Based Biomaterials for Bone Tissue Engineering. International Journal of Molecular Sciences, 15(3), 3640-3659.

Ghasemi Hamidabadi, H., Rezvani, Z., Nazm Bojnordi, M., Shirinzadeh, H., Seifalian, A. M., Joghataei, M. T., Razaghpour, M., Alibakhshi, A., Yazdanpanah, A., Salimi, M., Mozafari, M., Urbanska, A. M., Reis, R. L., Kundu, S. C., Gholipourmalekabadi, M. (2017). Chitosan-Intercalated Montmorillonite/Poly(vinyl alcohol) Nanofibers as a Platform to Guide Neuronlike Differentiation of Human Dental Pulp Stem Cells. ACS Applied Materials & Interfaces, 9(13), 11392-11404.

Ciardelli, G., Chiono, V., Vozzi, G., Pracella, M., Ahluwalia, A., Barbani, N., Cristallini, C., Giusti, P. (2005). Blends of Poly-(ε-caprolactone) and Polysaccharides in Tissue Engineering Applications. Biomacromolecules, 6(4), 1961-1976.

González-Carrasco, J., Cifuentes Cuellar, S., Lieblich Rodríguez, M. (2019). Metals. Bone Repair Biomaterials, 103-140.

Gonzalez-Perez, F., Hernández, J., Heimann, C., Phillips, J. B., Udina, E., Navarro, X. (2018). Schwann cells and mesenchymal stem cells in laminin- or fibronectin-aligned matrices and regeneration across a critical size defect of 15 mm in the rat sciatic nerve. Journal of Neurosurgery: Spine, 28(1), 109-118.

Goonoo, N., Bhaw-Luximon, A., Passanha, P., Esteves, S. R., Jhurry, D. (2017). Third generation poly(hydroxyacid) composite scaffolds for tissue engineering. Journal of Biomedical Materials Research Part B: Applied Biomaterials, 105(6), 1667-1684.

Gordon, J., Amini, S., White, M. K. (2013). Neuronal Cell Culture, 1078, 1-6.

Goulart, C. O., Ângelo Durço, D. de F. P., de Carvalho, L. A., Oliveira, J. T., Alves, L., Cavalcante, L. A., Blanco Martinez, A. M. (2016). Olfactory ensheathing glia cell therapy and tubular conduit enhance nerve regeneration after mouse sciatic nerve transection. Brain Research, 1650, 243-251.

Goulart, C. O., Pereira Lopes, F. R., Monte, Z. O., Dantas, S. V., Souto, A., Oliveira, J. T., Almeida, F. M., Tonda-Turo, C., Pereira, C. C., Borges, C. P., Martinez, A. M. B. (2016). Evaluation of biodegradable polymer conduits - poly(l-lactic acid) - for guiding sciatic nerve regeneration in mice. Methods, 99, 28-36.

Grimoldi, N., Colleoni, F., Tiberio, F., Vetrano, I. G., Cappellari, A., Costa, A., Belicchi, M., Razini, P., Giordano, R., Spagnoli, D., Pluderi, M., Gatti, S., Morbin, M., Gaini, S. M., Rebulla, P., Bresolin, N., Torrente, Y. (2015). Stem Cell Salvage of Injured Peripheral Nerve. Cell Transplantation, 24(2), 213-222.

Gu, B. K., Choi, D. J., Park, S. J., Kim, M. S., Kang, C. M., Kim, C.-H. (2016). 3-dimensional bioprinting for tissue engineering applications. Biomaterials Research, 20(1), 12.

Gu, Jian, Xu, H., Xu, Y.-P., Liu, H.-H., Lang, J.-T., Chen, X.-P., Xu, W.-H., Fan, J.-P. (2019). Olfactory ensheathing cells promote nerve regeneration and functional recovery after facial nerve defects. Neural Regeneration Research, 14(1), 124–131.

Gu, Jianhui, Hu, W., Deng, A., Zhao, Q., Lu, S., Gu, X. (2012). Surgical repair of a 30 mm long human median nerve defect in the distal forearm by implantation of a chitosan-PGA nerve guidance conduit. Journal of Tissue Engineering and Regenerative Medicine, 6(2), 163-168.

Gu, Q., Tomaskovic-Crook, E., Lozano, R., Chen, Y., Kapsa, R. M., Zhou, Q., Wallace, G. G., Crook, J. M. (2016). Functional 3D Neural Mini-Tissues from Printed Gel-Based Bioink and Human Neural Stem Cells. Advanced Healthcare Materials, 5(12), 1429-1438.

Gu, X., Ding, F., Williams, D. F. (2014). Neural tissue engineering options for peripheral nerve regeneration. Biomaterials, 35(24), 6143-6156.

Gu, X., Ding, F., Yang, Y., Liu, J. (2011). Construction of tissue engineered nerve grafts and their application in peripheral nerve regeneration. Progress in Neurobiology, 93(2), 204-230.

Gu, X., Ding, F., Yang, Y., Liu, J. (2015). Tissue Engineering in Peripheral Nerve Regeneration. Neural Regeneration, 73-99.

Guo, B.-F., Dong, M.-M. (2009). Application of neural stem cells in tissue-engineered artificial nerve. Otolaryngology–Head and Neck Surgery, 140(2), 159-164.

Gusel'nikova, V. V, Korzhevskiy, D. E. (2015). NeuN As a Neuronal Nuclear Antigen and Neuron Differentiation Marker. Acta Naturae, 7(2), 42-47.

Guy, R., Grynspan, F., Ben-Zur, T., Panski, A., Lamdan, R., Danon, U., Yaffe, D., Offen, D. (2019). Human Muscle Progenitor Cells Overexpressing Neurotrophic Factors Improve Neuronal Regeneration in a Sciatic Nerve Injury Mouse Model. Frontiers in Neuroscience, 13, 151.

Haider, A., Haider, S., Kang, I.-K. (2018). A comprehensive review summarizing the effect of electrospinning parameters and potential applications of nanofibers in biomedical and biotechnology. Arabian Journal of Chemistry, 11(8), 1165-1188.

Han, G.-H., Peng, J., Liu, P., Ding, X., Wei, S., Lu, S., Wang, Y. (2019). Therapeutic strategies for peripheral nerve injury: decellularized nerve conduits and Schwann cell transplantation. Neural Regeneration Research, 14(8), 1343-1351.

Haney, M. J., Zhao, Y., Harrison, E. B., Mahajan, V., Ahmed, S., He, Z., Suresh, P., Hingtgen, S. D., Klyachko, N. L., Mosley, R. L., Gendelman, H. E., Kabanov, A.V.,

Batrakova, E. V. (2013). Specific Transfection of Inflamed Brain by Macrophages: A New Therapeutic Strategy for Neurodegenerative Diseases. PLoS ONE, 8(4), e61852.

Hasirci, V., Hasirci, N. (2018). Fundamentals of Human Biology and Anatomy. In Fundamentals of Biomaterials (pp. 131–140). New York, NY: Springer New York.

Hei, W.-H., Kim, S., Park, J.-C., Seo, Y.-K., Kim, S.-M., Jahng, J. W., Lee, J.-H. (2016). Schwann-like cells differentiated from human dental pulp stem cells combined with a pulsed electromagnetic field can improve peripheral nerve regeneration. Bioelectromagnetics, 37(3), 163-174.

Heo, D. N., Lee, S.-J., Timsina, R., Qiu, X., Castro, N. J., Zhang, L. G. (2019). Development of 3D printable conductive hydrogel with crystallized PEDOT:PSS for neural tissue engineering. Materials Science and Engineering: C, 99, 582-590.

Hinüber, C., Chwalek, K., Pan-Montojo, F. J., Nitschke, M., Vogel, R., Brünig, H., Heinrich, G., Werner, C. (2014). Hierarchically structured nerve guidance channels based on poly-3-hydroxybutyrate enhance oriented axonal outgrowth. Acta Biomaterialia, 10(5), 2086-2095.

Ho, S., Labroo, P., Lin, K.-M., Sant, H., Shea, J., Gale, B., Agarwal, J. (2019). Designing a Novel Drug Delivering Nerve Guide: A Preliminary Study. Journal of Medical and Biological Engineering, 39(3), 294-304.

Houshyar, S., Bhattacharyya, A., Shanks, R. (2019). A Review-Peripheral Nerve Conduit: Materials and Structures. ACS Chemical Neuroscience.

Hsieh, F.-Y., Lin, H.-H., Hsu, S. (2015). 3D bioprinting of neural stem cell-laden thermoresponsive biodegradable polyurethane hydrogel and potential in central nervous system repair. Biomaterials, 71, 48-57.

Hsu, M.-N., Liao, H.-T., Li, K.-C., Chen, H.-H., Yen, T.-C., Makarevich, P., Parfyonova, Y., Hu, Y.-C. (2017). Adipose-derived stem cell sheets functionalized by hybrid baculovirus for prolonged GDNF expression and improved nerve regeneration. Biomaterials, 140, 189-200.

Hsueh, Y.-S., Savitha, S., Sadhasivam, S., Lin, F.-H., Shieh, M.-J. (2014). Design and synthesis of elastin-like polypeptides for an ideal nerve conduit in peripheral nerve regeneration. Materials Science and Engineering: C, 38, 119-126.

Hu, F., Zhang, X., Liu, H., Xu, P., Doulathunnisa, Teng, G., Xiao, Z. (2017). Neuronally differentiated adipose-derived stem cells and aligned PHBV nanofiber nerve scaffolds promote sciatic nerve regeneration. Biochemical and Biophysical Research Communications, 489(2), 171-178.

Hu, R., Cao, Q., Sun, Z., Chen, J., Zheng, Q., Xiao, F. (2018). A novel method of neural differentiation of PC12 cells by using Opti-MEM as a basic induction medium. International Journal of Molecular Medicine, 41(1), 195-201.

Hudson, T. W., Zawko, S., Deister, C., Lundy, S., Hu, C. Y., Lee, K., Schmidt, C. E. (2004). Optimized Acellular Nerve Graft Is Immunologically Tolerated and Supports Regeneration. Tissue Engineering, 10(11–12), 1641-1651.

Huhtamäki, T., Tian, X., Korhonen, J. T., Ras, R. H. A. (2018). Surface-wetting characterization using contact-angle measurements. Nature Protocols, 13(7), 1521-1538.

Hutmacher, D. W., Schantz, T., Zein, I., Ng, K. W., Teoh, S. H., Tan, K. C. (2001). Mechanical properties and cell cultural response of polycaprolactone scaffolds designed and fabricated via fused deposition modeling. Journal of Biomedical Materials Research, 55(2), 203-216.

Hutmacher, D. W., Woodfield, T. B. F., Dalton, P. D. (2014). Scaffold Design and Fabrication. Tissue Engineering, 311-346.

Jaiswal, M., Koul, V. (2013). Assessment of multicomponent hydrogel scaffolds of poly(acrylic acid-2-hydroxy ethyl methacrylate)/gelatin for tissue engineering applications. Journal of Biomaterials Applications, 27(7), 848-861.

Jang, C. H., Lee, H., Kim, M., Kim, G. (2016). Effect of polycaprolactone/collagen/hUCS microfiber nerve conduit on facial nerve regeneration. International Journal of Biological Macromolecules, 93, 1575-1582.

Jessen, K. R., Mirsky, R. (2016). The repair Schwann cell and its function in regenerating nerves. Journal of Physiology, 594(13), 3521-3531.

Jessen, K. R., Arthur-Farraj, P. (2019). Repair Schwann cell update: Adaptive reprogramming, EMT, and stemness in regenerating nerves. Glia, 67(3), 421-437.

Jia, H., Wang, Y., Chen, J., Li, J., Han, H., Tong, X., He, Z. Y., Ma, W. (2019). Combination of BMSCs-laden acellular nerve xenografts transplantation and G-CSF administration promotes sciatic nerve regeneration. Synapse, 73(7), e22093.

Jia, H., Wang, Y., Tong, X.-J., Liu, G.-B., Li, Q., Zhang, L.-X., Sun, X.-H. (2012). Sciatic nerve repair by acellular nerve xenografts implanted with BMSCs in rats xenograft combined with BMSCs. Synapse, 66(3), 256-269.

Jiang, L., Jones, S., Jia, X. (2017). Stem Cell Transplantation for Peripheral Nerve Regeneration: Current Options and Opportunities. International Journal of Molecular Sciences, 18(1).

Jiang, Z., Song, Y., Qiao, J., Yang, Y., Zhang, W., Liu, W., Han, B. (2019). Rat sciatic nerve regeneration across a 10-mm defect bridged by a chitin/CM-chitosan artificial nerve graft. International Journal of Biological Macromolecules, 129, 997-1005.

Jing, W., Ao, Q., Wang, L., Huang, Z., Cai, Q., Chen, G., Yang, X., Zhong, W. (2018). Constructing conductive conduit with conductive fibrous infilling for peripheral nerve regeneration. Chemical Engineering Journal, 345, 566-577.

Jones, I., Novikova, L. N., Novikov, L. N., Renardy, M., Ullrich, A., Wiberg, M., Carlsson, L., Kingham, P. J. (2018). Regenerative effects of human embryonic stem cell-derived neural crest cells for treatment of peripheral nerve injury. Journal of Tissue Engineering and Regenerative Medicine, 12(4), e2099–e2109.

Kabiri, M., Oraee-Yazdani, S., Shafiee, A., Hanaee-Ahvaz, H., Dodel, M., Vaseei, M., Soleimani, M. (2015). Neuroregenerative effects of olfactory ensheathing cells transplanted in a multi-layered conductive nanofibrous conduit in peripheral nerve repair in rats. Journal of Biomedical Science, 22(1), 35.

Kakinoki, S., Nakayama, M., Moritan, T., Yamaoka, T. (2014). Three-layer microfibrous peripheral nerve guide conduit composed of elastin-laminin mimetic artificial protein and poly(L-lactic acid). Frontiers in Chemistry, 2, 52.

Keilhoff, G., Stang, F., Goihl, A., Wolf, G., Fansa, H. (2006). Transdifferentiated Mesenchymal Stem Cells as Alternative Therapy in Supporting Nerve Regeneration and Myelination. Cellular and Molecular Neurobiology, 26(7–8), 1233-1250.

Keilhoff, G., Stang, F., Wolf, G., Fansa, H. (2003). Bio-compatibility of type I/III collagen matrix for peripheral nerve reconstruction. Biomaterials, 24(16), 2779-2787.

Kemp, S. W. P., Syed, S., Walsh, S. K., Zochodne, D. W., Midha, R. (2009). Collagen Nerve Conduits Promote Enhanced Axonal Regeneration, Schwann Cell Association, and Neovascularization Compared to Silicone Conduits. Tissue Engineering Part A, 15(8), 1975-1988.

Kijeńska, E., Prabhakaran, M. P., Swieszkowski, W., Kurzydlowski, K. J., Ramakrishna, S. (2014). Interaction of Schwann cells with laminin encapsulated PLCL core–shell nanofibers for nerve tissue engineering. European Polymer Journal, 50, 30-38.

Kingham, P. J., Kalbermatten, D. F., Mahay, D., Armstrong, S. J., Wiberg, M., Terenghi, G. (2007). Adipose-derived stem cells differentiate into a Schwann cell phenotype and promote neurite outgrowth in vitro. Experimental Neurology, 207(2), 267-274.

Kingham, P. J., Kolar, M. K., Novikova, L. N., Novikov, L. N., Wiberg, M. (2014). Stimulating the Neurotrophic and Angiogenic Properties of Human Adipose-Derived Stem Cells Enhances Nerve Repair. Stem Cells and Development, 23(7), 741-754.

Klimanskaya, I. (2019). Embryonic Stem Cells: Derivation, Properties, and Challenges. Principles of Regenerative Medicine, 113-123.

Klimczak, A., Kozlowska, U. (2016). Mesenchymal Stromal Cells and Tissue-Specific Progenitor Cells: Their Role in Tissue Homeostasis. Stem Cells International, 2016, 1-11.

Ko, C.-H., Shie, M.-Y., Lin, J.-H., Chen, Y.-W., Yao, C.-H., Chen, Y.-S. (2017). Biodegradable Bisvinyl Sulfonemethyl-crosslinked Gelatin Conduit Promotes

Regeneration after Peripheral Nerve Injury in Adult Rats. Scientific Reports, 7(1), 17489.

Koshy, S. T., Ferrante, T. C., Lewin, S. A., Mooney, D. J. (2014). Injectable, porous, and cell-responsive gelatin cryogels. Biomaterials, 35(8), 2477-2487.

Kouhi, M., Jayarama Reddy, V., Fathi, M., Shamanian, M., Valipouri, A., Ramakrishna, S. (2019). Poly (3-hydroxybutyrate-co-3-hydroxyvalerate) /fibrinogen /bredigite nanofibrous membranes and their integration with osteoblasts for guided bone regeneration. Journal of Biomedical Materials Research Part A, 107(6), 1154-1165.

Kuang, T., Chang, L., Chen, F., Sheng, Y., Fu, D., Peng, X. (2016). Facile preparation of lightweight high-strength biodegradable polymer/multi-walled carbon nanotubes nanocomposite foams for electromagnetic interference shielding. Carbon, 105, 305-313.

Kuang, T., Chen, F., Chang, L., Zhao, Y., Fu, D., Gong, X., Peng, X. (2017). Facile preparation of open-cellular porous poly (l-lactic acid) scaffold by supercritical carbon dioxide foaming for potential tissue engineering applications. Chemical Engineering Journal, 307, 1017-1025.

Kuo, Y.-C., Yeh, C.-F. (2011). Effect of surface-modified collagen on the adhesion, biocompatibility and differentiation of bone marrow stromal cells in poly(lactide-co-glycolide)/chitosan scaffolds. Colloids and Surfaces B: Biointerfaces, 82(2), 624-631.

Labet, M., Thielemans, W. (2009). Synthesis of polycaprolactone: a review. Chemical Society Reviews, 38(12), 3484.

Labroo, P., Goodwin, I., Davis, B., Edwards, K., Ho, S., Sant, H. J., Gale, B. K., Shea, J. E., Agarwal, J. (2017). Effect Of Ngf Delivering Conduit On Peripheral Nerve Regeneration. Plastic and Reconstructive Surgery - Global Open, 5, 97-98.

Lai, J.-Y., Cheng, H.-Y., Ma, D. H.-K. (2015). Investigation of Overrun-Processed Porous Hyaluronic Acid Carriers in Corneal Endothelial Tissue Engineering. PLOS ONE, 10(8), e0136067.

Lavasani, M., Thompson, S. D., Pollett, J. B., Usas, A., Lu, A., Stolz, D. B., Clark, K. A., Sun, B., Péault, B., Huard, J. (2014). Human muscle–derived stem/progenitor cells promote functional murine peripheral nerve regeneration. Journal of Clinical Investigation, 124(4), 1745-1756.

Lee, B.-K., Ju, Y. M., Cho, J.-G., Jackson, J. D., Lee, S. J., Atala, A., Yoo, J. J. (2012). End-to-side neurorrhaphy using an electrospun PCL/collagen nerve conduit for complex peripheral motor nerve regeneration. Biomaterials, 33(35), 9027-9036.

Lee, H., Yun, S., Kim, I.-S., Lee, I.-S., Shin, J. E., Park, S. C., Kim, W. J., Park, K. I. (2014). Human Fetal Brain-Derived Neural Stem/Progenitor Cells Grafted into the

Adult Epileptic Brain Restrain Seizures in Rat Models of Temporal Lobe Epilepsy. PLoS ONE, 9(8), e104092.

Lee, S.-J., Nowicki, M., Harris, B., Zhang, L. G. (2017). Fabrication of a Highly Aligned Neural Scaffold via a Table Top Stereolithography 3D Printing and Electrospinning. Tissue Engineering Part A, 23(11–12), 491-502.

Lee, S.-J., Zhu, W., Nowicki, M., Lee, G., Heo, D. N., Kim, J., Zuo, Y. Y., Zhang, L. G. (2018). 3D printing nano conductive multi-walled carbon nanotube scaffolds for nerve regeneration. Journal of Neural Engineering, 15(1), 016018.

Li, B.-B., Yin, Y.-X., Yan, Q.-J., Wang, X.-Y., Li, S.-P. (2016). A novel bioactive nerve conduit for the repair of peripheral nerve injury. Neural Regeneration Research, 11(1), 150-155.

Li, C.-W., Wang, G.-J. (2017). Double-Layer Nerve Guide Conduit With Palisade Poly(Lactic-Co-Glycolic Acid) Tube Wrapped by Microporous Chitosan-Collagen Composite. In Volume 4: 22nd Design for Manufacturing and the Life Cycle Conference; 11th International Conference on Micro- and Nanosystems, V004T09A001.

Li, M., Zhu, Q., Liu, J. (2018). Olfactory ensheathing cells in facial nerve regeneration. Brazilian Journal of Otorhinolaryngology.

Li, Ruijun, Liu, Z., Pan, Y., Chen, L., Zhang, Z., Lu, L. (2014). Peripheral Nerve Injuries Treatment: a Systematic Review. Cell Biochemistry and Biophysics, 68(3), 449-454.

Li, Runxin, Liu, H., Huang, H., Bi, W., Yan, R., Tan, X., Wen, W., Wang, C., Song, W., Zhang, Y., Zhang, F., Hu, M. (2018). Chitosan conduit combined with hyaluronic acid prevent sciatic nerve scar in a rat model of peripheral nerve crush injury. Molecular Medicine Reports, 17(3), 4360-4368.

Li, Xiaowei, Liu, W., Ye, G., Zhang, B., Zhu, D., Yao, K., Liu, Z., Sheng, X. (2005). Thermosensitive N-isopropylacrylamide–N–propylacrylamide-vinyl pyrrolidone terpolymers: Synthesis, characterization and preliminary application as embolic agents. Biomaterials, 26(34), 7002-7011.

Li, Xiufang, Wang, L., Li, L., Luo, Z., Yan, S., Zhang, Q., You, R. (2019). Water-stable silk fibroin nerve conduits with tunable degradation prepared by a mild freezing-induced assembly. Polymer Degradation and Stability, 164, 61-68.

Li, Y., Guo, L., Ahn, H. S., Kim, M. H., Kim, S.-W. (2014). Amniotic mesenchymal stem cells display neurovascular tropism and aid in the recovery of injured peripheral nerves. Journal of Cellular and Molecular Medicine, 18(6), 1028-1034.

Liard, O., Segura, S., Sagui, E., Nau, A., Pascual, A., Cambon, M., Darlix, J. L., Fusai, T., Moyse, E. (2012). Adult-Brain-Derived Neural Stem Cells Grafting into a Vein

Bridge Increases Postlesional Recovery and Regeneration in a Peripheral Nerve of Adult Pig. Stem Cells International, 2012, 128732.

Lin, S. C.-Y., Wang, Y., Wertheim, D. F., Coombes, A. G. A. (2017). Production and in vitro evaluation of macroporous, cell-encapsulating alginate fibres for nerve repair. Materials Science and Engineering: C, 73, 653-664.

Lin, Y.-C., Ramadan, M., Van Dyke, M., Kokai, L. E., Philips, B. J., Rubin, J. P., Marra, K. G. (2012). Keratin Gel Filler for Peripheral Nerve Repair in a Rodent Sciatic Nerve Injury Model. Plastic and Reconstructive Surgery, 129(1), 67-78.

Liu, B.-S. (2008). Fabrication and evaluation of a biodegradable proanthocyanidin-crosslinked gelatin conduit in peripheral nerve repair. Journal of Biomedical Materials Research Part A, 87A(4), 1092-1102.

Liu, C., Wang, C., Zhao, Q., Li, X., Xu, F., Yao, X., Wang, M. (2018). Incorporation and release of dual growth factors for nerve tissue engineering using nanofibrous bicomponent scaffolds. Biomedical Materials, 13(4), 044107.

Liu, S., Sun, X., Wang, T., Chen, S., Zeng, C., Xie, G., Zhu, Q., Liu, X., Quan, D. (2018). Nano-fibrous and ladder-like multi-channel nerve conduits: Degradation and modification by gelatin. Materials Science and Engineering: C, 83, 130-142.

Lizarraga-Valderrama, L. R., Nigmatullin, R., Taylor, C., Haycock, J. W., Claeyssens, F., Knowles, J. C., Roy, I. (2015). Nerve tissue engineering using blends of poly(3-hydroxyalkanoates) for peripheral nerve regeneration. Engineering in Life Sciences, 15(6), 612-621.

Lizarraga-Valderrama, L. R., Taylor, C. S., Claeyssens, F., Haycock, J. W., Knowles, J. C., Roy, I. (2019). Unidirectional Neuronal Cell growth and Differentiation on Aligned Polyhydroxyalkanoate Blend Microfibres with Varying Diameters. Journal of Tissue Engineering and Regenerative Medicine.

Lu, C., Meng, D., Cao, J., Xiao, Z., Cui, Y., Fan, J., Cui, X., Chen, B., Yao, Y., Zhang, Z., Ma, J., Pan, J., Dai, J. (2015). Collagen scaffolds combined with collagen-binding ciliary neurotrophic factor facilitate facial nerve repair in mini-pigs. Journal of Biomedical Materials Research Part A, 103(5), 1669-1676.

Lu, J., Sun, X., Yin, H., Shen, X., Yang, S., Wang, Y., Jiang, W., Sun, Y., Zhao, L., Sun, X., Lu, S., Mikos, A. G., Peng, J., Wang, X. (2018). A neurotrophic peptide-functionalized self-assembling peptide nanofiber hydrogel enhances rat sciatic nerve regeneration. Nano Research, 11(9), 4599-4613.

Lu, T., Li, Y., Chen, T. (2013). Techniques for fabrication and construction of three-dimensional scaffolds for tissue engineering. International Journal of Nanomedicine, 8, 337-350.

Lu, Y., Li, R., Zhu, J., Wu, Y., Li, D., Dong, L., Li, Y., Wen, X., Yu, F., Zhang, H., Ni, X., Du, S., Li, X., Xiao, J., Wang, J. (2019). Fibroblast growth factor 21 facilitates

peripheral nerve regeneration through suppressing oxidative damage and autophagic cell death. Journal of Cellular and Molecular Medicine, 23(1), 497-511.

Ma, P. X. (2008). Biomimetic materials for tissue engineering. Advanced Drug Delivery Reviews, 60(2), 184-198.

Ma, Y., Dong, L., Zhou, D., Li, L., Zhang, W., Zhen, Y., Wang, T., Su, J., Chen, D., Mao, C., Wang, X. (2019). Extracellular vesicles from human umbilical cord mesenchymal stem cells improve nerve regeneration after sciatic nerve transection in rats. Journal of Cellular and Molecular Medicine, 23(4), 2822-2835.

Madduri, S., Feldman, K., Tervoort, T., Papaloïzos, M., Gander, B. (2010). Collagen nerve conduits releasing the neurotrophic factors GDNF and NGF. Journal of Controlled Release, 143(2), 168-174.

Manavitehrani, I., Fathi, A., Badr, H., Daly, S., Shirazi, A. N., Dehghani, F. (2016). Biomedical applications of biodegradable polyesters. Polymers, 8(1), 20.

Manavitehrani, I., Le, T. Y. L., Daly, S., Wang, Y., Maitz, P. K., Schindeler, A., Dehghani, F. (2019). Formation of porous biodegradable scaffolds based on poly(propylene carbonate) using gas foaming technology. Materials Science and Engineering: C, 96, 824-830.

Marconi, S., Castiglione, G., Turano, E., Bissolotti, G., Angiari, S., Farinazzo, A., Constantin, G., Bedogni, G., Bedogni, A., Bonetti, B. (2012). Human adipose-derived mesenchymal stem cells systemically injected promote peripheral nerve regeneration in the mouse model of sciatic crush. Tissue Engineering Part A, 18(11-12), 1264-1272.

Marpu, S., Benton, E. (2018). Shining Light on Chitosan: A Review on the Usage of Chitosan for Photonics and Nanomaterials Research. International Journal of Molecular Sciences, 19(6), 1795.

Martin, R. A., Wendling, M., Mohrenweiser, B., Qian, Z., Zhao, F., Mullins, M. E. (2019). Formation of aligned core/sheath microfiber scaffolds with a poly-L-lactic acid (PLLA) sheath and a conductive poly(3,4-ethylenedioxythiophene) (PEDOT) core. Journal of Materials Research, 34(11), 1931-1943.

Martini, F. H., Nath, J. L., Bartholomew, E. F. (2018). Fundamentals of Anatomy and Physiology. 11th edition. Pearson.

Mazzoli, A. (2013). Selective laser sintering in biomedical engineering. Medical and Biological Engineering and Computing, 51(3), 245-256.

Mazzoli, A., Ferretti, C., Gigante, A., Salvolini, E., Mattioli-Belmonte, M. (2015). Selective laser sintering manufacturing of polycaprolactone bone scaffolds for applications in bone tissue engineering. Rapid Prototyping Journal, 21(4), 386-392.

Menzies, K. L., Jones, L. (2010). The impact of contact angle on the biocompatibility of biomaterials. Optometry and Vision Science: Official Publication of the American Academy of Optometry, 87(6), 387-399.

Millán-Rivero, J. E., Nadal-Nicolás, F. M., García-Bernal, D., Sobrado-Calvo, P., Blanquer, M., Moraleda, J. M., Vidal-Sanz, M., Agudo-Barriuso, M. (2018). Human Wharton's jelly mesenchymal stem cells protect axotomized rat retinal ganglion cells via secretion of anti-inflammatory and neurotrophic factors. Scientific Reports, 8(1), 16299.

Mithieux, S. M., Weiss, A. S. (2005). Elastin. In Advances in protein chemistry, 70, 437-461.

Mobini, S., Spearman, B. S., Lacko, C. S. (2017). Recent advances in strategies for peripheral nerve tissue engineering. Current Opinion in Biomedical Engineering, 4, 134-142.

Mohseni, M., Hutmacher, D. W., Castro, N. J., Mohseni, M., Hutmacher, D. W., Castro, N. J. (2018). Independent Evaluation of Medical-Grade Bioresorbable Filaments for Fused Deposition Modelling/Fused Filament Fabrication of Tissue Engineered Constructs. Polymers, 10(1), 40.

Molnar, C., Gair, J. (2015). Concepts of Biology-1st Canadian Edition, 1, 1007.

Mondal, D., Griffith, M., Venkatraman, S. S. (2016). Polycaprolactone-based biomaterials for tissue engineering and drug delivery: Current scenario and challenges. International Journal of Polymeric Materials and Polymeric Biomaterials, 65(5), 255-265.

Monteiro, I. P., Shukla, A., Marques, A. P., Reis, R. L., Hammond, P. T. (2015). Spray-assisted layer-by-layer assembly on hyaluronic acid scaffolds for skin tissue engineering. Journal of Biomedical Materials Research Part A, 103(1), 330-340.

Mori, K., Yamamoto, T., Oyama, K., Ueno, H., Nakao, Y., Honma, K. (2008). Modified Three-Dimensional Skull Base Model With Artificial Dura Mater, Cranial Nerves, and Venous Sinuses for Training in Skull Base Surgery. Neurologia Medico-Chirurgica, 48(12), 582-588.

Mottaghitalab, F., Farokhi, M., Zaminy, A., Kokabi, M., Soleimani, M., Mirahmadi, F., Shokrgozar, M. A., Sadeghizadeh, M. (2013). A Biosynthetic Nerve Guide Conduit Based on Silk/SWNT/Fibronectin Nanocomposite for Peripheral Nerve Regeneration. PLoS ONE, 8(10), 10.

Mukhatyar, V. J., Salmerón-Sánchez, M., Rudra, S., Mukhopadaya, S., Barker, T. H., García, A. J., Bellamkonda, R. V. (2011). Role of fibronectin in topographical guidance of neurite extension on electrospun fibers. Biomaterials, 32(16), 3958-3968.

Myers, D. G., DeWall, N. C. (2017). Psychology in Everyday Life (4th ed.).

Nadi, M., Midha, R. (2018). Management of Peripheral Nerve Injuries. Principles of Neurological Surgery, 832-841.

Naghavi Alhosseini, S., Moztarzadeh, F., Kargozar, S., Dodel, M., Tahriri, M. (2015). Development of Polyvinyl Alcohol Fibrous Biodegradable Scaffolds for Nerve Tissue Engineering Applications: In Vitro Study. International Journal of Polymeric Materials and Polymeric Biomaterials, 64(9), 474-480.

Naghieh, S., Sarker, M. D., Abelseth, E., Chen, X. (2019). Indirect 3D bioprinting and characterization of alginate scaffolds for potential nerve tissue engineering applications. Journal of the Mechanical Behavior of Biomedical Materials, 93, 183-193.

Nakamura, Y., Horiuchi, S., Koshinuma, E., Imai, S., Nishioka, Y. (2017). Cultivation of Rat Nerve Cells on Biodegradable Sheet Made of Poly (lactic-co-glycolic acid) Thin Film with Micropatterns of Polylysine Containing Laminin Layer. ECS Meeting Abstracts, MA2017-02(55), 2337.

Naseri-Nosar, M., Salehi, M., Hojjati-Emami, S. (2017). Cellulose acetate/poly lactic acid coaxial wet-electrospun scaffold containing citalopram-loaded gelatin nanocarriers for neural tissue engineering applications. International Journal of Biological Macromolecules, 103, 701-708.

Necas, J., Bartosikova, L., Brauner, P., Kolar, J. (2008). Hyaluronic acid (hyaluronan): a review. Veterinarni Medicina, 53(8), 397-411.

Nguyen, D. Y., Tran, R. T., Costanzo, F., Yang, J. (2015). Tissue-Engineered Peripheral Nerve Guide Fabrication Techniques. Nerves and Nerve Injuries, 971-992.

Nichol, J. W., Koshy, S. T., Bae, H., Hwang, C. M., Yamanlar, S., Khademhosseini, A. (2010). Cell-laden microengineered gelatin methacrylate hydrogels. Biomaterials, 31(21), 5536-5544.

Niu, Y., Chen, K. C., He, T., Yu, W., Huang, S., Xu, K. (2014). Scaffolds from block polyurethanes based on poly(ε-caprolactone) (PCL) and poly(ethylene glycol) (PEG) for peripheral nerve regeneration. Biomaterials, 35(14), 4266-4277.

Nune, M., Krishnan, U. M., Sethuraman, S. (2016). PLGA nanofibers blended with designer self-assembling peptides for peripheral neural regeneration. Materials Science and Engineering: C, 62, 329-337.

Nune, M., Manchineella, S., Govindaraju, T., Narayan, K.S. (2019). Melanin incorporated electroactive and antioxidant silk fibroin nanofibrous scaffolds for nerve tissue engineering. Materials Science and Engineering: C, 94, 17-25.

O'Brien, J., Wilson, I., Orton, T., Pognan, F. (2000). Investigation of the Alamar Blue (resazurin) fluorescent dye for the assessment of mammalian cell cytotoxicity. European Journal of Biochemistry, 267(17), 5421-5426.

Oatari, M., Uehara, M., Shimizu, F. (2018). Evaluation of the effects of a polyglycolic acid–collagen tube in the regeneration of facial nerve defects in rats. The International Journal of Artificial Organs, 41(10), 664-669.

Obermeyer, J. M., Tuladhar, A., Payne, S. L., Ho, E., Morshead, C. M., Shoichet, M. S. (2019). Local Delivery of Brain-Derived Neurotrophic Factor Enables Behavioral Recovery and Tissue Repair in Stroke-Injured Rats. Tissue Engineering Part A.

Oh, S. H., Kang, J. G., Kim, T. H., Namgung, U., Song, K. S., Jeon, B. H., Lee, J. H. (2018). Enhanced peripheral nerve regeneration through asymmetrically porous nerve guide conduit with nerve growth factor gradient. Journal of Biomedical Materials Research Part A, 106(1), 52-64.

Owens, C. M., Marga, F., Forgacs, G., Heesch, C. M. (2013). Biofabrication and testing of a fully cellular nerve graft. Biofabrication, 5(4), 045007.

Ozbolat, I. T., Yu, Y. (2013). Bioprinting toward organ fabrication: Challenges and future trends. IEEE Transactions on Biomedical Engineering, 60(3), 691-699.

Pace, L. A., Plate, J. F., Smith, T. L., Van Dyke, M. E. (2013). The effect of human hair keratin hydrogel on early cellular response to sciatic nerve injury in a rat model. Biomaterials, 34(24), 5907-5914.

Pan, X., Sun, B., Mo, X. (2018). Electrospun polypyrrole-coated polycaprolactone nanoyarn nerve guidance conduits for nerve tissue engineering. Frontiers of Materials Science, 12(4), 438-446.

Panahi-Joo, Y., Karkhaneh, A., Nourinia, A., Abd-Emami, B., Negahdari, B., Renaud, P., Bonakdar, S. (2016). Design and fabrication of a nanofibrous polycaprolactone tubular nerve guide for peripheral nerve tissue engineering using a two-pole electrospinning system. Biomedical Materials, 11(2), 025017.

Parenteau-Bareil, R., Gauvin, R., Berthod, F. (2010). Collagen-Based Biomaterials for Tissue Engineering Applications. Materials, 3(3), 1863-1887.

Passipieri, J. A., Dienes, J., Frank, J., Glazier, J., Portell, A., Venkatesh, K. P., Bliley, J. M., Grybowski, D., Schilling, B. K., Marra, K. G., Christ, G. J. (2019). Adipose Stem Cells Enhance Nerve Regeneration and Muscle Function in a Peroneal Nerve Ablation Model. Tissue Engineering Part A, ten.tea.2018.0244.

Peng, J., Wang, Y., Zhang, L., Zhao, B., Zhao, Z., Chen, J., Guo, Q., Liu, S., Sui, X., Xu, W., Lu, S. (2011). Human umbilical cord Wharton's jelly-derived mesenchymal stem cells differentiate into a Schwann-cell phenotype and promote neurite outgrowth in vitro. Brain Research Bulletin, 84(3), 235-243.

Pestana, F. M., Domingues, R. C. C., Oliveira, J. T., Durço, D. F. P. A., Goulart, C. O., Mendonça, H. R., dos Santos, A. C. R., de Campos, N. T., da Silva B. T., Pereira, C. C., Borges, C. P., Martinez, A. M. B. (2018). Comparison of morphological and functional outcomes of mouse sciatic nerve repair with three biodegradable polymer

conduits containing poly(lactic acid). Neural Regeneration Research, 13(10), 1811-1819.

Petcu, E. B., Midha, R., McColl, E., Popa-Wagner, A., Chirila, T. V, Dalton, P. D. (2018). 3D printing strategies for peripheral nerve regeneration. Biofabrication, 10(3), 032001.

Porzionato, A., Barbon, S., Stocco, E., Dalzoppo, D., Contran, M., De Rose, E., Parnigotto, P. P., Macchi, V., Grandi, C., De Caro, R. (2019). Development of Oxidized Polyvinyl Alcohol-Based Nerve Conduits Coupled with the Ciliary Neurotrophic Factor. Materials, 12(12), 1996.

Prabhakaran, M. P., Vatankhah, E., Ramakrishna, S. (2013). Electrospun aligned PHBV/collagen nanofibers as substrates for nerve tissue engineering. Biotechnology and Bioengineering, 110(10), 2775-2784.

Qian, Y., Zhao, X., Han, Q., Chen, W., Li, H., Yuan, W. (2018). An integrated multi-layer 3D-fabrication of PDA/RGD coated graphene loaded PCL nanoscaffold for peripheral nerve restoration. Nature Communications, 9(1), 323.

Qing, H., Jin, G., Zhao, G., Huang, G., Ma, Y., Zhang, X., Sha, B., Luo, Z., Lu, T. J., Xu, F. (2018). Heterostructured Silk-Nanofiber-Reduced Graphene Oxide Composite Scaffold for SH-SY5Y Cell Alignment and Differentiation. ACS Applied Materials & Interfaces, 10(45), 39228-39237.

Quan, Q., Meng, H.-Y., Chang, B., Liu, G.-B., Cheng, X.-Q., Tang, H., Wang, Y., Peng, J., Zhao, Q., Lu, S.-B. (2019). Aligned fibers enhance nerve guide conduits when bridging peripheral nerve defects focused on early repair stage. Neural Regeneration Research, 14(5), 903.

Raimondo, S., Fornaro, M., Di Scipio, F., Ronchi, G., Giacobini-Robecchi, M. G., Geuna, S. (2009). Chapter 5 Methods and Protocols in Peripheral Nerve Regeneration Experimental Research. In International review of neurobiology, 87, 81–103.

Ramachandran, S., Midha, R. (2019). Recent advances in nerve repair. Neurology India, 67(7), 106.

Rando, T. A. (2006). Stem cells, ageing and the quest for immortality. Nature, 441(7097), 1080-1086.

Rao, F., Yuan, Z., Li, M., Yu, F., Fang, X., Jiang, B., Wen, Y., Zhang, P. (2019). Expanded 3D nanofibre sponge scaffolds by gas-foaming technique enhance peripheral nerve regeneration. Artificial Cells, Nanomedicine, and Biotechnology, 47(1), 491-500.

Rao, J., Cheng, Y., Liu, Y., Ye, Z., Zhan, B., Quan, D., Xu, Y. (2017). A multi-walled silk fibroin/silk sericin nerve conduit coated with poly(lactic-co-glycolic acid) sheath for peripheral nerve regeneration. Materials Science and Engineering: C, 73, 319-332.

Resch, A., Wolf, S., Mann, A., Weiss, T., Stetco, A.-L., Radtke, C. (2018). Co-Culturing Human Adipose Derived Stem Cells and Schwann Cells on Spider Silk—A New Approach as Prerequisite for Enhanced Nerve Regeneration. International Journal of Molecular Sciences, 20(1), 71.

Rimington, R. P., Capel, A. J., Christie, S. D. R., Lewis, M. P. (2017). Biocompatible 3D printed polymers via fused deposition modelling direct C 2 C 12 cellular phenotype in vitro. Lab on a Chip, 17(17), 2982-2993.

Rivera-Briso, A. L., Serrano-Aroca, Á. (2018, July 3). Poly(3-Hydroxybutyrate-co-3-Hydroxyvalerate): Enhancement strategies for advanced applications. Polymers, 10(7): 732.

Roloff, F., Scheiblich, H., Dewitz, C., Dempewolf, S., Stern, M., Bicker, G. (2015). Enhanced Neurite Outgrowth of Human Model (NT2) Neurons by Small-Molecule Inhibitors of Rho/ROCK Signaling. PLOS ONE, 10(2), e0118536.

Ruini, F., Tonda-Turo, C., Raimondo, S., Tos, P., Pugliese, P., Geuna, S., Ciardelli, G. (2016). Nerve guidance conduits based on bi-layer chitosan membranes for peripheral nerve regeneration. Biomedical Science and Engineering, 1(1).

Rupp, F., Gittens, R. A., Scheideler, L., Marmur, A., Boyan, B. D., Schwartz, Z., Geis-Gerstorfer, J. (2014). A review on the wettability of dental implant surfaces I: theoretical and experimental aspects. Acta biomaterialia, 10(7), 2894-2906.

Salehi, M., Ehtrami, A., Bastami, F., Farzamfar, S., Hosseinpour, S., Vahedi, H., Vaez, A., Rahvar, M., Goodarzi, A. (2019). Polyurethane/Gelatin Nanofiber Neural Guidance Conduit in Combination with Resveratrol and Schwann Cells for Sciatic Nerve Regeneration in the Rat Model. Fibers and Polymers, 20(3), 490-500.

Salehi, M., Naseri-Nosar, M., Ebrahimi-Barough, S., Nourani, M., Khojasteh, A., Farzamfar, S., Mansouri, K., Ai, J. (2018). Polyurethane/Gelatin Nanofibrils Neural Guidance Conduit Containing Platelet-Rich Plasma and Melatonin for Transplantation of Schwann Cells. Cellular and Molecular Neurobiology, 38(3), 703-713.

Salih, V. (2009). Biodegradable scaffolds for tissue engineering. Cellular Response to Biomaterials, 185-211.

Saltzman, E. B., Villa, J. C., Doty, S. B., Feinberg, J. H., Lee, S. K., & Wolfe, S. W. (2018). A Comparison Between Two Collagen Nerve Conduits and Nerve Autograft: A Rat Model of Motor Nerve Regeneration. The Journal of Hand Surgery.

Salvatore, L., Madaghiele, M., Parisi, C., Gatti, F., Sannino, A. (2014). Crosslinking of micropatterned collagen-based nerve guides to modulate the expected half-life. Journal of Biomedical Materials Research Part A, 102(12), 4406-4414.

Sango, K., Kawakami, E., Yanagisawa, H., Takaku, S., Tsukamoto, M., Utsunomiya, K., Watabe, K. (2012). Myelination in coculture of established neuronal and Schwann cell lines. Histochemistry and Cell Biology, 137(6), 829-839.

Sarhane, K. A., Tuffaha, S. H., Ibrahim, Z., Cashman, C. R., Krick, K., Martin, R., Broyles, J. M., Cooney, D. S., Lee, W. P. A., Mi, R., Mao, H. Q., Höke, A., Brandacher, G. (2019). Glial Cell Line–Derived Neurotrophic Factor and Chondroitinase Promote Axonal Regeneration in a Chronic Denervation Animal Model. Neurotherapeutics, 1-13.

Sarker, M. D., Naghieh, S., McInnes, A. D., Schreyer, D. J., Chen, X. (2018). Regeneration of peripheral nerves by nerve guidance conduits: Influence of design, biopolymers, cells, growth factors, and physical stimuli. Progress in Neurobiology, 171, 125-150.

Schmidt, C. E., Leach, J. B. (2003). Neural tissue engineering: strategies for repair and regeneration. Annu Rev Biomed Eng, 5, 293-347.

Scholz, T., Sumarto, A., Krichevsky, A., Evans, G. R. D. (2011). Neuronal Differentiation of Human Adipose Tissue–Derived Stem Cells for Peripheral Nerve Regeneration In Vivo. Archives of Surgery, 146(6), 666-674.

Seddon, H. J. (1943). Peripheral Nerve Injuries. Glasgow Medical Journal, 139(3), 61.

Sensharma, P., Madhumathi, G., Jayant, R. D., Jaiswal, A. K. (2017). Biomaterials and cells for neural tissue engineering: Current choices. Materials Science and Engineering: C, 77, 1302–1315.

Sha, L., Chen, Z., Chen, Z., Zhang, A., Yang, Z. (2016). Polylactic Acid Based Nanocomposites: Promising Safe and Biodegradable Materials in Biomedical Field. International Journal of Polymer Science, 2016, 1-11.

Shimizu, M., Matsumine, H., Osaki, H., Ueta, Y., Tsunoda, S., Kamei, W., Hashimoto, K., Niimi, Y., Watanabe, Y., Miyata, M., Sakurai, H. (2018). Adipose-derived stem cells and the stromal vascular fraction in polyglycolic acid-collagen nerve conduits promote rat facial nerve regeneration. Wound Repair and Regeneration, 26(6), 446-455.

Shin, H., Olsen, B. D., Khademhosseini, A. (2012). The mechanical properties and cytotoxicity of cell-laden double-network hydrogels based on photocrosslinkable gelatin and gellan gum biomacromolecules. Biomaterials, 33(11), 3143-3152.

Shirazi, S. F. S., Gharehkhani, S., Mehrali, M., Yarmand, H., Metselaar, H. S. C., Adib Kadri, N., Osman, N. A. A. (2015). A review on powder-based additive manufacturing for tissue engineering: selective laser sintering and inkjet 3D printing. Science and Technology of Advanced Materials, 16(3), 033502.

Shirian, S., Ebrahimi-Barough, S., Saberi, H., Norouzi-Javidan, A., Mousavi, S. M. M., Derakhshan, M. A., Arjmand, B., Ai, J. (2016). Comparison of Capability of Human Bone Marrow Mesenchymal Stem Cells and Endometrial Stem Cells to Differentiate into Motor Neurons on Electrospun Poly(ε-caprolactone) Scaffold. Molecular Neurobiology, 53(8), 5278-5287.

Shrestha, B. K., Shrestha, S., Baral, E. R., Lee, J. Y., Kim, B.-S., Park, C. H., Kim, C. S. (2019). π-Conjugated polyaniline-assisted flexible titania nanotubes with controlled surface morphology as regenerative medicine in nerve cell growth. Chemical Engineering Journal, 360, 701-713.

Singh, A., Shiekh, P. A., Das, M., Seppälä, J., Kumar, A. (2019). Aligned Chitosan-Gelatin Cryogel-Filled Polyurethane Nerve Guidance Channel for Neural Tissue Engineering: Fabrication, Characterization, and In Vitro Evaluation. Biomacromolecules, 20(2), 662-673.

Sivak, W. N., White, J. D., Bliley, J. M., Tien, L. W., Liao, H. T., Kaplan, D. L., Marra, K. G. (2017). Delivery of chondroitinase ABC and glial cell line-derived neurotrophic factor from silk fibroin conduits enhances peripheral nerve regeneration. Journal of Tissue Engineering and Regenerative Medicine, 11(3), 733-742.

Skoog, S. A., Goering, P. L., Narayan, R. J. (2014). Stereolithography in tissue engineering. Journal of Materials Science: Materials in Medicine, 25(3), 845-856.

Slaughter, B. V., Khurshid, S. S., Fisher, O. Z., Khademhosseini, A., Peppas, N. A. (2009). Hydrogels in Regenerative Medicine. Advanced Materials, 21(32–33), 3307-3329.

Song, J., Sun, B., Liu, S., Chen, W., Zhang, Y., Wang, C., Mo, X., Che, J., Ouyang, Y., Yuan, W., Fan, C. (2016). Polymerizing Pyrrole Coated Poly (l-lactic acid-co-ε-caprolactone) (PLCL) Conductive Nanofibrous Conduit Combined with Electric Stimulation for Long-Range Peripheral Nerve Regeneration. Frontiers in Molecular Neuroscience, 9, 117.

Srinivasan, A., Toh, Y.-C. (2019). Human Pluripotent Stem Cell-Derived Neural Crest Cells for Tissue Regeneration and Disease Modeling. Frontiers in Molecular Neuroscience, 12, 39.

Srivas, P. K., Kapat, K., Dadhich, P., Pal, P., Dutta, J., Datta, P., Dhara, S. (2017). Osseointegration assessment of extrusion printed Ti6Al4V scaffold towards accelerated skeletal defect healing via tissue in-growth. Bioprinting, 6, 8-17.

Stocco, E., Barbon, S., Lora, L., Grandi, F., Sartore, L., Tiengo, C., Petrelli, L., Dalzoppo, D., Parnigotto, P. P., Macchi, V., De Caro, R., Porzionato, A., Grandi, C. (2018). Partially oxidized polyvinyl alcohol conduitfor peripheral nerve regeneration. Scientific Reports, 8(1), 604.

Storti, G., Lattuada, M. (2017). Synthesis of bioresorbable polymers for medical applications. Bioresorbable Polymers for Biomedical Applications, 153-179.

Strem, B. M., Hicok, K. C., Zhu, M., Wulur, I., Alfonso, Z., Schreiber, R. E., Fraser, J. K., Hedrick, M. H. (2005). Multipotential differentiation of adipose tissue-derived stem cells. The Keio Journal of Medicine, 54(3), 132-141.

Su, C.-F., Chang, L.-H., Kao, C.-Y., Lee, D.-C., Cho, K.-H., Kuo, L.-W., Chang, H., Wang, Y.-H, Chiu, I.-M. (2018). Application of amniotic fluid stem cells in repairing sciatic nerve injury in minipigs. Brain Research, 1678, 397-406.

Su, D., Zhou, J., Ahmed, K. S., Ma, Q., Lv, G., Chen, J. (2019). Fabrication and characterization of collagen-heparin-polypyrrole composite conductive film for neural scaffold. International Journal of Biological Macromolecules, 129, 895-903.

Sun, A. X., Prest, T. A., Fowler, J. R., Brick, R. M., Gloss, K. M., Li, X., DeHart, M., Shen, H., Yang, G., Brown, B. N., Alexander, P. G., Tuan, R. S. (2019). Conduits harnessing spatially controlled cell-secreted neurotrophic factors improve peripheral nerve regeneration. Biomaterials, 203, 86-95.

Sun, J., Wei, Z. Z., Gu, X., Zhang, J. Y., Zhang, Y., Li, J., Wei, L. (2015). Intranasal delivery of hypoxia-preconditioned bone marrow-derived mesenchymal stem cells enhanced regenerative effects after intracerebral hemorrhagic stroke in mice. Experimental Neurology, 272, 78-87.

Sunderland, S. (1951). A Classification of Peripheral Nerve Injuries Producing Loss of Function. Brain, 74(4), 491-516.

Suzuki, H., Araki, K., Matsui, T., Tomifuji, M., Yamashita, T., Kobayashi, Y., Shiotani, A. (2016). Value of a novel PGA-collagen tube on recurrent laryngeal nerve regeneration in a rat model. The Laryngoscope, 126(7), E233-E239.

Tajiri, N., Acosta, S. A., Shahaduzzaman, M., Ishikawa, H., Shinozuka, K., Pabon, M., Hernandez-Ontiveros, D., Kim, D.W., Metcalf, C., Staples, M., Dailey, T., Vasconcellos, J., Franyuti, G., Gould, L., Patel, N., Cooper, D., Kaneko, Y., Borlongan, C. V., Bickford, P. C. (2014). Intravenous Transplants of Human Adipose-Derived Stem Cell Protect the Brain from Traumatic Brain Injury-Induced Neurodegeneration and Motor and Cognitive Impairments: Cell Graft Biodistribution and Soluble Factors in Young and Aged Rats. Journal of Neuroscience, 34(1), 313-326.

Tang, Y., Yu, P., Cheng, L. (2017). Current progress in the derivation and therapeutic application of neural stem cells. Cell Death & Disease, 8(10), e3108.

Tegenge, M. A., Roloff, F., Bicker, G. (2011). Rapid Differentiation of Human Embryonal Carcinoma Stem Cells (NT2) into Neurons for Neurite Outgrowth Analysis. Cellular and Molecular Neurobiology, 31(4), 635-643.

Teo, T. J., Yang, G., Chen, I.-M. (2014). Compliant Manipulators. In Handbook of Manufacturing Engineering and Technology (pp. 1–63). London: Springer London.

Teuschl, A. H., Schuh, C., Halbweis, R., Pajer, K., Márton, G., Hopf, R., Mosia, S., Rünzler, D., Redl, H., Nógrádi, A., Hausner, T. (2015). A New Preparation Method for Anisotropic Silk Fibroin Nerve Guidance Conduits and Its Evaluation In Vitro and

in a Rat Sciatic Nerve Defect Model. Tissue Engineering Part C: Methods, 21(9), 945-957.

Thomas, A., Kolan, K. C. R., Leu, M. C., Hilmas, G. E. (2017). Freeform extrusion fabrication of titanium fiber reinforced 13–93 bioactive glass scaffolds. Journal of the Mechanical Behavior of Biomedical Materials, 69, 153-162.

Tian, B., Liu, J., Dvir, T., Jin, L., Tsui, J. H., Qing, Q., Suo, Z., Langer, R., Kohane, D. S., Lieber, C. M. (2012). Macroporous nanowire nanoelectronic scaffolds for synthetic tissues. Nature Materials, 11, 986-994.

Toba, T., Nakamura, T., Shimizu, Y., Matsumoto, K., Ohnishi, K., Fukuda, S., Yoshitani, M., Ueda, H., Hori, Y., Endo, K. (2001). Regeneration of canine peroneal nerve with the use of a polyglycolic acid-collagen tube filled with laminin-soaked collagen sponge: a comparative study of collagen sponge and collagen fibers as filling materials for nerve conduits. Journal of Biomedical Materials Research, 58(6), 622-630.

Toloue, E. B., Karbasi, S., Salehi, H., Rafienia, M. (2019). Potential of an electrospun composite scaffold of poly (3-hydroxybutyrate)-chitosan/alumina nanowires in bone tissue engineering applications. Materials Science and Engineering: C, 99, 1075-1091.

Tsujimoto, G., Sunada, K., Nakamura, T. (2017). Effect of cervical sympathetic ganglionectomy on facial nerve reconstruction using polyglycolic acid-collagen tubes. Brain Research, 1669, 79-88.

Uemura, T., Ikeda, M., Takamatsu, K., Yokoi, T., Okada, M., Nakamura, H. (2015). Long-Term Efficacy and Safety Outcomes of Transplantation of Induced Pluripotent Stem Cell-Derived Neurospheres with Bioabsorbable Nerve Conduits for Peripheral Nerve Regeneration in Mice. Cells Tissues Organs, 200(1), 78-91.

Vaezi, M., Zhong, G., Kalami, H., Yang, S. (2018). Extrusion-based 3D printing technologies for 3D scaffold engineering. Functional 3D Tissue Engineering Scaffolds, 235-254.

Vigneswari, S., Murugaiyah, V., Kaur, G., Abdul Khalil, H. P. S., Amirul, A. A. (2016). Simultaneous dual syringe electrospinning system using benign solvent to fabricate nanofibrous P(3HB-co-4HB)/collagen peptides construct as potential leave-on wound dressing. Materials Science and Engineering: C, 66, 147-155.

Vojnits, K., Pan, H., Dai, X., Sun, H., Tong, Q., Darabi, R., Huard, J., Li, Y. (2017). Functional Neuronal Differentiation of Injury-Induced Muscle-Derived Stem Cell-Like Cells with Therapeutic Implications. Scientific Reports, 7(1), 1177.

Volova, T. G., Shumilova, A. A., Nikolaeva, E. D., Kirichenko, A. K., Shishatskaya, E. I. (2019). Biotechnological wound dressings based on bacterial cellulose and degradable copolymer P(3HB/4HB). International Journal of Biological Macromolecules, 131, 230-240.

Wang, B., Yuan, J., Chen, X., Xu, J., Li, Y., Dong, P. (2016). Functional regeneration of the transected recurrent laryngeal nerve using a collagen scaffold loaded with laminin and laminin-binding BDNF and GDNF. Scientific Reports, 6(1), 32292.

Wang, G., Wu, W., Yang, H., Zhang, P., Wang, J. (2019). Intact polyaniline coating as a conductive guidance is beneficial to repairing sciatic nerve injury. Journal of Biomedical Materials Research Part B: Applied Biomaterials, 1-15.

Wang, J., Tian, L., He, L., Chen, N., Ramakrishna, S., So, K.-F., Mo, X. (2018). Lycium barbarum polysaccharide encapsulated Poly lactic-co-glycolic acid Nanofibers: cost effective herbal medicine for potential application in peripheral nerve tissue engineering. Scientific RePoRTs, 8, 8669.

Wang, J., Cheng, Y., Chen, L., Zhu, T., Ye, K., Jia, C., Wang, H., Zhu, M., Fan, C., Mo, X. (2019). In vitro and in vivo studies of electroactive reduced graphene oxide-modified nanofiber scaffolds for peripheral nerve regeneration. Acta Biomaterialia, 84, 98-113.

Wang, Q., Chen, J., Niu, Q., Fu, X., Sun, X., Tong, X. (2017). The application of graphene oxidized combining with decellularized scaffold to repair of sciatic nerve injury in rats. Saudi Pharmaceutical Journal, 25(4), 469-476.

Wang, W., Wang, C. (2012). Polyurethane for biomedical applications: A review of recent developments. The Design and Manufacture of Medical Devices, 115-151.

Wang, X.-W., Li, Q., Liu, C.-M., Hall, P. A., Jiang, J.-J., Katchis, C. D., Kang, S., Dong, B. C., Li, S., Zhou, F.-Q. (2018). Lin28 Signaling Supports Mammalian PNS and CNS Axon Regeneration. Cell Reports, 24(10), 2540-2552.

Wang, Y.-L., Gu, X.-M., Kong, Y., Feng, Q.-L., Yang, Y.-M. (2015). Electrospun and woven silk fibroin/poly(lactic-co-glycolic acid) nerve guidance conduits for repairing peripheral nerve injury. Neural Regeneration Research, 10(10), 1635-1642.

Wang, L., Lu, C., Liu, H., Lin, S., Nan, K., Chen, H., Li, L. (2016). A double network strategy to improve epithelization of a poly (2-hydroxyethyl methacrylate) hydrogel for corneal repair application. RSC Advances, 6(2), 1194-1202.

Watabe, K., Fukuda, T., Tanaka, J., Honda, H., Toyohara, K., Sakai, O. (1995). Spontaneously immortalized adult mouse Schwann cells secrete autocrine and paracrine growth-promoting activities. Journal of Neuroscience Research, 41(2), 279-290.

Wei, Z.-J., Fan, B.-Y., Liu, Y., Ding, H., Tang, H.-S., Pan, D.-Y., Shi, J.-X., Zheng, P.-Y., Shi, H.-Y., Wu, H., Li, A., Feng, S.-Q. (2019). MicroRNA changes of bone marrow-derived mesenchymal stem cells differentiated into neuronal-like cells by Schwann cell-conditioned medium. Neural Regeneration Research, 14(8), 1462-1469.

White, J. D., Wang, S., Weiss, A. S., Kaplan, D. L. (2015). Silk–tropoelastin protein films for nerve guidance. Acta Biomaterialia, 14, 1-10.

Wood, R. L., Karlinsey, K. S., Thompson, A. D., Rigby, M. N., Boatright, G. D., Pitt, W. G., Roeder, B. L., Steffensen, S. C, Cook, A. D. (2018). Baseline effects of lysophosphatidylcholine and nerve growth factor in a rat model of sciatic nerve regeneration after crush injury. Neural Regeneration Research, 13(5), 846-853.

Wu, X., He, L., Li, W., Li, H., Wong, W.-M., Ramakrishna, S., Wu, W. (2017). Functional self-assembling peptide nanofiber hydrogel for peripheral nerve regeneration. Regenerative Biomaterials, 4(1), 21-30.

Wu, Y., Wang, L., Guo, B., Shao, Y., Ma, P. X. (2016). Electroactive biodegradable polyurethane significantly enhanced Schwann cells myelin gene expression and neurotrophin secretion for peripheral nerve tissue engineering. Biomaterials, 87, 18-31.

Wu, Y., Wang, L., Hu, T., Ma, P. X., Guo, B. (2018). Conductive micropatterned polyurethane films as tissue engineering scaffolds for Schwann cells and PC12 cells. Journal of Colloid and Interface Science, 518, 252-262.

Xia, Y., Zhou, P., Cheng, X., Xie, Y., Liang, C., Li, C., Xu, S. (2013). Selective laser sintering fabrication of nano-hydroxyapatite/poly-ε-caprolactone scaffolds for bone tissue engineering applications. International Journal of Nanomedicine, 8, 4197-4213.

Xie, J., Willerth, S. M., Li, X., Macewan, M. R., Rader, A., Sakiyama-Elbert, S. E., Xia, Y. (2009). The differentiation of embryonic stem cells seeded on electrospun nanofibers into neural lineages. Biomaterials, 30(3), 354-362.

Xu, D., Fan, L., Gao, L., Xiong, Y., Wang, Y., Ye, Q., Yu, A., Dai, H., Yin, Y., Cai, J., Zhang, L. (2016). Micro-Nanostructured Polyaniline Assembled in Cellulose Matrix via Interfacial Polymerization for Applications in Nerve Regeneration. ACS Applied Materials & Interfaces, 8(27), 17090-17097.

Xu, H., Yan, Y., Li, S. (2011). PDLLA/chondroitin sulfate/chitosan/NGF conduits for peripheral nerve regeneration. Biomaterials, 32(20), 4506-4516.

Xu, W., Wang, Z., Liu, Y., Wang, L., Jiang, Z., Li, T., Zhang, W., Liang, Y. (2018). Carboxymethyl chitosan/gelatin/hyaluronic acid blended-membranes as epithelia transplanting scaffold for corneal wound healing. Carbohydrate Polymers, 192, 240-250.

Xu, X., Yee, W.-C., Hwang, P. Y., Yu, H., Wan, A. C., Gao, S., Boon, K. L., Mao, H. Q., Leong, K. W., Wang, S. (2003). Peripheral nerve regeneration with sustained release of poly(phosphoester) microencapsulated nerve growth factor within nerve guide conduits. Biomaterials, 24(13), 2405-2412.

Xu, Y., Huang, Z., Pu, X., Yin, G., Zhang, J. (2019). Fabrication of Chitosan/Polypyrrole-coated poly(L-lactic acid)/Polycaprolactone aligned fibre films for enhancement of neural cell compatibility and neurite growth. Cell Proliferation, 52(3), e12588.

Xu, Y., Zhang, Z., Chen, X., Li, R., Li, D., Feng, S. (2016). A Silk Fibroin/Collagen Nerve Scaffold Seeded with a Co-Culture of Schwann Cells and Adipose-Derived Stem Cells for Sciatic Nerve Regeneration. PLOS ONE, 11(1), e0147184.

Xue, J., Wu, T., Dai, Y., Xia, Y. (2019). Electrospinning and Electrospun Nanofibers: Methods, Materials, and Applications. Chemical Reviews, 119(8), 5298-5415.

Yadegari, A., Fahimipour, F., Rasoulianboroujeni, M., Dashtimoghadarm, E., Omidi, M., Golzar, H., Tahriri, M. (2017). Specific considerations in scaffold design for oral tissue engineering. Biomaterials for Oral and Dental Tissue Engineering, 157-183.

Yamamoto, T., Osako, Y., Ito, M., Murakami, M., Hayashi, Y., Horibe, H., Iohara, K., Takeuchi, N., Okui, N., Hirata, H., Nakayama, H., Kurita, K., Nakashima, M. (2016). Trophic Effects of Dental Pulp Stem Cells on Schwann Cells in Peripheral Nerve Regeneration. Cell Transplantation, 25(1), 183-193.

Yamazaki, A., Obara, K., Tohgi, N., Shirai, K., Mii, S., Hamada, Y., Arakawa, N., Aki, R., Hoffman, R. M., Amoh, Y. (2017). Implanted hair-follicle-associated pluripotent (HAP) stem cells encapsulated in polyvinylidene fluoride membrane cylinders promote effective recovery of peripheral nerve injury. Cell Cycle, 16(20), 1927-1932.

Yang, H., He, B.-R., Hao, D.-J. (2015). Biological Roles of Olfactory Ensheathing Cells in Facilitating Neural Regeneration: A Systematic Review. Molecular Neurobiology, 51(1), 168-179.

Yang, H. Y., Thompson, I., Yang, S. F., Chi, X. P., Evans, J. R. G., Cook, R. J. (2008). Dissolution characteristics of extrusion freeformed hydroxyapatite–tricalcium phosphate scaffolds. Journal of Materials Science: Materials in Medicine, 19(11), 3345-3353.

Yang, M.-H., Chen, K.-C., Chiang, P.-W., Chung, T.-W., Chen, W.-J., Chu, P.-Y., Chen S.C.-J., Lu, Y.-S., Yuan, C.-H., Wang, M.-C., Lin, C.-Y., Huang, Y.-F., Jong, S.-B., Lin, P.-C., Tyan, Y.-C. (2016). Proteomic Profiling of Neuroblastoma Cells Adhesion on Hyaluronic Acid-Based Surface for Neural Tissue Engineering. BioMed Research International, 2016, 1-13.

Yang, W., Xu, H., Lan, Y., Zhu, Q., Liu, Y., Huang, S., Shi, S., Hancharou, A., Tang, B., Guo, R. (2019). Preparation and characterisation of a novel silk fibroin/hyaluronic acid/sodium alginate scaffold for skin repair. International Journal of Biological Macromolecules, 130, 58-67.

Yang, Y.-C., Shen, C.-C., Huang, T.-B., Chang, S.-H., Cheng, H.-C., Liu, B.-S. (2010). Characteristics and biocompatibility of a biodegradable genipin-cross-linked gelatin/β-tricalcium phosphate reinforced nerve guide conduit. Journal of Biomedical Materials Research Part B: Applied Biomaterials, 95B(1), 207-217.

Yao, L., O'Brien, N., Windebank, A., Pandit, A. (2009). Orienting neurite growth in electrospun fibrous neural conduits. Journal of Biomedical Materials Research Part B: Applied Biomaterials, 90B(2), 483-491.

Yen, C.-M., Shen, C.-C., Yang, Y.-C., Liu, B.-S., Lee, H.-T., Sheu, M.-L., Tsai, M.-H., Cheng, W.-Y. (2019). Novel electrospun poly(ε-caprolactone)/type I collagen nanofiber conduits for repair of peripheral nerve injury. Neural Regeneration Research, 14(9), 1617-1625.

Yeong, W.-Y., Chua, C.-K., Leong, K.-F., Chandrasekaran, M. (2004). Rapid prototyping in tissue engineering: challenges and potential. Trends in Biotechnology, 22(12), 643-652.

Yi, S., Yuan, Y., Chen, Q., Wang, X., Gong, L., Liu, J., Gu, X., Li, S. (2016). Regulation of Schwann cell proliferation and migration by miR-1 targeting brain-derived neurotrophic factor after peripheral nerve injury. Scientific Reports, 6(1), 29121.

Yin, D.-P., Chen, Q.-Y., Liu, L. (2016). Synergetic effects of ciliary neurotrophic factor and olfactory ensheathing cells on optic nerve reparation (complete translation). Neural Regeneration Research, 11(6), 1006-1012.

Yucel, D., Kose, G. T., Hasirci, V. (2010). Polyester based nerve guidance conduit design. Biomaterials, 31(7), 1596-1603.

Yussuf, A., Al-Saleh, M., Al-Enezi, S., Abraham, G. (2018). Synthesis and Characterization of Conductive Polypyrrole: The Influence of the Oxidants and Monomer on the Electrical, Thermal, and Morphological Properties. International Journal of Polymer Science, 2018, 1-8.

Zack-Williams, S. D., Butler, P. E., Kalaskar Shomari DL Zack-Williams, D. M., Kalaskar, D. M. (2015). Current progress in use of adipose derived stem cells in peripheral nerve regeneration. World J Stem Cells, 7(1), 51-64.

Zarbakhsh, S., Goudarzi, N., Shirmohammadi, M., Safari, M. (2016). Histological Study of Bone Marrow and Umbilical Cord Stromal Cell Transplantation in Regenerating Rat Peripheral Nerve. Cell Journal, 17(4), 668–677.

Zargar, V., Asghari, M., and Dashti, A. (2015). A Review on Chitin and Chitosan Polymers: Structure, Chemistry, Solubility, Derivatives, and Applications. ChemBioEng Reviews, 2(3), 204-226.

Zhan, J., Liu, J., Wang, C., Fan, C., EI-Hamshary, H. A., Al-Deyab, S. S., Mo, X. (2016). Electrospun silk fibroin–poly (lactic-co-glycolic acid) membrane for nerve tissue engineering. Journal of Bioactive and Compatible Polymers, 31(2), 208-224.

Zhang, H., Wei, Y., Tsang, K., Sun, C., Li, J., Huang, H., Cui, F. Z., An, Y. (2008). Implantation of neural stem cells embedded in hyaluronic acid and collagen composite

conduit promotes regeneration in a rabbit facial nerve injury model. Journal of Translational Medicine, 6(1), 67.

Zhang, J. Y., Luo, X. G., Xian, C. J., Liu, Z. H., Zhou, X. F. (2000). Endogenous BDNF is required for myelination and regeneration of injured sciatic nerve in rodents. The European Journal of Neuroscience, 12(12), 4171-4180.

Zhang, L., Yang, W., Tao, K., Song, Y., Xie, H., Wang, J., Li, X., Shuai, X., Gao, J., Chang, P., Wang, G., Wang, Z., Wang, L. (2017). Sustained Local Release of NGF from a Chitosan–Sericin Composite Scaffold for Treating Chronic Nerve Compression. ACS Applied Materials & Interfaces, 9(4), 3432-3444.

Zhang, L., Li, B., Liu, B., Dong, Z. (2019). Co-transplantation of Epidermal Neural Crest Stem Cells and Olfactory Ensheathing Cells Repairs Sciatic Nerve Defects in Rats. Frontiers in Cellular Neuroscience, 13, 253.

Zhang, L., Xu, L., Li, G., Yang, Y. (2019). Fabrication of high-strength mecobalamin loaded aligned silk fibroin scaffolds for guiding neuronal orientation. Colloids and Surfaces B: Biointerfaces, 173, 689-697.

Zhang, P.-X., Han, N., Kou, Y.-H., Zhu, Q.-T., Liu, X.-L., Quan, D.-P., Chen, J.-G., Jiang, B.-G. (2019). Tissue engineering for the repair of peripheral nerve injury. Neural Regeneration Research, 14(1), 51-58.

Zhang, S., Gelain, F., Zhao, X. (2005). Designer self-assembling peptide nanofiber scaffolds for 3D tissue cell cultures. Seminars in Cancer Biology, 15(5), 413-420.

Zhang, Y.-G., Sheng, Q.-S., Qi, F.-Y., Hu, X.-Y., Zhao, W., Wang, Y.-Q., Lan, L.-F., Huang, J.-H., Luo, Z.-J. (2013). Schwann cell-seeded scaffold with longitudinally oriented micro-channels for reconstruction of sciatic nerve in rats. Journal of Materials Science: Materials in Medicine, 24(7), 1767-1780.

Zhang, Y., Luo, H., Zhang, Z., Lu, Y., Huang, X., Yang, L., Xu, J., Yang, W., Fan, X., Du, B., Gao, P., Hu, G., Jin, Y. (2010). A nerve graft constructed with xenogeneic acellular nerve matrix and autologous adipose-derived mesenchymal stem cells. Biomaterials, 31(20), 5312-5324.

Zheng, Z., Huang, L., Yan, L., Yuan, F., Wang, L., Wang, K., Lawson, T., Lin, M., Liu, Y. (2019). Polyaniline Functionalized Graphene Nanoelectrodes for the Regeneration of PC12 Cells via Electrical Stimulation. International Journal of Molecular Sciences, 20(8), 2013.

Zhou, J.-F., Wang, Y.-G., Cheng, L., Wu, Z., Sun, X.-D., and Peng, J. (2016). Preparation of polypyrrole-embedded electrospun poly(lactic acid) nanofibrous scaffolds for nerve tissue engineering. Neural Regeneration Research, 11(10), 1644-1652.

Zhou, Z.-F., Zhang, F., Wang, J.-G., Chen, Q.-C., Yang, W.-Z., He, N., Jiang, Y.-Y., Chen, F., Liu, J.-J. (2016). Electrospinning of PELA/PPY Fibrous Conduits:

Promoting Peripheral Nerve Regeneration in Rats by Self-Originated Electrical Stimulation. ACS Biomaterials Science & Engineering, 2(9), 1572–1581.

Zhu, C., Huang, J., Xue, C., Wang, Y., Wang, S., Bao, S., Chen, R., Li, Y., Gu, Y. (2018). Skin derived precursor Schwann cell-generated acellular matrix modified chitosan/silk scaffolds for bridging rat sciatic nerve gap. Neuroscience Research, 135, 21-31.

Zhu, L., Wang, K., Ma, T., Huang, L., Xia, B., Zhu, S., Yang, Y., Liu, Z., Quan, X., Luo, K., Kong, D., Huang, J., Luo, Z. (2017). Noncovalent Bonding of RGD and YIGSR to an Electrospun Poly(ε-Caprolactone) Conduit through Peptide Self-Assembly to Synergistically Promote Sciatic Nerve Regeneration in Rats. Advanced Healthcare Materials, 6(8), 1600860.

Zhu, W., George, J. K., Sorger, V. J., and Grace Zhang, L. (2017). 3D printing scaffold coupled with low level light therapy for neural tissue regeneration. Biofabrication, 9(2).

APPENDICES

A. ETHICAL COMMITTEE APPROVAL

T.C.
HACETTEPE ÜNİVERSİTESİ
Hayvan Deneyleri Yerel Etik Kurulu

Sayı : 52338575 - 128

HAYVAN DENEYLERİ YEREL ETİK KURUL KARARI

TOPLANTI TARİHİ	:	28.11.2017 (SALI)
TOPLANTI SAYISI	:	2017/11
DOSYA KAYIT NUMARASI	:	2017/73
KARAR NUMARASI	:	2017/73 -01
ARAŞTIRMA YÜRÜTÜCÜSÜ	:	Prof. Dr. Mehmet Yıldırım SARA
HAYVAN DENEYLERİNDEN		
SORUMLU ARAŞTIRMACI	:	Tuğba Dursun USAL, Dr. Metin YEŞİLTEPE, Arwa Al BERKDAR
YARDIMCI ARAŞTIRMACILAR	:	Prof. Dr. Vasıf HASIRCI
ONAYLANAN HAYVAN TÜRÜ ve		
SAYISI	:	*40 Adet Wistar Sıçan (Erişkin)*

Üniversitemiz Tıp Fakültesi Tıbbi Farmakoloji Anabilim Dalı öğretim üyelerinden Prof. Dr. Mehmet Yıldırım SARA' nın araştırma yürütücüsü olduğu 2017/73 kayıt numaralı *"Kollajen Temelli Kompozit Sinir Tüpü Geliştirilmesi"* isimli çalışma Hayvan Deneyleri Yerel Etik Kurulu Yönergesi'ne göre uygun bulunarak oy birliği ile onaylanmasına karar verilmiştir. Kurul üyesi Prof. Dr. Mehmet Yıldırım SARA çıkar çatışması nedeni ile tartışma ve oylamaya katılmamıştır.
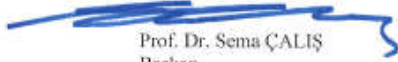
Prof. Dr. Sema ÇALIŞ
Başkan

HAYVAN DENEYLERİ YEREL ETİK KURULU GÜNDEMİ - İMZA SİRKÜLERİ
TOPLANTI TARİHİ : 28.11.2017 (SALI)
TOPLANTI SAYISI : 2017/11
TOPLANTI SAATİ : 13.30

Prof. Dr. Sema ÇALIŞ (Başkan)	(İZİNLİ) Prof. Dr. Nüket Örnek BÜKEN (Üye)	Prof. Dr. M. Yıldırım SARA (Üye)
Doç. Dr. Meltem TUNCER (Üye)	Doç. Dr. A. Cevdet AKMAN (Üye)	İZİNLİ Prof. Dr. Mehmet Ali ONUR (Üye)
(İZİNLİ) Doç. Dr. Güneş ESENDAĞLI (Üye)	Doç. Dr. Aytekin AKYOL (Üye)	Doç. Dr. Ersoy KONAŞ (Üye)
Doç. Dr. İ. ÜNBAŞILAR (Üye)	Doç. Dr. Mehmet Alper ÇETİNKAYA (Üye)	Yrd. Doç. Dr. Banu Cahide TEL (Üye)
Mevlüt ÖKSÜZOĞLU (Üye)	Serdar ÇAKIROĞLU (Üye)	Avukat Yasemin ÖZSELÇUK (Üye)
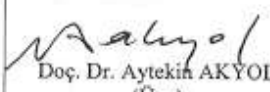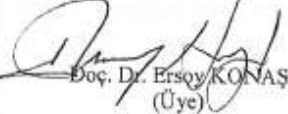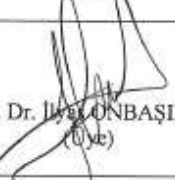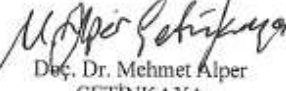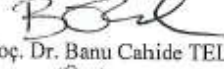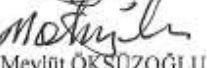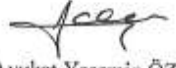
B. EQUATION FOR ALAMAR BLUE CALCULATIONS

$$\text{Percent Reduction (\%)} = \frac{\left((\varepsilon_{ox})_{\lambda_2} \text{x } A_{\lambda_1}\right) - \left((\varepsilon_{ox})_{\lambda_1} \text{x } A_{\lambda_2}\right)}{\left((\varepsilon_{red})_{\lambda_1} \text{x } A'_{\lambda_2}\right) - \left((\varepsilon_{red})_{\lambda_2} \text{x } A'_{\lambda_1}\right)} \text{ x } 100$$

$\lambda_1 = 570$ nm $\lambda_2 = 595$ nm

$(\varepsilon_{ox})_{\lambda_1} = 117.216$ $(\varepsilon_{red})_{\lambda_1} = 155.677$

$(\varepsilon_{ox})_{\lambda_1} = 80.586$ $(\varepsilon_{red})_{\lambda_2} = 14.652$ where,

A_{λ_1} = Absorbance of the test well, at $\lambda_1 = 570$ nm

A_{λ_2} = Absorbance of the test well, at $\lambda_2 = 595$ nm

A'_{λ_1} = Absorbance of the negative control (blank), at $\lambda_1 = 570$ nm and

A'_{λ_1} = Absorbance of the negative control, at $\lambda_2 = 595$ nm.

C. CALIBRATION CURVES FOR ALAMAR BLUE ASSAY

SCs P8 Alamar Blue Calibration Curve

$y = 6E{-}05x$
$R^2 = 0{,}983$

PC12 Alamar Blue Calibration Curve

$y = 3E{-}05x$
$R^2 = 0{,}9858$

SCs and PC12 Alamar Blue Calibration Curve

y = 2E-05x
R² = 0,9609

% Reduced Dye

Cell Number
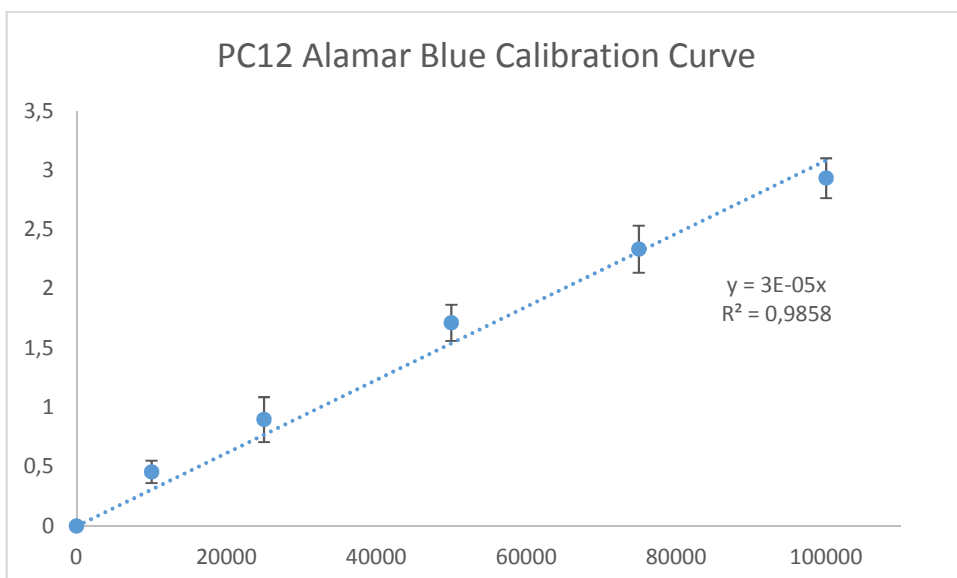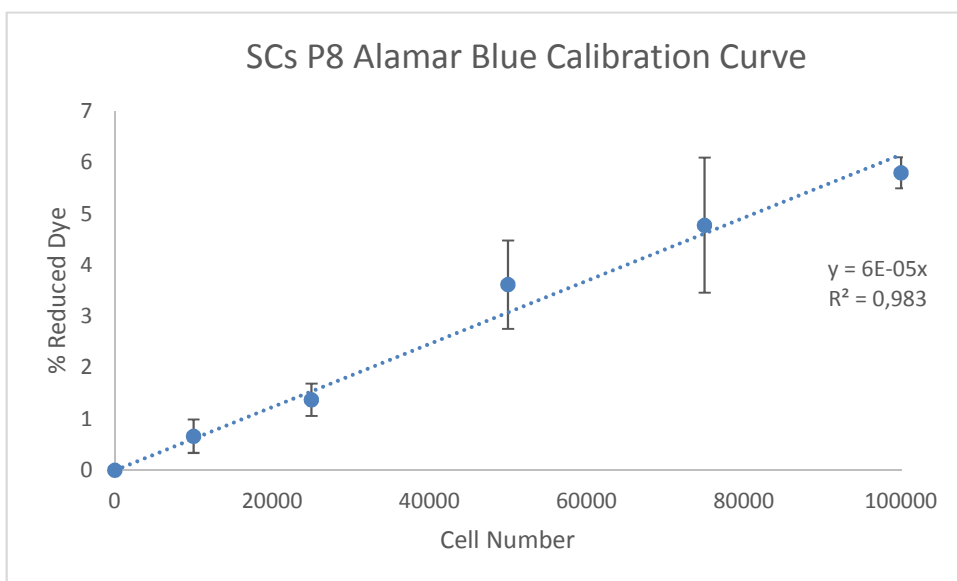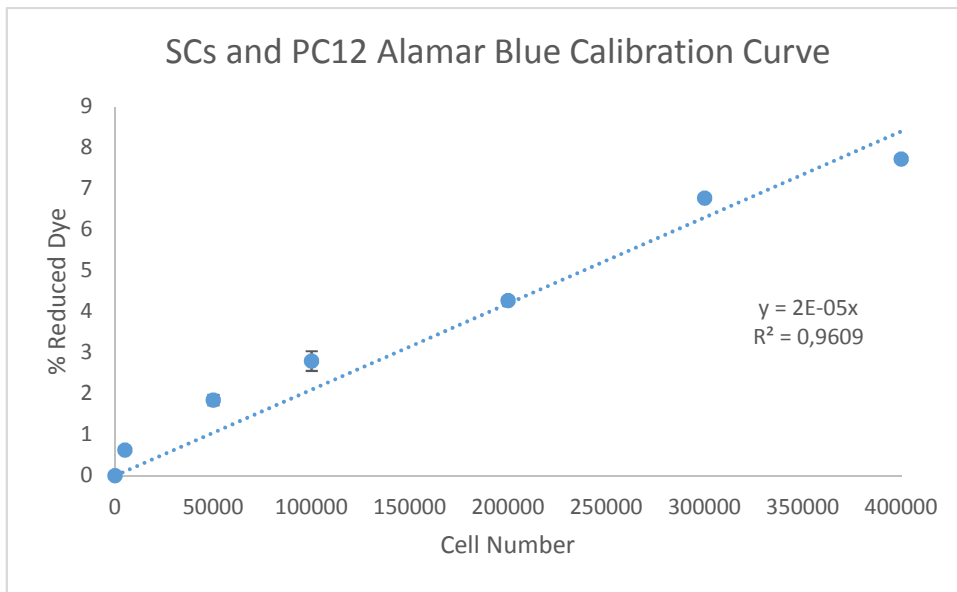
CURRICULUM VITAE

PERSONAL INFORMATION

Surname, Name   : Dursun Usal, Tuğba
Nationality   : Turkish (TC)
Date and Place of Birth   : 16 April 1989, Samsun
Phone   : +90 544 244 58 18
E-mail   : tugbad@metu.edu.tr

EDUCATION

Degree	Institution	Year of Graduation
MS	METU Biotechnology	2013
BS	METU Molecular Biology and Genetics	2011
High School	Ankara Science High School, Ankara	2006

WORK EXPERIENCE

Year	Place	Enrollment
2011-Present	METU Biological Sciences	Research Assistant
2011-Present	METU BIOMATEN	Researcher

FOREIGN LANGUAGES

Advanced English, Beginner German

PUBLICATIONS

Research Articles

Dursun Usal T, Yucel D, Hasirci V. (2019). A novel GelMA-pHEMA hydrogel nerve guide for the treatment of peripheral nerve damages. International Journal of Biological Macromolecules. 121; 699-706.

Dursun Usal T, Yucel D, Hasirci V. (2018). Differentiation of BMSCs into Nerve Precursor Cells on Fiber-Foam Constructs for Peripheral Nerve Tissue Engineering. Journal of Siberian Federal University.Biology. 11; 2.

Reviews

Tamay DG, Dursun Usal T, Alagoz AS, Yucel, D, Hasirci N, Hasirci V. (2019). 3D and 4D Printing of Polymers for Tissue Engineering Applications. Frontiers in Bioengineering and Biotechnology, 7; 164.

Arslantunali D, Dursun T, Yucel D, Hasirci N, Hasirci V. (2014) Review: Peripheral nerve conduits: technology update. Medical Devices, Evidence and Research, 7; 405-424.

Book Chapters

Ermis M**,** Baran ET, Dursun T, Antmen E, Hasirci V. Contribution of physical forces on the design of biomimetic tissue substitutes. Brennan, AB, & Kirschner, CM (Eds.). (2014). Bio-inspired Materials for Biomedical Engineering. John Wiley & Sons, pp. 59-76, ISBN: 978-1-118-36936-4.

CONFERENCE PRESENTATIONS

Oral Presentations

T. Dursun Usal, D. Yucel, V. Hasirci (2018). GelMA-pHEMA hydrogel composite nerve guide for peripheral nerve regeneration. 2nd International Biomedical Engineering Congress (IBMEC 2018), 24-27 May 2018, Nicosia, North Cyprus.

T. Dursun, D. Yucel, V. Hasirci (2017). Development of a methacrylated gelatin based nerve guide. 28th Annual Conference of the Society for Biomaterials (ESB 2017), 4-8 September 2017, Athens, Greece.

V. Hasirci, S. Alagoz, T. Dursun, C. Kilic Bektaş, N. Hasirci (2015). Biopolymers in Tissue Engineering and Regenerative Medicine. 8th European Symposium on Biopolymers (ESBP 2015), September 15-18, Rome, Italy.

T. Dursun, D. Yucel, V. Hasirci (2014). Influence of Inner Organization of Nerve Guide on Rat Bone Marrow Stem Cells (rBMSCs). 26th Annual Conference European Society of Biomaterials, 31st August-3rd September, Liverpool, England.

T. Dursun, D. Yucel, V. Hasirci (2014). Study on the Influence of Scaffold Inner Organization on the treatment of Peripheral Nerve Injury. 2nd International Symposium of Peripheral Nerve Regeneration, 23-25 February, Torino, Italy.

T. Dursun, D. Yucel, V. Hasirci. (2013). Effects of the Architecture of a Nerve Guide for Use in the Treatment of Spinal Cord Injury. 19th International Biomedical Science and Technology Symposium, 12-15 November, Kuşadası, İzmir, Turkey.

Poster Presentations

T. Dursun Usal, D. Yucel, V. Hasirci (2018). Production of a 3D Printed PCL Nerve Guide. 23rd International Biomedical Science and Technology Symposium (BIOMED 2018), 15-16 December 2018, Istanbul, Turkey. (Poster presentation)

G. E. Köle, T. Dursun Usal, V. Hasirci D. Yucel (2018). Development of Tubular Conjunction with Tissue Engineering Method. 23rd International Biomedical Science and Technology Symposium (BIOMED 2018), 15-16 December 2018, Istanbul, Turkey. (Poster presentation)

T. Dursun, D. Yucel, V. Hasirci (2017). Development of GelMA-pHEMA hydrogel blend for nerve tissue engineering applications. 22nd International Biomedical Science and Technology Symposium (BIOMED 2017), 12-14 May 2017, Ankara, Turkey.

T. Dursun, D. Yucel, V. Hasirci (2015). Development of Collagen Based Composite Nerve Guide. 21th International Biomedical Science and Technology Symposium (BIOMED 2015), 22-24 October 2015, Antalya, Turkey.

T. Dursun, D. Yucel, V. Hasirci (2013). Nerve guides with different architecture for use in the treatment of spinal cord injury. TERMIS-EU Chapter Meeting, 17-20 June, Istanbul, Turkey.

HOBBIES

Reading, Pilates, Swimming, Playing Flute